COPIES 1 — 25

COPY NO. 1

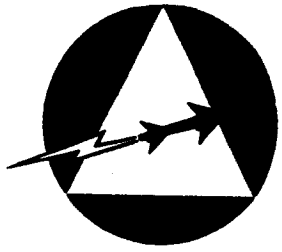

RADIOPLANE

A DIVISION OF NORTHROP CORPORATION

8000 WOODLEY AVENUE • VAN NUYS, CALIFORNIA

LANDING SYSTEMS FOR MARS AND VENUS SPACECRAFT

Radioplane Report 2368

12 April 1961

RADIOPLANE, A Division of
Northrop Corporation
8000 Woodley Avenue
Van Nuys, California

LANDING SYSTEMS FOR MARS

AND

VENUS SPACECRAFT

Radioplane Report No. 2368

12 April 1961

This work was performed for the Jet Propulsion Laboratory, California Institute of Technology, sponsored by the National Aeronautics and Space Administration under Contract NAS7-100.

Prepared By:

M. Neustadt
Dr. M. Neustadt
Research and Advanced Engineering Section

Approved By:

Don Walt
Don Walt, Jr.
Chief
Advanced Design Group

FOREWORD

This report titled "Landing Systems for Mars and Venus Spacecraft" was prepared by personnel of the Research and Advanced Engineering Section and the Paradynamics Group of the Radioplane Engineering Department. Work Authorization Number 7421 and Contract Release Notice Number 188 provided the authorization for accomplishment of the work involved in preparing this document.

By this report a basis is established for further applied research work and proposal activity in the area of spacecraft landing systems for the National Aeronautics and Space Administration.

TABLE OF CONTENTS

TABLE OF CONTENTS (cont'd)

TABLE OF CONTENTS (cont'd)

FIGURES

FIGURES (Con.)

FIGURES (Con.)

TABLES

SECTION 1

INTRODUCTION

Radioplane, A Division of the Northrop Corporation, in an effort to project its capability for the design, development, and manufacture of re-entry and landing systems from Earth to planetary vehicles, has embarked on an applied research program of spacecraft recovery systems development.

Recent and current Radioplane Division sponsored programs of study and materials tests of lunar vehicle landing system devices for the NASA Surveyor and Prospector projects are evidence of this technological progress. This report is directed toward planetary spacecraft landing systems. As such, it was prepared for distribution to the NASA, Jet Propulsion Laboratory, Pasadena, California, and applies to the JPL Planetary Exploration Programs.

These programs which are intended to probe the environment of the planets Mars and Venus with vehicles to be called Mariner and Voyager are important projects in the U.S. national space exploration effort.

The purpose of this document is to suggest to the Planetary Program Office of JPL that appropriate instrumentation payloads should be installed on early flights of the Mariner vehicle, or its ejected data capsule, to measure those atmospheric and

surface environmental parameters of Mars and Venus needed to design optimum re-entry and recovery system for follow on Mariner and Voyager flight vehicles. If optimum and reliable entry and landing systems can be installed on these vehicles, the JPL planetary exploration program can proceed to its ultimate objectives.

Section 2 briefly describes the NASA/JPL Planetary Research Programs as published by JPL.

Mars and Venus estimated data are given in Section 3.

Those parameters needed to design planetary entry and landing hardware systems are given in Section 4. It is this information that should be obtained on early Mariner flights to get the data necessary for optimum systems design.

Section 5 describes the instrumentation in Mariner and Voyager vehicle payloads required to measure the parameters of Section 4.

Aerodynamic decelerator concepts are given in Section 6 while retro-thrust devices are described in Section 7.

Section 8 names some of the concepts applicable to Mars and Venus for entry and landing systems. Because these planets have atmospheres the point is made that advantage should be taken of these atmospheres to adapt Earth type landing concepts to a Mars or Venus landing.

Section 9 details the impact deceleration hardware pertinent to the problem of absorbing the energy of touchdown.

The aerothermodynamic considerations of entry into the atmosphere of Mars and Venus is discussed in Section 10.

A list of References used in compiling the information contained herein are given in Section 11.

SECTION 2

NASA-JPL PLANETARY RESEARCH PROGRAMS

The National Aeronautical and Space Administration has initiated a program of planetary research which has as its ultimate goal the successful manned exploration of the planets. By directive, the Jet Propulsion Laboratory, Pasadena, California has been assigned by NASA the program management of this planetary exploration project.

Mr. R. J. Parks, Planetary Program Director of JPL has outlined the planetary program objectives in Reference 1 . The material presented in this section was obtained from this reference and also from Reference 2 .

2.1 PROGRAM OBJECTIVES

The primary long-range objective of the JPL Planetary-Interplanetary Program is the development of automatic, unmanned, interplanetary spacecraft technology and the use of this technology in the form of space probes to gather fundamental scientific knowledge concerning the planetary environments, the planets themselves, and solar phenomenon, both within and out of the plane of the ecliptic.

The secondary long-range objective of the Program is the development of technology and the collection of scientific data which will contribute to the successful manned exploration of the planets and the interplanetary space.

The goal by 1970 is to have demonstrated and exploited, in terms of acquired scientific data, spacecraft capable of being put in orbit and landing on the surfaces of Mars and Venus. Further it is the goal by 1970 to have made initial efforts toward probing the planets Mercury and Jupiter as well as probing interplanetary space out of the plane of the ecliptic.

The fundamental scientific knowledge that is sought in the exploration is directed at answering three questions: (1) Is there extraterrestrial life? (2) What can be learned of the origin and evolution of the solar system and its multitude of component bodies? (3) What must be learned to assure the success of the more difficult missions of the future?

The success of the program will depend on the degree to which these three questions are answered.

2.2 MARINER AND VOYAGER

A factor strongly influencing the plans is the launch vehicle availability. Launch vehicles will be provided to JPL by the NASA Marshall Space Flight Center. The CENTAUR is the first vehicle which provides adequate payload performance for the planetary and interplanetary missions envisioned. Spacecraft utilizing the CENTAUR will be called MARINERS and will be employed for fly-by missions with extensive planetary directional measurements. The CENTAUR can carry payloads of the order of

1000 pounds. Planetary orbiters and orbiter-landers then become possible later with the availability of the SATURN C-1 and C-2 vehicles, which can inject payloads in the thousands of pounds. Spacecraft in this class are called VOYAGERS.

Table 2-1 is an indication of the Mariner and Voyager planetary spacecraft program and shows the current JPL planning for these vehicles.

2.3 MARINER AND VOYAGER FLIGHT PLANNING

At the present time, the Mariner program comprises seven interplanetary missions, all Venus and Mars fly-bys. Venus will be the first U.S. fly-by using Mariner. This will take place in 1962, and will be a shot designed to give a close-up instrumented "look" at the cloud wreathed planet. The first launching of a prototype of the Mars spacecraft is scheduled for 1963. This will be a development mission and a prelude to the 1964 Mars fly-by mission. A trajectory will be chosen to provide the best over-all test of this spacecraft involving some form of Earth-return orbit.

Toward the end of the 1960 decade the Mariners will be replaced by Voyagers which will use Saturn C-1 and C-2 launch vehicles. These will be able to carry 10,000 to 20,000 lbs. payloads respectively and will be used for planetary orbiters and orbiter-landers.

The Venus and Mars program plan is shown in Figure 2-1.

Figure 2-2 shows, in a general way, the proximity of Venus and Mars to Earth. When all factors including payload performance, communication distance, launch azimuth, injection instrumentation and many others are considered, it appears that there are launching opportunities at Venus and Mars consisting of roughly a one to two-hour period each day for approximately one month in each of the years shown in Figure 2-3. It is important to note that in the case of a planetary mission a one-month slip in launching date schedule usually means a delay of a year or more.

TABLE 2-1

MARINER & VOYAGER

UNMANNED PLANETARY SPACECRAFT PROGRAM

Program	Booster	Mission	Injected Wt.	Spacecraft Propulsion
		Under Development		
Mariner A-1	Atlas Centaur	Venus Prob 1962	1100	Liquid motor for multiple mid-course correction, restart experiment near target
		Understudy		
Mariner A-2	Atlas Centaur	Deep Space Prob	To be determined	Unspecified mid-course correction probable
Mariner B-1	Atlas Centaur	Venus Fly By	To be determined	Unspecified mid-course correction probable
Mariner B-2	Atlas Centaur	Mars Split Capsule	To be determined	Mid-course correction rocket; rocket to split capsule for manpower landing
Voyager	Saturn C-1	Deep Space Probe Venus Orbiter	To be determined	Unspecified; possible need for mid-course correction rocket, retro rocket, and terminal maneuver
Voyager	Saturn C-2	Venus, Mars, and deep-space missions	To be determined	Unspecified, possible need for mid-course correction rocket, retro rocket, and terminal maneuver

Reference: "Solid Rockets for Spacecraft" by Winston Gin and L. Piasecki, Jet Propulsion Laboratory Pasadena, California, Page 32 of March 1961 issue of Astronautics Magazine.(Published by American Rocket Society) Reference 2.

VENUS AND MARS PROGRAM PLAN

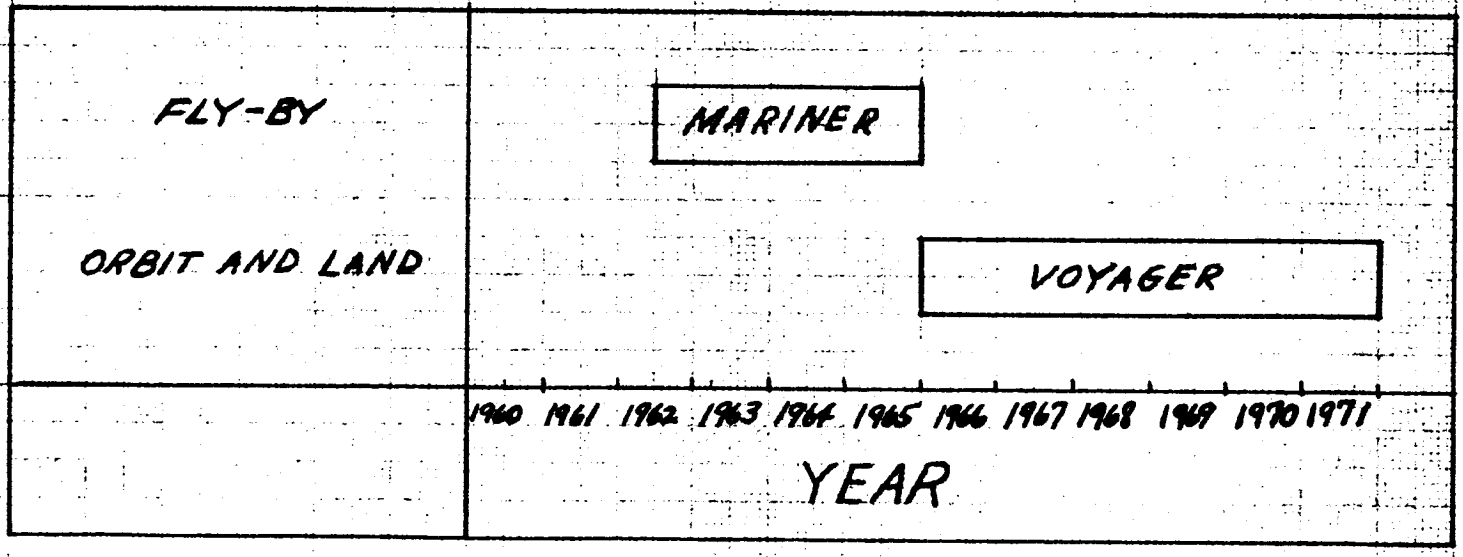

FIGURE 2-1

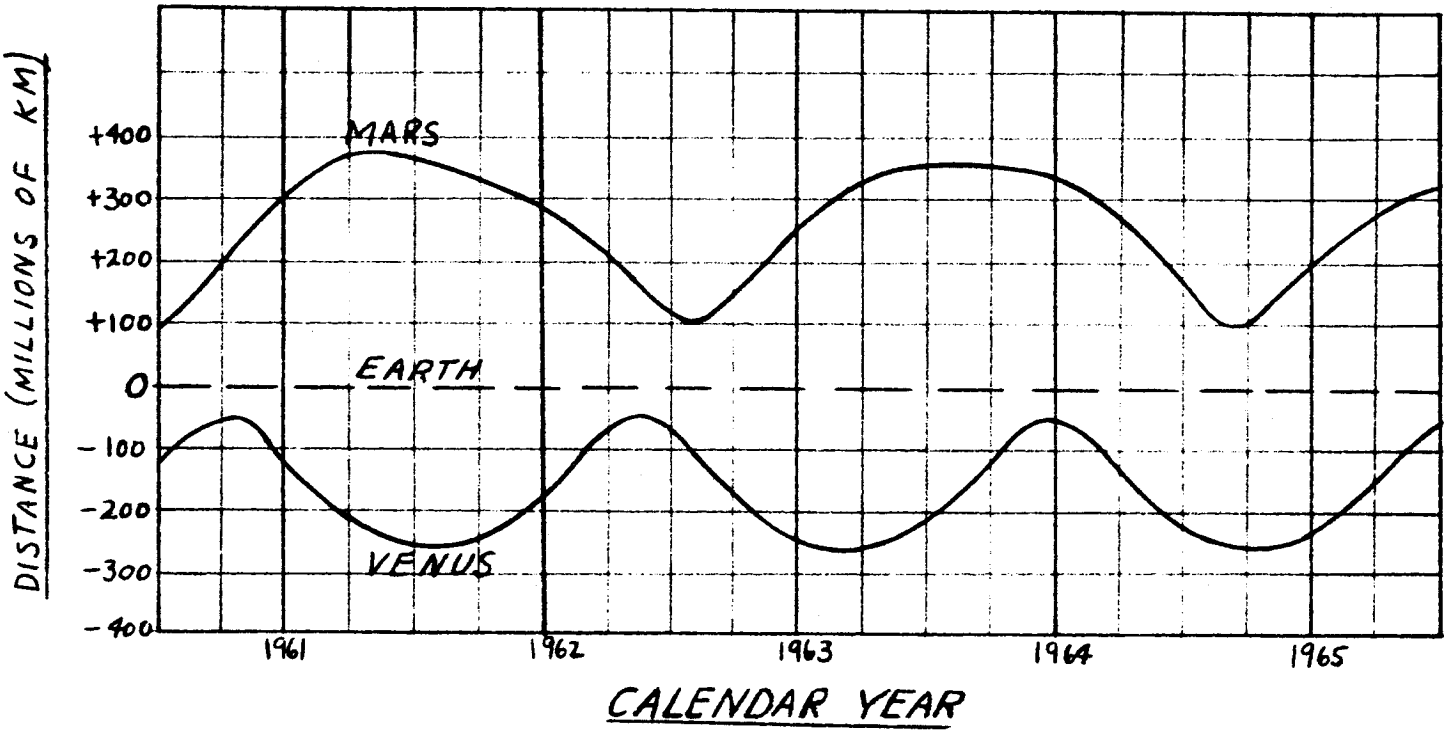

RELATIVE PLANET DISTANCES AND PERIODS

FIGURE 2-2

1960 -		MARS
1961 -	VENUS	
1962 -	VENUS	MARS
1963 -		
1964 -	VENUS	MARS
1965 -	VENUS	
1966 -		MARS
1967 -	VENUS	
1968 -		MARS
1969 -	VENUS	
1970 -	VENUS	

BEST YEARS FOR LAUNCHING FLIGHTS TO VENUS AND MARS.

FIGURE 2-3

SECTION 3

MARS AND VENUS PLANETARY DATA

Some of the measured and estimated data on the characteristics of Mars and Venus are presented in this Section. It is realized that the values presented for the various items will differ depending on which reference one wishes to quote. Zdenek Kopal, of the University of Manchester, Department of Astronomy, describes in Reference 3 the methods and results of quantitative studies of planetary atmospheres. He states that data to date has been obtained essentially by two methods - spectroscopic and photometric (or polarimetric).

It remains, however, necessary for a spacecraft to actually penetrate the atmospheres of Mars and Venus and land on their surfaces to obtain data to substantiate the estimated planetary data now available. This is, in effect, the mission of Mariner and Voyager.

Report No. 2368

PLANETARY DATA

The following are data relating to Venus, Earth and Mars (Reference 4).

Table 3-1
Planetary Data

	Venus	Earth	Mars
Mean Distance from Sun (N. Miles)	58.3×10^6	80.7×10^6	122.9×10^6
Diameter (Earth = 1)	0.967	1.000	0.523
Mean Diameter (N. Miles)	6649	6876	3596
Surface Gravity (Earth = 1)	0.88	1.00	0.38
Surface Gravity (ft/sec^2)	28.3	32.2	12.25
Velocity of Escape (ft/sec)	34,100	36,700	16,700
Probable Surface Temperature (°K)	*	288	289
Sidereal Period:			
Mean Days	224.70	365.26	686.98
Tropical Years	0.615	1.000	1.881
Period of Axial Rotation	$224^d 16^h 49^m 9^s$	$0^d 23^h 56^m 4^s$	$0^d 24^h 37^m 23^s$
Mean Orbit Velocity (n. miles/sec)	18.89	16.06	13.01
Mass (Earth = 1)	0.8136	1.000	0.1069

*Reference 4 gives a probable surface temperature of 293°K, or 20°C. However, recent measurements of the surface temperature of Venus at the Naval Research Laboratory, using radio signals emitted by Venus, give a temperature of 580°K or 307°C.

An isothermal atmosphere may be assumed given by

$$\sigma = \frac{\rho}{\rho_{SL}} = e^{-\frac{M'gh}{RT}} = e^{-ah} \qquad (1)$$

where ρ = atmospheric density,

ρ_{SL} = atmospheric density at sea level,

M' = molecular weight of atmosphere,

g = gravitational acceleration on the planet,

h = altitude measured from sea level,

R = universal gas constant,

T = absolute temperature

$\alpha = \frac{M'gh}{RT}$.

The composition of the atmospheres of Venus and Mars is (Reference 5)

Table 3-2

Atmospheres of Venus and Mars

	N_2	O_2	CO_2
Venus	10%	--	90%
Mars	95%	--	5%

The sea level density and values of α are

Table 3-3

Sea Level Densities and Exponential Coefficients

	ρ_{SL} (lbs/ft^3)	α (ft^{-1})
Venus	1.0	4.88×10^{-5}
Earth	0.0765	4.15×10^{-5}
Mars	0.0062	1.67×10^{-5}

The above data for ρ_{SL} and α are from Reference 3 with the exception of α for Mars which is from Reference 6

A plot of $\rho = \rho_{SL} e^{-ah}$ for Venus, Earth and Mars is given in Figure 3-1.

Venus is obscured by thick clouds and its surface has never been seen. According to recent measurements Venus appears to have a high surface temperature and therefore surface bodies of water such as oceans or lakes probably do not exist. High winds and wind dynamic pressure are expected on the surface of Venus.

The surface of Mars probably consists of large sandy plains with no oceans or sharp mountain ranges. It is quite possible that some primitive vegetation occurs on these plains and is responsible for the traces of color seen from time to time. Maximum height of mountains is estimated to be 9000 feet (Reference ?). There are seasonal changes in the size of the polar caps and in the climate. Wind velocities of the same magnitude as on Earth have been reported in the literature. Since the surface atmospheric density is about 1/10 that of Earth, wind dynamic pressures on Mars should be quite small.

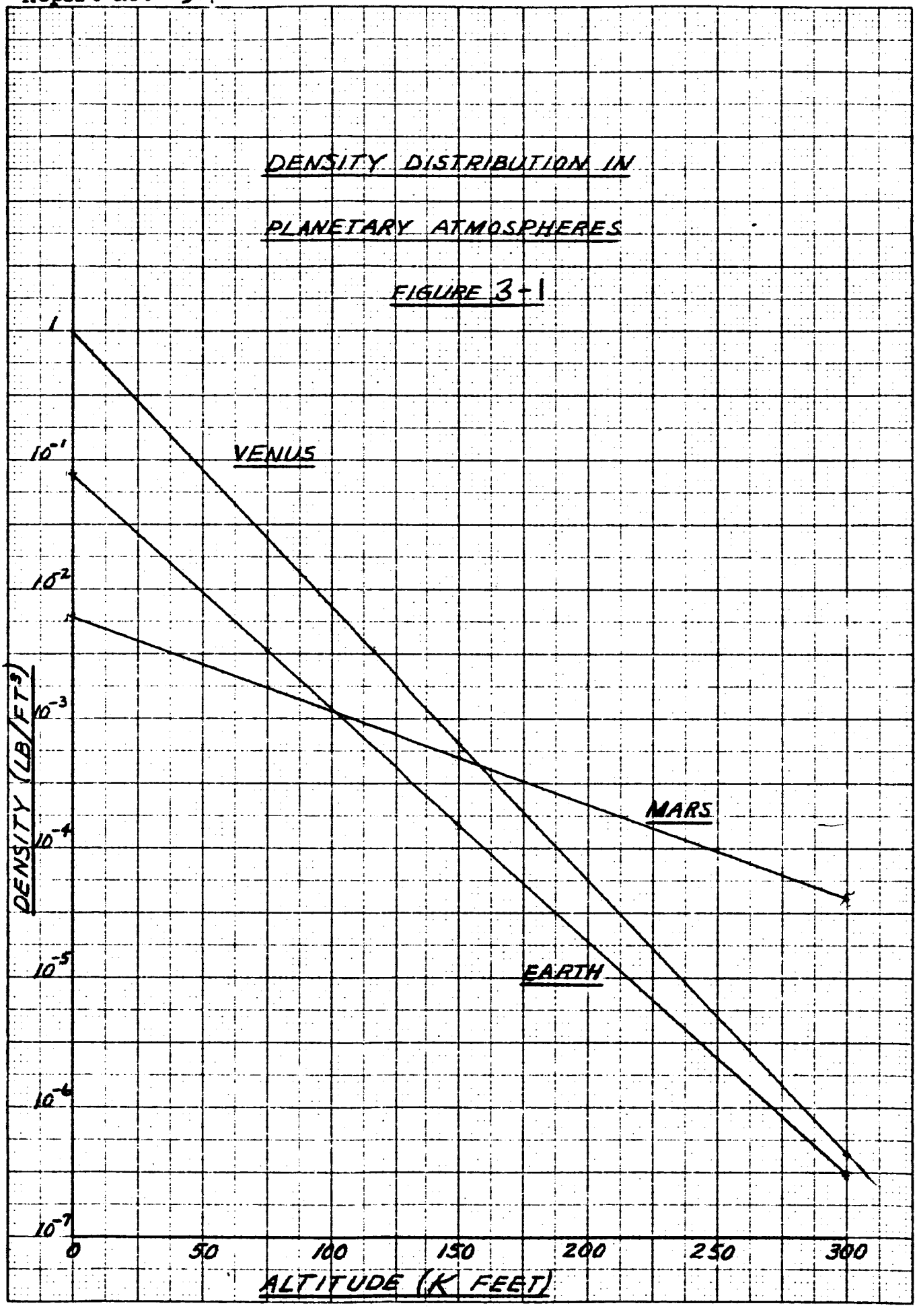
DENSITY DISTRIBUTION IN
PLANETARY ATMOSPHERES
FIGURE 3-1
1
10^{-1}
10^{-2}
10^{-3}
10^{-4}
10^{-5}
10^{-6}
10^{-7}
DENSITY (LB/FT^3)
VENUS
MARS
EARTH
0
50
100
150
200
250
300
ALTITUDE (K FEET)

SECTION 4

INFORMATION REQUIRED FOR DESIGN OF PLANETARY VEHICLE LANDING SYSTEMS

If it is intended to accomplish re-entry and landing of a spacecraft on the surface of the planet, the configuration and operating characteristics of the re-entry control and final landing systems of the spacecraft will depend, to a large degree, on the atmospheric conditions and surface environment of the planet.

The information needed to design re-entry and landing systems for Mars and Venus spacecraft is contained in the following list:

4.1 REQUIRED MARS AND VENUS ATMOSPHERIC CHARACTERISTICS DATA

A. Composition of the atmosphere and proportion of the components

B. Temperature - altitude profile

C. Radiation Fields - their location and content

The above data will influence the re-entry system and final descent system material selection.

D. Density - altitude distribution of the atmosphere

E. Density - gravity ratio profile

The above data will influence the weight and volume of the re-entry system and the final descent system.

When considering the weight, volume and materials for the re-entry and landing system, consideration must, of course, be given to the allowable limits of vehicle and payload deceleration g's and aerodynamic heating.

4.2 REQUIRED MARS AND VENUS SURFACE DATA

A. Surface composition, hardness, roughness and proturberances

B. Surface slope

C. Ratio of land mass to liquid surface

D. Surface wind velocity and direction

E. Surface temperature

The above data will influence the design and materials selection of the final descent and impact absorption system. It will also indicate the need to consider a flotation system if a liquid landing is probable.

Information such as the planet mass; rotation rate; spin axis; mean diameter; mean orbital velocity and surface area, while useful, is not absolutely necessary in landing systems design.

The first Mariner probes to Mars and Venus will attempt to gather information to assure the success of the more difficult missions to follow. The above information should be obtained by either the Mariner vehicle itself or an ejected data capsule in early

flights, so that re-entry and landing systems can be optimized on follow-on flights. If an optimum and reliable re-entry and landing system is provided for the follow-on Mariner flights and for the entire Voyager flight program, the Mars and Venus scientific planetary exploration program can proceed with an added assurance of success.

SECTION 5

INSTRUMENTATION TO OBTAIN RE-ENTRY-RECOVERY SYSTEM DESIGN INFORMATION

For gathering environmental data required for the design of recovery systems the following instruments are needed: pressure gauges, temperature gauges, atmosphere composition analysis devices. For observation the following instruments would seem desirable: television for far-scanning of the Martian terrain; radar to be utilized both in orbit and on the surface to determine not only position but contour of the land and perhaps some of the surface structure.

5.1 INSTRUMENTATION TO OBTAIN ENVIRONMENTAL DATA

5.1.1 Reliability

In designing instrumentation for planetary atmospheric studies, it must constantly be kept in mind that extreme reliability is the essential requirement. Not only are the boosters used to power planetary flight very expensive but the optimum departure times for these flights are often years apart.

It is utterly meaningless to talk about flights to Venus and Mars if the equipment to be sent there has no reasonable probability of continuing to work for the duration of the flight and for a useful period after arrival. Keeping modest amounts of equipment working, unattended, for many months is possible, but it requires a good knowledge of the environments, careful design and extensive ground testing. Since reliability

SECTION 5

INSTRUMENTATION TO OBTAIN RE-ENTRY-RECOVERY SYSTEM DESIGN INFORMATION

For gathering environmental data required for the design of recovery systems the following instruments are needed: pressure gauges, temperature gauges, atmosphere composition analysis devices. For observation the following instruments would seem desirable: television for far-scanning of the Martian terrain; radar to be utilized both in orbit and on the surface to determine not only position but contour of the land and perhaps some of the surface structure.

5.1 INSTRUMENTATION TO OBTAIN ENVIRONMENTAL DATA

5.1.1 Reliability

In designing instrumentation for planetary atmospheric studies, it must constantly be kept in mind that extreme reliability is the essential requirement. Not only are the boosters used to power planetary flight very expensive but the optimum departure times for these flights are often years apart.

It is utterly meaningless to talk about flights to Venus and Mars if the equipment to be sent there has no reasonable probability of continuing to work for the duration of the flight and for a useful period after arrival. Keeping modest amounts of equipment working, unattended, for many months is possible, but it requires a good knowledge of the environments, careful design and extensive ground testing. Since reliability

is so important it is therefore essential that a maximum information gathering capability be maintained even under the most adverse and unexpected conditions. In view of these requirements, the instrumentation philosophy might well consist of attempting to make all instruments provide as much information as possible even when partially or almost totally inoperative.

To best achieve this goal, instruments of as nearly passive a nature as possible are necessary.

5.1.2 Atmospheric Density

A number of devices are available which measure atmospheric pressure (and thus indirectly) atmospheric density. Among these are the conventional vacuum gauges (McLeod Gauge and its modifications) Ionization Gauges and Hot Wire Gauges. The applicability of each will be described below and is summarized in Table 5.1.

5.1.2.1 McLeod Gauge

The McLeod Gauge is a mercury manometer wherein a fixed volume of gas is compressed a known amount. Using the gas law the original ambient pressure can be computed from the pressure in the compressed volume. The McLeod Gauge in its present form is a cumbersome and heavy device which needs a gravitational field and is also fragile because of large unreinforced glass areas. Even if above objections were overcome, the complex

INSTRUMENT CHARACTERISTICS

Instrument	Parameter	Range	Accuracy	Volume	Typical Wt.	Status
McLeod Gauge	Pressure	10-- 10^{-7}mm Hg	10^{-3}mm Hg 4% 10^{-4}mm Hg 1.4% 10^{-5}mm Hg 5% 10^{-6}mm Hg 14% 10^{-7}mm Hg 50%	150 in^3	5 lbs.	Well developed in lab but tremendously difficult to adapt for space flight.
Pirani Gauge	Pressure	1-- 10^{-3}mm Hg	± 10%	15 in^3	1/21b.	Off-the-shelf but some development probably required for specific deep space use.
Thermocouple Gauge	Pressure	1-- 10^{-3}mm Hg	± 10%	30 in^3	3/4lb.	Off-the-shelf.
Ionization Gauge	Pressure	10^{-3}-- 10^{-10}mmHg	± 5%	20 in^3	1 lb.	Off-the-shelf with modifications.
Phillips Gauge	Pressure	10^{-2}-- 10^{-7}mmHg	± 5%	25 in^3	1½ lb.	Off-the-shelf with modifications.
Inpact Microphone	Dynamic Pressure ($\frac{1}{2}\rho V^2$)	$5X10^{-3}$mm Hg for = satellite velocity = 10^{-15} gm/cc	± 5%	40 in^3	2 lb.	Under development working models exist.
Mass Spectrograph	Composition	With specimen storage, unlimited	± 1%	200in^3	12lbs.	Developed but not off-the-shelf
Optical Spectrometer	Composition	With integrable recording, almost unlimited	± 1%	100in^3	4 lb.	Well developed but not off-the-shelf.

cycle of containing the ambient atmosphere, compressing it, measuring the pressure and returning the gauge to its original state is time consuming as well as suspect from reliability considerations. For the above reasons a McLeod type gauge is probably the least desirable atmospheric pressure sensor available.

5.1.2.2 Ionization Gauge

Ionization gauges all use a stream of energetic electrons to ionize a sample of the ambient atmosphere and then measure the ion current to determine the atmospheric pressure. The ionization gauge may either use a heated filament as a source of electrons or alternatively, in the Philips Gauge, the electrons are emitted from a cold cathode and made to spiral by a magnetic field. By virtue of the spiraling action, the electron-atom collision probability is increased and the sensitivity goes up. The ionization gauge is rugged and dependable but the sensitivity is dependent on the type of atoms present. If an isothermal atmosphere is postulated for Venus, the ionization gauge must be used at an altitude of less than 200 miles to be effective. For a Mars mission the ionization gauge will be valuable even at altitudes of 500 to 600 miles.

5.1.2.3 Hot Wire (Pirani) Gauge

The hot wire gauge essentially measures the heat conducted from a hot wire by a gas. Since the heat conductivity of a gas at low pressures is almost linear with pressure, the hot wire

gauge may be calibrated to the accuracy of the meter movement (or equivalent read-out device) used. Since conditions on the space vehicle will probably not be static, however, allowance must be made for the gas flow past the wire. In any case the range of the hot wire gauge is limited (760 to 10^{-3} mm Hg) to such an extent that it is not well suited to measurements which must range over many orders of magnitude.

5.2 DYNAMIC PRESSURE

Dynamic pressure can be found from drag effects or by a recently developed molecular microphone.

5.2.1 Drag Determination

If the drag coefficient C_D of a body is known, then the drag force F is $1/2\ \rho v^2 C_D A$. A is the cross sectional area. This drag force produces a deceleration along the flight path of F/M or $\frac{\rho v^2 C_D A}{2M}$. M is the vehicle mass. The preceding relations are true, however, only if the atmosphere consists entirely of neutral particles. If there are sufficient charged particles so that a charged particle interaction with the vehicle occurrs, errors which may be significant are possible. For Mars, exclusively neutral particle drag may be a fairly safe assumption but so little is known about the Venusian atmosphere with regard to ionization that drag measurements may not give true density measurements.

5.2.2 Molecular Microphone

Recently, an instrument for measuring dynamic pressure by recording the effect of this pressure on a sensitive microphone has been developed. This device consists of an aperture in the vehicle nose through which molecules are allowed to impinge on the microphone. The molecular flow is chopped to provide an alternating current signal and this signal is proportional to the dynamic pressure $q_\infty (= 1/2 \rho v^2)$. The microphone system has been proven reliable at $10^{-15} gm/cm^3$ densities and it is expected that this figure can be lowered with refinement of this technique. Since v can be determined accurately ρ will be relatively accurate and a comparision of this density with ionization gauge density will give an indication of the molecular partial densities. Since the microphone is limited to densities on the order of 10^{-15} gm/cm^3 it would be limited to altitudes of 100 miles or so on Venus and 300 miles or so on Mars (if the atmosphere were isothermal). It is expected that these ranges will be extended considerably in later models of the apparatus.

5.3 TEMPERATURE MEASUREMENTS

At super-satellite velocities the direct measurement of temperature is a formidable problem. Since the vehicle velocity is of the same order of magnitude as the thermal velocities, most of the ordinary temperature measuring devices are not applicable to the problem. The use of the above mentioned microphone technique

provides a method of measurement of atmospheric temperature at the same time as the dynamic pressure is being determined. The temperature can be deduced by the spreading of the beam of ambient molecules. These molecules will spread due to the transverse thermal velocity components and the amount of spreading will be proportional to the square root of the absolute temperature. If the beam is scanned by the microphone, the velocity distribution is mapped and kinetic temperature can be computed if the molecular weight of the gas is known.

5.4 DIRECT SURFACE WIND VELOCITY DETERMINATION

Surface winds on a planet can be measured directly by tracking any reasonably low density object in its descent to the surface. In addition, the local wind velocities on Venus might possibly be detected using a differential Doppler technique. Assuming the major Doppler return frequency F_d to be a function of the radial velocity of the vehicle with respect to Venus, then the total Doppler return will be equal to $F_d + \Delta F$ where ΔF is a function of the rotational velocity of Venus and surface wind velocities. If the vehicle is at such a distance that its Doppler radar beam envelopes the entire planet the Doppler component due to the rotation of Venus should cancel out. Since the surface winds are probably traveling in many different directions it is probable that the Doppler return due to wind would also cancel under the above conditions.

However, as the vehicle moves close to Venus and the Doppler radar beam covers only a small part of the planet, the surface winds within the area covered by the beam could possibly show a local trend which could give rise to a unique Doppler return which could be detected by heterodyning the Doppler return with the integrated Doppler signal to observe low amplitude deviations in Doppler signal due to surface winds.

It is felt that this system would require extensive development and may not be practical unless most of the Doppler gear is already on board for other purposes.

5.5 INDIRECT SURFACE WIND DETERMINATION

An indirect measurement can be performed from a distance of many thousands of miles away to determine the velocity of the surface winds on Venus or Mars. It is known that for Reynolds numbers greater than about 1000 turbulence replaces laminar flow. If Re, the Reynolds number is set equal to 1000, and the altitude, h, of turbulent mixing is used as the characteristic length, then the velocity is defined as:

$$v = \frac{Re\,\eta}{\rho h}$$

Using the isothermal approximation, $\rho = \rho_o e^{-\alpha h}$ and η is the sum of the viscosities of atmospheric constituents weighed in proportion to their partial pressures at the temperature of the planetary surface.

$$v = \frac{1000\, e^{(4.88\times10^{-5})h}}{\rho_o h}\,\eta$$ for Venus

If the surface temperature of Venus is assumed to be 0°C then

$$v = \frac{1000\, e^{(4.88\times10^{-5})h}\,(3.0\times10^{-7})}{h}$$ ft/sec.

if the surface temperature of Venus is assumed to be 300°C

$$v = \frac{1000\, e^{(4.88\times10^{-5})h}\,(5.8\times10^{-7})}{h}$$ ft/sec.

(10% N_2 & 90% CO_2)

For Mars

$$v = \frac{1000\, e^{(4.15\times10^{-5})h}\,(3.9\times10^{-7})}{.0062\, h}$$ ft/sec

(assuming a temperature of 40°C and 95% N_2 + 5% CO_2)

If either radar or optical techniques can be used to determine the altitude of the onset of atmospheric stratification, then by use of the above method a rough estimate of surface wind velocity can be obtained. The velocity found in such a way will be low since the turbulence will tend to disturb the stratified atmosphere above it and give an overly large value of h.

Öpik has used this system with the known wind velocities of Earth and found h to be 130 km. This points out that extra-terrestrial beings using the above equations would get the terrestrial wind velocity within ± 50%. (See Reference 8)

5.6 ATMOSPHERIC COMPOSITION

Atmospheric composition can be determined directly by sampling. It is assumed that the method of collecting samples used in the terrestrial atmosphere by the Department of Aeronautics of the University of Michigan (See Mitra, Chapter 12) can be used equally well by a Mars or Venus Probe. In addition a chemical grid technique or mass and/or optical spectrometry can be used.

5.7 CHEMICAL REACTION GRID

A simple metallic grid constructed of various metals can be used to detect atmospheric corrosive effects. The grid is formed by vacuum deposition of various metals in ships across a common conductor as shown below. By vacuum depositing a layer

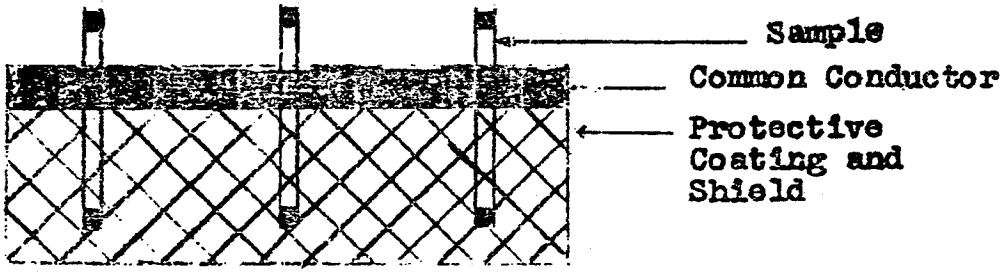

of silicon dioxide over the legs of the above strips on one side of the common conductor chemical action can be prevented on this side and these legs will act as control samples and balancing reference resistances to a bridge circuit which will detect changes in resistance as shown below.

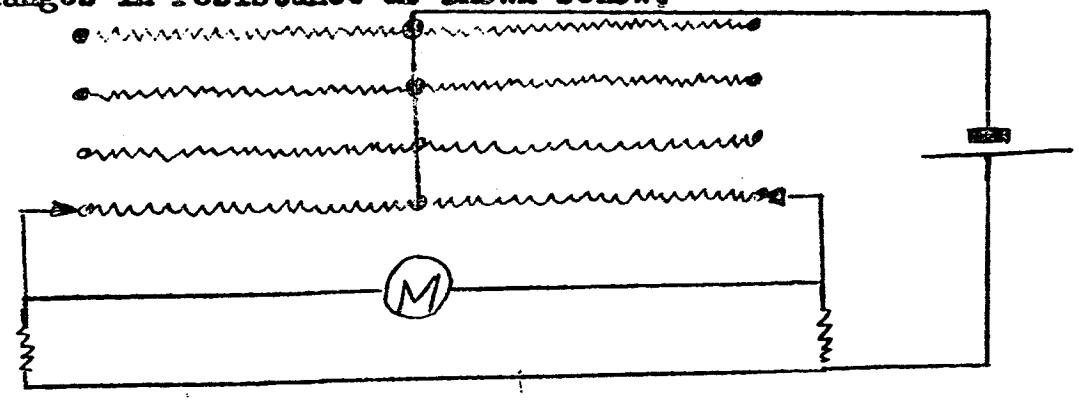

After exposure of the above grid has been accomplished, the grid would be sealed to prevent re-exposure to another atmosphere. The bridge outputs would be sampled upon return to the vicinity of the Earth to determine the amount of chemical reaction which had occurred when samples were exposed to the atmospheres of Venus and Mars.

5.7.1 Mass Spectrometer

A mass spectrometer may be thought of as a versitile ionization gauge which sorts ions of different molecular masses. It consists of an electron source used for ionizing ambient molecules, an electric field to accelerate the ions so formed, a magnetic field to bend the beam and spread it and detectors to monitor the spectrum formed. Perhaps the device which is best suited for very tenuous atmospheric measurements should be called a mass spectrograph rather than a mass spectrometer since it will measure the ion energies only accurately enough to determine their species and not necessarily their energy. An instrument like this, necessarily has a lower detection threshold because of the integration of fine structural components of the spectrum. In using the spectrograph approach, the instrument configuration can be such that the minimum payload volume and weight is used and at the same time, by sacrificing resolution, as mentioned above, the sensitivity can be made to approach a value such that an atmosphere of 10^{-11} mm Hg can be analysed. The need for a

magnet power supply can be eliminated by using a "ceramic magnet" which has a very long life and excellent stability. The high voltage for the mass spectrometer can be supplied by a radio-active battery having a half-life of approximately 10 years. The output of the battery could be further regulated by means of a radio-actively stabilized glow discharge shunt regulator tube. Such a mass spectrometer could be completely contained in a 12 pound package.

5.7.2 Atmospheric Composition From Absorbtion Spectra

A great deal can be learned about the composition of an atmosphere by an analysis of its absorbtion spectrum especially in the visible and the infra-red.

Since the solar spectrum has been studied extensively, the sun provides an excellent source of continuous radiation for trans-mission measurements in the Venusian or Martian atmosphere. To use the solar radiation scanner to detect atmospheric pro-perties of a planet, the planet must occult the sun during the vehicle trajectory. The solar transmission scanner must therefore be tied to a sun seeker or contain its own sun seeker. The optical spectrum can be scanned mechanically or by using a grating made by creating ultra-sonic waves in a liquid. The ultra-sonic frequency can be modulated causing the grating spacing to change rapidly, and the spectrum to be scanned.

A spectrometer using the liquid grating technique may not have the resolution required to pick out fine structure in the spectrum but bands can certainly be detected. In case the mechanical scanning technique is used the spectrometer may be miniturized to about 100 cubic inches total volume but this would require development work of a serious nature.

To scan the radio or microwave frequencies a broadband antenna such as a log-spiral and a varicap-tuned receiver will probably need to be used. The bands chosen should, of course, correspond to the radar and radio frequencies which have good possibilities for use in both landing and communications systems from the planets. It is assumed that the radio scanner will be a modification of the basic vehicle antenna and not a unique instrument. Sensitivity and weight are therefore omitted here.

Because of the rapid motion with respect to the line-of-sight through the planetary atmosphere both optical and radio scanners will have to be fast.

The above techniques can be used on the Mariner fly-by, capsule from Mariner, Voyager orbiter or capsule from Voyager. As the orbiter passes in and out of the shadow of the planet repeated experiments would be made of the optical absorption properties of the atmosphere.

There is need for efficient, high-power transponders for the spacecraft, and for high gain, directional, large, yet stowable,

spacecraft antennas. A particular problem occurring in fly-by experiments is that the time of encounter near the planet is brief and considerable data are desired. These data can be stored during the encounter but it may take days to transmit the same data back over the long communication distances to Earth.

5.8 RECORDER TIMER

The exact time of arrival of a planetary probe in the proximity of the target planet cannot be predicted with sufficient accuracy to permit the on-board timers alone to control the turning on and off of the data recorders. A device capable of sensing the proximity of the target planet would be desirable if it could not be tripped by the passing of other bodies. The combination of a proximity device in conjunction with a timer set to the earliest possible time of arrival would overcome the above objections to these devices.

The recorder would be turned on when the elapsed time from start of trip becomes equal to or greater than the minimum possible transit time, and the proximity detector senses the presence of a body in the vicinity of the vehicle. The recorder would be turned off when the elapsed recorded time becomes greater than the minimum possible passing time and the proximity detector no longer senses the presence of a body in the vicinity of the vehicle.

Such a device, tied to other vehicle sensors, would occupy only a few cubic inches and would be valuable in preventing abortive data recording.

5.9 Mariner Payload

It is to be hoped that the Mariner itself will carry:

(1) Impact Microphone
(2) Ionization Gauge
(3) Mass Spectrograph
(4) Chemical Reaction Sensing Grid
(5) Optical Spectrometer (and/or I.R. Scanner)
(6) Recorder Timer
(7) Communication Equipment

5.10 Capsule From Mariner

It is highly desirable to obtain atmospheric data all the way to the surface of the target planet. A capsule could be launched from Mariner to measure certain atmospheric characteristics until it impacted upon the surface of the planet. This capsule could carry the following instruments and relay the data to a recorder aboard the Mariner:

Mass Spectrometer (atmospheric composition)
Ionization Gauge (pressure)
Impact Microphone (Dynamic pressure and temperature)
Doppler Velocity Indicator (wind velocity)

The Doppler velocity indicator provides the velocity information required to reduce the data from the other instruments. The above would also be used in the capsule from Voyager.

5.11 COMMUNICATION OF DATA TO EARTH

The spacecraft must be able to communicate the engineering and scientific data to the Earth over distances 30 to 250 millions of miles. Because of distance the transmitting equipment must utilize a directiona antenna pointed at the earth. Two-way communications are necessary for the spacecraft to receive commands and also for precision tracking to determine orbits and make orbital corrections.

SECTION 6

AERODYNAMIC DECELERATOR DEVICES

Prior to deployment of the main recovery system on the Mariner and Voyager vehicles or their ejected data capsules, it may be required, during planetary re-entry, to employ aerodynamic drag producing devices to:

1. Decrease the vehicle velocity
2. Control re-entry deceleration and aerodynamic heating values
3. Control the trajectory so as to minimize impact dispersion
4. Provide system stability to the vehicle

This Section describes the aero-space deceleration devices presently available to the missile and space craft designer and names some of the problems attendant to the use of these devices. The solution to the listed problems will lead to the establishment of aerodynamic decelerator design criteria and deployment techniques.

6.1 TYPES OF AERO-SPACE DECELERATOR DEVICES

A variety of aerodynamic drag devices are available for possible use with air or space vehicles. These devices may be generally categorized by the manner in which they are connected to the vehicle; that is, there are drag devices attached as part of the primary structure and drag devices towed by lines

or cable. A list of drag devices in each category is given below:

1. Trailing Types
   - A. Parachute
     - a. Shaped solid or ventilated canopies
     - b. Clusters of small canopies
     - c. Autorotating systems
   - B. Balloon
   - C. Cascade (plates, cones, caps, etc.)
   - D. Towed after-body

2. Attached Types
   - A. Autorotor
     - a. Folding blade
     - b. Flexible blade
   - B. Semi-rigid flaps and spoilers
     - a. Umbrella frame and fabric
     - b. Annular parachute
     - c. Toroidal bladder
   - C. Rigid flaps and spoilers
     - a. Hinged surfaces
     - b. Extensible surfaces

Representative configurations of some of these aerodynamic drag devices are illustrated in Figure 6-1.

Trailing Devices

Attached Devices

Simple Parachute

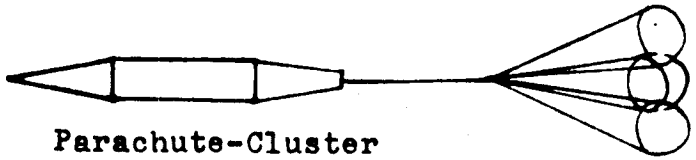

Parachute-Cluster

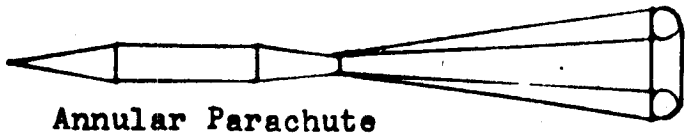

Annular Parachute

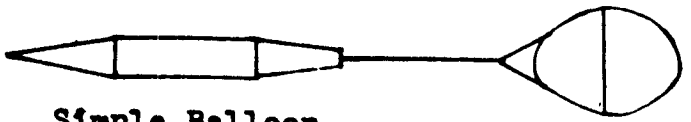

Simple Balloon

Cascade of Plates

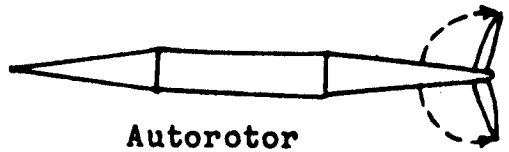

Autorotor

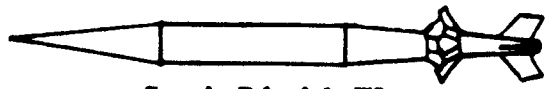

Semi-Rigid Flaps

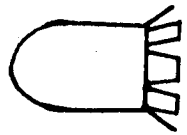

Rigid Flaps

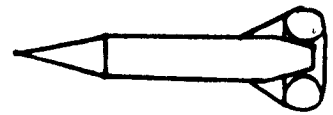

Toroidal Balloon

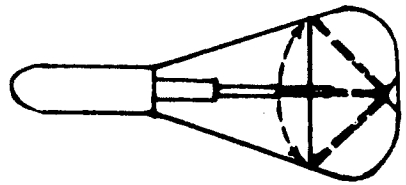

Extensible "Umbrella" Parachute

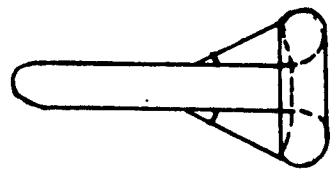

Annular Parachute (Attached)

REPRESENTATIVE AERODYNAMIC DRAG DEVICES

FIGURE 6-1

In many cases, there is no sharp dividing line between the different types of drag devices and, although some may be described as flexible, semi-rigid, or rigid in respect to their manner of support and attachment to the vehicle, specific examples of each may be found in more than one category.

Towed devices, such as parachutes, balloons and cascades of plates are commonly attached to the vehicle by flexible lines or cables, but semi-rigid attachments are also envisioned. These systems are well adapted to packaging and stowage in the vehicle. A deceleration system using the towing principle lends itself to considerable standardization and may be adapted to various vehicles with minor changes to itself or the vehicle. Towed devices, do, however, introduce extension and opening or deployment and inflation problems.

Ridigly attached devices, in general, require a greater degree of tailoring to be adaptable to a given vehicle. Most of these devices become effective when extended from the vehicle, and as such must be designed to withstand large bending moments and to minimize the forces required for deployment. Both flaps and autorotors may be made in semi-rigid as well as folding configurations to facilitate stowage in the vehicle.

The cascade of drag plates is formed by attaching transverse plates in series on a single cable. By this means, a large

drag area per unit frontal area can be developed. Packaging and adaptability considerations of this system are similar to a cluster of parachutes.

6.2 CLASSIFICATION OF VEHICLE-DECELERATOR CONFIGURATIONS

The range of Mach numbers, altitudes, and temperatures for which aerodynamic drag devices are discussed encompasses the flight regimes of ballistic as well as lifting re-entry shapes for Mariner and Voyager vehicles as well as data capsules ejected from these vehicles. Each of these vehicle classes offers its own drag device deployment problems with respect to:

1. Flight conditions at time of deployment
2. Geometric configuration of the basic vehicle
3. Allowable limits of temperature and deceleration rates
4. Aerodynamic stability
5. Structural load considerations

6.3 DECELERATOR TECHNICAL CONSIDERATIONS

6.3.1 Trajectory Considerations

A velocity-altitude plots showing the probable region of continuous flight for entry in Mars and Venus are presented in Section 10.

For the region of high dynamic pressure, the vehicles are essentially at their maximum temperature prior to deployment of the drag devices. After deployment, stagnation and skin temperatures of the vehicle will decrease continously with the passage of time, due to the rapid decrease in vehicle speed. This will be especially true for small values of the vehicle's flight path angle, θ.

Attached drag devices (flaps and spoilers) will probably be exposed to the same temperatures as the vehicle structure prior to deployment. A particularly important consideration in the case of the re-entering vehicle is that the use of spoilers or drag flaps will certainly increase the local heat transfer coefficients and may serve to trip the laminar boundary layer over most of the vehicle surface resulting in greatly increased heat transfer rates. Deflection of a control surface or a drag flap has been known to promote a boundary layer transition which propagates upstream (in the inner subsonic region of the boundary layer) against a supersonic free stream and causes transition forward of the flap hinge line.

Parachutes, on the other hand, will probably be shielded from high temperatures prior to deployment and hence, will experience a build-up of temperature when deployed. Peak temperatures of the parachute should be somewhat less than the maximum vehicle temperatures due to the time lag of temperature build-up and the rapid deceleration associated with the use of drag device.

The high q region trajectory problems appear, therefore, to be associated more with the problems of deployment techniques, initiating inflation, opening shock loads, and deceleration rate than with those of maximum temperatures and heating rates.

For the low q range, re-entry vehicles which deploy their drag devices prior to entrance into the denser layers of the atmosphere are of most concern. At time of deployment, both the drag device and the vehicle itself are relatively cold. Their trajectories upon re-entry into the atmosphere and their heating rates and surface temperatures experienced during re-entry are governed by the following parameters:

1. Ballistic parameter (W/C_DA_c) where
   - W = vehicle weight
   - C_D = total drag coefficient
   - A_c = cross-sectional area on which C_D is based
2. Initial re-entry angle (θ) and velocity (V)
3. Surface emissivity (ϵ)
4. Ratio of surface area to cross-sectional area (A_s/A_c)

Analysis of References 5 through 12 yields the following information about zero lift re-entry trajectories:

1. Effects of variation of ballistic parameter $\frac{W}{C_DA_c}$:
   Lower values of the ballistic parameter will result in lower maximum heating rates and surface temperatures, (Figure 6-2. Peak deceleration rate will be essentially unaffected by variations in this parameter, though decreases in the value of (W/C_DA_c) will result in the peak deceleration occurring at higher altitudes, Figure 6-3 depicts this situation for entry into the Earth's atmosphere. The same condition would apply for entry into any atmosphere.

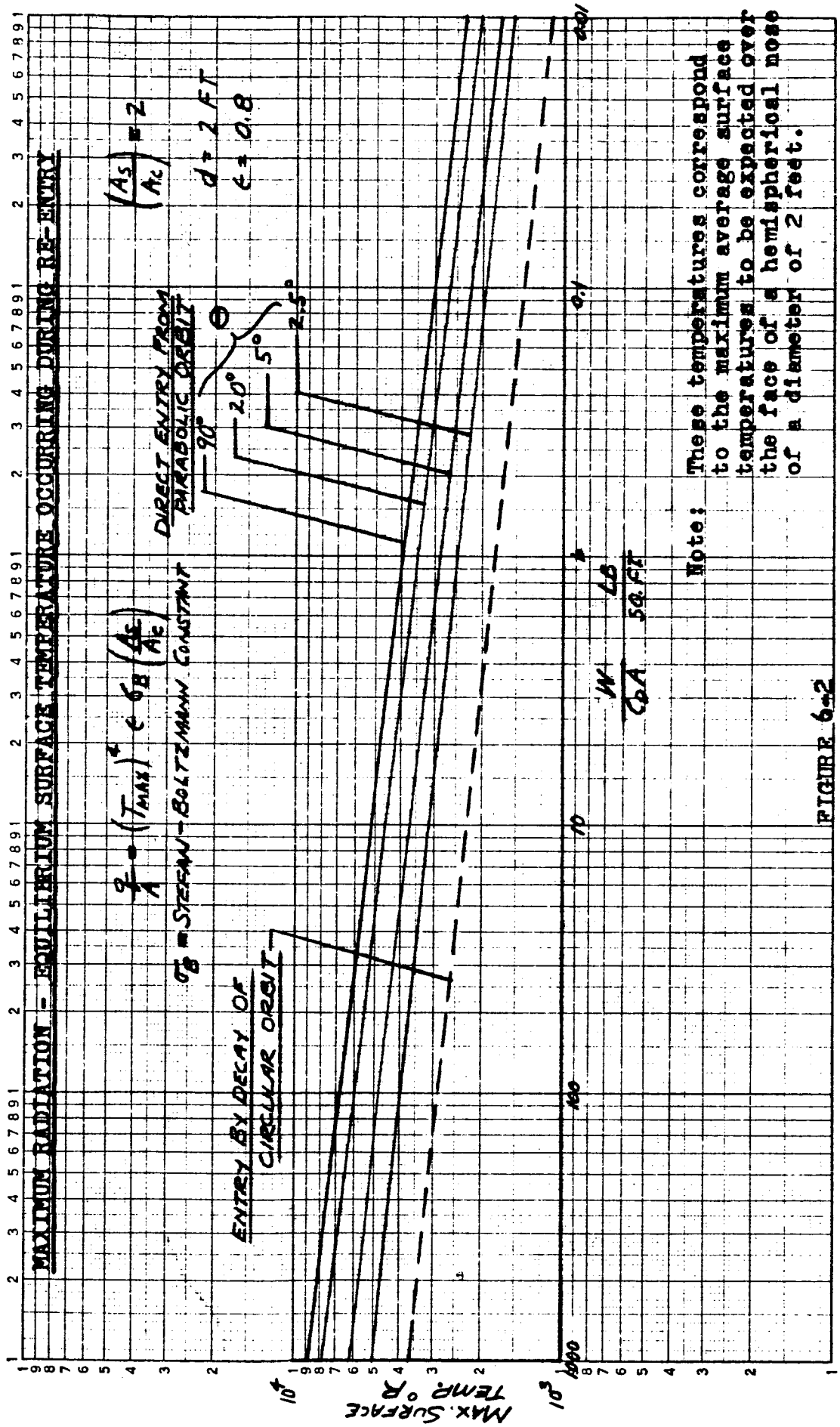
MAXIMUM RADIATION - EQUILIBRIUM SURFACE TEMPERATURE OCCURRING DURING RE-ENTRY
$\frac{q}{A} = \epsilon \sigma_B \left(\frac{A_s}{A_c}\right) (T_{MAX})^4$
σ_B = STEFAN-BOLTZMANN CONSTANT
$\left(\frac{A_s}{A_c}\right) = 2$
$d = 2$ FT
$\epsilon = 0.8$
DIRECT ENTRY FROM PARABOLIC ORBIT
θ
90°
20°
5°
2.5°
ENTRY BY DECAY OF CIRCULAR ORBIT
$\frac{W}{C_D A}$ LB / SQ FT
MAX. SURFACE TEMP °R
10^4
10^3
Note: These temperatures correspond to the maximum average surface temperatures to be expected over the face of a hemispherical nose of a diameter of 2 feet.

FIGURE 6-2

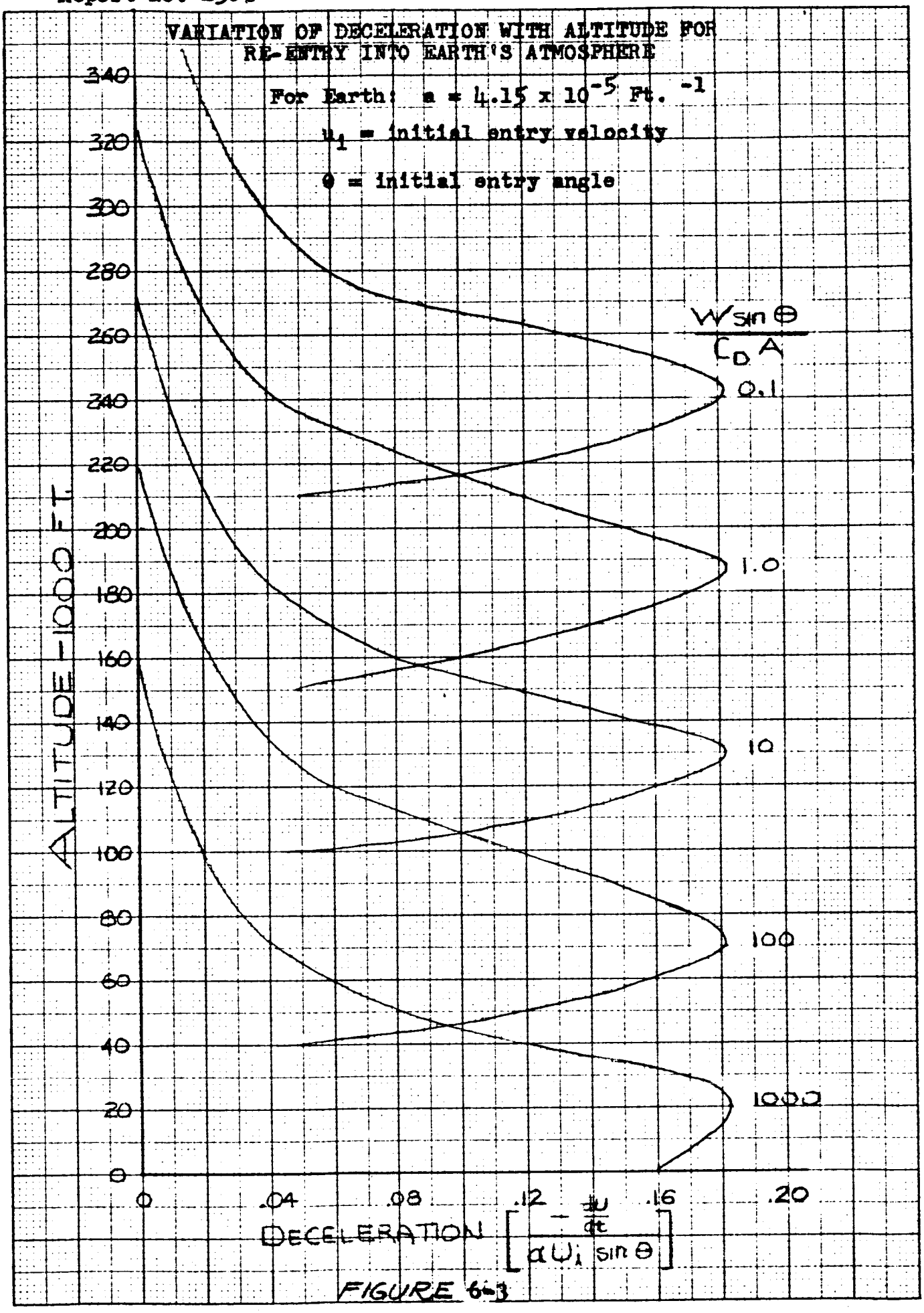
VARIATION OF DECELERATION WITH ALTITUDE FOR RE-ENTRY INTO EARTH'S ATMOSPHERE
For Earth: a = 4.15 x 10^-5 Ft.^-1
u_1 = initial entry velocity
θ = initial entry angle
$\frac{W \sin\theta}{C_D A}$
0.1
1.0
10
100
1000
ALTITUDE-1000 FT.
340
320
300
280
260
240
220
200
180
160
140
120
100
80
60
40
20
0
0
.04
.08
.12
.16
.20
DECELERATION $\left[\frac{-\frac{du}{dt}}{a u_i \sin\theta}\right]$

FIGURE 6-3

2. Effects of variation in initial re-entry angle and velocity:

   Increases in the initial re-entry angle and velocity will result in greater peak deceleration rates, heating rates and surface temperatures.

3. Effects of variation in surface emissivity:

   Decreases in surface emissivity are associated with higher surface temperatures.

4. Effects of variation in ratio of surface to cross-sectional area ratio:

   Decreases in the ratio of surface area to cross-sectional area will result in higher surface temperatures. (The actual size of the body influences the temperature in that it affects the flight Reynolds Number and hence, the convective heat transfer).

The use of an aerodynamic drag device to decrease the value of the ballistic parameter to approximately 1.0 psf will result in relatively low maximum surface temperatures (1000-2000°F) for low values of re-entry angle ($\theta_E = 5^\circ$) and reasonable values of emissivity ($\epsilon = .7$ to $.8$) and area ratio ($A_p/A_c = 2$) for entry into the Earth's atmosphere. Similar values for entry into planetary atmosphere can be calculated.

6.3.2. Effects of Variable Drag

For re-entry type vehicles, the use of variable drag area offers the possibility of the control of deceleration rates throughout the entire trajectory. For example, Reference 5 indicates that for both direct entry from a parabolic orbit and entry by decay of circular orbit, a constant value of deceleration rate will be obtained if $\frac{\sigma}{(W/C_DA_c)}$ is a constant (σ = ratio of density at altitude to density at sea level). As can be seen, the maintenance of a constant value of $\frac{\sigma}{(W/C_DA_c)}$ requires that the drag area (C_DA_c) be continuously decreased as altitude decreases. The desirability of achieving rates of deceleration lower than those experienced with a constant value of the ballistic parameter is apparent, especially for a manned re-entry body. Trajectories of this type will, however, cause higher velocities in the lower regions of the atmosphere, with higher heating rates resulting. Detailed trajectory studies, including the effects of various types of drag area (C_DA_c) programming will yield more information on the nature of the aerodynamic heating problems associated with the use of variable drag devices. Investigation of mechanical and structural

problems, in light of the information obtained from the trajectory studies, should enable the design of variable drag area devices which will offer a reasonable compromise between decreases in deceleration rates and increases in heating rates.

6.3 3. Aerodynamic Stability

Blunt nose, capsule type vehicle configurations have a tendency to be unstable at transonic and supersonic flight speeds. Drag devices, especially trailing types, can be employed to provide aerodynamic stability to these configurations. In the case of the Project Mercury capsule, the drogue parachute exerts a drag force on the capsule that enables capsule stability to be maintained from supersonic speeds down to the subsonic deployment speeds of the main recovery parachute.

During and after deployment of the drag producing device, pitch and yaw control will, in some design concepts, be unavailable for the vehicle-drag device combination. A safe margin of longitudinal and directional stability must, therefore, be achieved for the combination if reasonable trim attitudes are to be maintained. Where it is desirable to follow a zero lift trajectory, as might be the case when a closely predictable landing area is desired, the combination should be made as near rotationally symmetric as possible both geometrically and weight distribution-wise. Asymmetries in either geometry or weight distribution will cause a statically stable vehicle to trim at a non-zero angle of attack. For unmanned re-entry vehicles with attached drag devices, imparting some spin to the combination will tend to offset the

effects of geometric or mass asymmetries due to imperfect fabrication techniques.

The dynamic stability of a re-entry body with an attached drag device presents some unusual problems which can influence both the vehicle structures and the payload. In Reference 11. equations were derived to describe the oscillatory behavior of a ballistic body at supersonic speeds. The general solution for the angle of attack, α , is

$$\alpha = e^{K_1 e^{-\beta y}}\left[C_1 J_0\left(2\sqrt{k_2+k_1}\, e^{-\frac{\beta y}{2}}\right)+C_2 Y_0\left(2\sqrt{k_2+k_1}\, e^{-\frac{\beta y}{2}}\right)\right]$$

In the equation $J_0(\quad)$ and $Y_0(\quad)$ are the zero-order Bessel function of the first and second kind, respectively. The "dynamic stability" factor is:

$$K_1=\left[g\rho_0 A/4\beta W\sin\theta\right]\left[C_D-C_{L_\alpha}+\left(C_{m_q}+C_{m_{\dot\alpha}}\right)\left(\frac{l}{\sigma}\right)^2\right]$$

while the "static stability" factor is:

$$K_2=\left[g\rho_0 A/4\beta^2 W\sin\theta\right]\left[-\frac{C_{m_\alpha} l}{\sigma^2}+C_{L_\alpha}\beta\sin\theta\right]$$

Nomenclature:

C_D - Drag Coefficient

C_{L_α} - Lift Curve Slope

C_{m_q} - Pitch Damping Parameter

$C_{m_{\dot{\alpha}}}$ - Angle of Attack Rate Damping Parameter

C_{m_α} - Rate of Change of Pitching Moment Coefficient With Angle of Attack

l - Characteristic Length

σ - Radius of Gyration

C_1, C_2 - Constants of Integration

ρ_0 - Sea Level Density

β - Constant in Density Altitude Relation

y - Altitude

g - Acceleration of Gravity

W - Weight

A - Reference Area

θ - Trajectory Flight Path Angle Below the Horizon

If the body, on entering the atmosphere, has its axis misaligned by an angle with the respect to the flight path, but has no angular velocity, then C_2 is zero and the solution becomes:

$$\frac{\alpha}{\alpha_E} = e^{K_1 e^{-\beta y}} J_0\left(2\sqrt{K_2 + K_1}\, e^{-\beta y/2}\right)$$

The importance of the "dynamic stability" factor (K_1) is clearly evident. For large negative values of this factor the motion is completely damped while the vehicle is still at relatively high altitudes. With $K_1 = 0$ the amplitude decays, but is still finite at impact. Large positive values cause the amplitude to build up as the vehicle penetrates the denser layers of the atmosphere.

The non-dimensional coefficients which enter into the determination of K_1 vary considerably with Mach number, particularly in the transonic range. Studies, reported in Reference 12, have been made to determine the effects upon the amplitude of the oscillatory motion of a re-entry vehicle which has varying K_1 value in the transonic range and negative values of K_1 at subsonic and supersonic speeds. Positive K values (associated with positive values of $(C_{m_q} + C_{m_{\dot{\alpha}}})$ are tolerable in the transonic range if the vehicle impacts subsonically, as the passage through the transonic range is accomplished in a relatively short time.

For re-entry vehicles with trailing drag devices (e.g., parachutes) the dynamic stability problem is somewhat more complex in that the vehicle and drag device may each have their own oscillatory motions. The only constraints would be at the harness attachments joining the drag device to the vehicle. The effects of an initial angle of attack (α_E)

may be more severe in that the semi-independent motions may set up large time variant stresses tending to separate the drag device from the vehicle. It would appear that this would be especially important in situations where the drag forces are high in relation to the gravity forces, the effects of angle of attack on the drag of the basic vehicle are high, and the frequency of the (α/α_E) oscillations is high.

6.3.4. Effects of Drag on Dynamic Heating During Re-entry

During entry into the atmosphere a body's kinetic energy is converted into thermal energy of the surrounding air. The percentage of the thermal energy transferred to the body as heat from the surrounding air depends on the relationships of pressure drag and skin friction drag, with the heating rate varying directly with the latter. Accordingly, assuming total drag remains essentially constant, the blunt shape configuration with high pressure drag would appear to be satisfactory from the standpoint of minimizing heat transfer.

It is conceivable that some deceleration devices could fall in the above high pressure drag category. Therefore, the optimum drag device configuration to minimize temperatures should be achieved without special consideration or limitations to the basic vehicle design configuration. In addition to heating caused by skin friction, radiation effects from the hot gas downstream of the shock fronts associated with hypersonic flow conditions, are also significant. The complex nature of these gas properties are difficult to predict analytically because, contingent on velocities attained, these extreme gas temperatures can excite the vibrating modes

of the diatomic molecules, disassociate the diatomic molecules and possibly ionize the atoms. This points out the importance of utilizing experimental data to augment theory in determination of gas temperatures and corresponding heat transfer relationships. Although the body is subjected to severe air temperatures, obviously the actual surface temperatures experienced are determined by equating a heat balance of: (1) convective and radiation inputs, (2) material heat storage, and (3) radiation losses. The factor which influences the degree of dynamic heating for all bodies is the mass-drag parameter defined as $\frac{W \sin \Theta}{C_D A_c}$ where Θ is the trajectory flight path angle.

Small values of this parameter cause deceleration high in the atmosphere, while large values delay deceleration until the lower atmosphere is reached. Thus, the use of a high-drag, light body at a small entry angle is advantageous from the standpoint of reducing aerodynamic heating, since surface heating of the body increases with both atmospheric density and body velocity.

A study of the mass-drag parameter for each type of deceleration device and trajectory, particularly pertaining to variable drag devices, will afford a basis for the establishment of an optimum drag deployment vs. time schedule to reduce heating rates. Due to the fact that the altitude of maximum heating will vary with the mass-drag parameter, a programmed drag deployment presents a method of alleviating heating conditions.

As previously mentioned, the skin friction drag coefficient is paramount in determining the heating rate to the body configuration, and subsequently the total heat absorbed. There are well known analytical relationships which correlate heating rates as a function of Reynolds and Mach numbers for various configurations. However, if the space vehicle-decelerator device design program is one involving advanced state-of-the-art, it is probable that studies will be required to further basic relationships of heating parameters in the various flow regimes.

The variation in body surface temperatures during Mars and Venus descent depends not only on type of entry and the aforementioned configuration parameters, but also on the particular system heat storage and dissipation capabilities. To accommodate transient heat loads the body could be protected by a thick heat absorbing material, an insulation, or an ablating type material.

SECTION 7

RETRO-ROCKET DECELERATOR SYSTEMS

In addition to the aerodynamic decelerators discussed in Section 6, retor-rocket devices could be used on the Mariner or Voyager vehicles, or their ejected data capsules, to slow the spacecraft during planetary approach.

7.1 RETRO-ROCKET SYSTEMS CONCEPT

The landing velocity of the vehicle could be reduced to essentially zero by the firing of retro-rockets. Retro-rockets could be used to decelerate the vehicle from the time of entry into the planet's atmosphere until touch down. Another technique would be to fire the retro-rockets a few hundred feet from the surface after the vehicle has been decelerated to 50-100 ft/sec velocity by means of a parachute system or other aerodynamic decelerator. A system of this type would also require a landing gear or strut device which would include one of the methods of energy absorption described in Section 9 to absorb any shock which might occur due to errors in the guidance or retro-thrust systems. A variable thrust solid propellant retrorocket is suggested for this method of landing a vehicle on Venus or Mars in order that miminum landing shock can be achieved. A retro-rocket of this type would have the capability of correcting any errors in the systems mentioned above. Solid propellant motors are suggested for this application because of their simplicity and

high reliability. This is particularily important when the flight time of months and the space environment is considered for landing a payload on Venus or Mars. Throttleable high performance solid propellent motors with an I_{sp} of 275-300 seconds should be available for the long range Voyager program.

Depending on the vehicle configuration and space available for placement of retrorockets, either a single or multiple rocket could be adapted to this application.

7.2 ATTITUDE CONTROL WITH RETRO-ROCKETS

Another requirement for this system is that the motors be capable of providing directional control to correct for any thrust mis-alignment or horizontal velocity component in order that the vehicle be aligned vertically at touch down. An alternate method would be to use low thrust gas jets.

The correction of drift can be delayed until just prior to impact, at which time the drift vector is measured with a proximity sensing probe and corrected with a lateral impulse in the proper direction supplied by a retro-rocket deceleration system.

Without a human pilot, sensing the drift vector and orienting the vehicle, or retro-thrust system, to counter it is a complex engineering problem. However, automatic means of accomplishing

this have been envisioned for other space programs such as Surveyor and Prospector lunar projects. One of the important bits of information needed for design of the final system is the probable velocities of surface winds on Venus and Mars. This knowledge will help determine both the type of drift correction system to use and the total impulse required.

The cost of the drift sensing and correcting system will be least if it is made an integral part of a retro-thrust landing decelerator system. As noted in Reference 13, for a low impact velocity, the landing system of least weight, within the present state of the art, is provided by an optimum combination of parachutes and retro-rockets. The retro-rocket system can be designed so that with proper controls and intelligence inputs the resultant thrust vector can be applied through the vehicle center of gravity to reduce both vertical and horizontal velocity components to within tolerable levels at impact.

7.3 RETRO-ROCKETS IN COMBINATION WITH PARACHUTE SYSTEMS

A system of employing retro-thrust decelerators with parachute systems has been worked out by Mr. E. G. Ewing of the Radioplane Paradynamics Group, Engineering Department. He has published this concept in a paper titled, "A Minimum Weight Landing System for Interplanetary Spacecraft". This paper was presented by Mr. Ewing at the Recovery of Space Vehicles Symposium sponsored by the Institute of Aero Space Science, at Los Angeles California, August 31 - September 1, 1960. This paper is listed as Reference 13.

The following information is taken directly from this Reference.

7.3.1 THEORY OF RETRO-THRUST - PARACHUTE COMBINATIONS

The weight of the parachute system has a well-defined relationship to the area of the drag surface and thence to the equilibrium rate of descent with a given gross load (References 14 and 15). The weight of the rocket system is determined by the total impulse required which, through the net change in momentum, also can be expressed in terms of the vertical descent velocity of the parachute (Reference 15). These relationships may be stated more precisely as follows.

The Parachute: $$W_p = f\ (C_D S) \qquad (1)$$

Where: W_p = Weight of parachute system

$C_D S$ = Effective drag area.

The effective drag area of the parachutes is defined by this variation of the classical drag equation.

$$C_D S = \frac{2\ F_c}{\rho\ V_e^2} \qquad (2)$$

Where: $F_c = W$ = Total drag of parachute system

W = Gross landing weight

ρ = Mass density of air

V_e = Equilibrium rate of descent.

The Rocket: $$W_R = f\ (I_R) \qquad (3)$$

Where: W_R = Weight of rocket system

I_R = Total impulse required.

The total impulse required of the rockets may be defined as

$$I_R = \frac{\overline{W_L}}{g_o}\ (V_e - V_L) + K_e \overline{W_L} t_b \qquad (4)$$

Where: $\overline{W_L}$ = Mean landing weight

V_L = Vertical velocity at impact

K_e = Fraction of weight effective during t_b

t_b = Rocket burning time

g_o = Surface gravity.

We are interested in determining the conditions under which the ratio $(W_p + W_R)/W$ is a minimum and what minimum value is attainable by present parachute and rocket technology.

As noted, a parachute system in equilibrium descent develops a total drag equal to the gross weight.

From (2) $$F_c = 1/2 \rho V_e^2\ C_D S = W \qquad (5)$$

When the unit weights of the textile materials used are constant, the weight of the parachute can be expressed as a linear function of its surface area or effective drag area.

$$W_p = K_1\ (C_D S) \qquad (6)$$

By substitution in (5).

$$\frac{W_p}{W} = \frac{2K_1}{\rho V_e^2} \qquad (7a)$$

At sea level we may say $\rho = \rho_o$ = constant, and write

$$\frac{W_p}{W} = \frac{K}{V_e^2} \qquad (7b)$$

Where: $K = \frac{2K_1}{\rho_o}$ = Constant for a defined range of descent velocities

V_e = Equilibrium rate of descent at sea level

ρ_o = Mean density of atmosphere at sea level.

In actual practice, the unit weights of materials used in the parachute structure can be constant only over a narrow range of descent velocities because the increase in unit canopy loading with velocity develops higher stress levels necessitating use of proportionately stronger textiles. The general effect of this on W_p/W can be allowed for by using an exponent for V_e other than 2, as shown in Figure 1 of Reference 13 , but a more accurate result is obtained by determining a K value for 7b which is applicable to the limited descent velocity range of special interest.

The weight of the rocket is

$$W_R = \frac{I_R}{I_w} \qquad (8)$$

Where: i_w = Over-all impulse/weight ratio of the rocket in lb/sec/lb.

Then by (4) and (8)

$$W_R = \frac{W}{i_w}\left(\frac{V_e - V_L}{g} + K_e\, t_b\right) \qquad (9)$$

A slightly conservative answer is obtained by letting $W_L = W$, which neglects the weights of both parachute system and rocket propellant.

Of particular interest here is the requirement for landing with zero impact, i.e., $V_L = 0$.

Then:
$$\frac{W_R}{W} = \frac{1}{i_w}\left(\frac{V_e}{g} + K_e\, t_b\right) \qquad (10)$$

Adding (7b) and (10), the combined weight of parachutes and rockets is

$$\frac{W_p + W_R}{W} = \frac{K}{V_e^2} + \frac{1}{i_w}\left(\frac{V_e}{g} + K_e\, t_b\right) \qquad (11a)$$

$$= \frac{K}{V_e^2} + \frac{V_e}{i_w g} + \frac{K_e\, t_b}{i_w} \qquad (11b)$$

At what rate of descent is this ratio a minimum? It will be noted that as V_e approaches zero the parachute term becomes infinitely large, i.e., it is impractical to operate at "low" descent velocities. The rocket terms are more complicated, showing the desirability of using the lowest practicable descent velocity and the highest impulse

weight ratio attainable in combination with a "short" burning time. The orders of magnitude indicated by the terms "low" and "short" remain to be determined.

Differentiating (11b) with respect to V_e.

$$\frac{d\left(\frac{W_{P+}W_R}{W}\right)}{dV_e} = -2\frac{K}{V_e^3} + \frac{1}{i_w g} \qquad (12)$$

Thus, the minimum occurs when (12) is zero,

$$V_e = 3\sqrt{2K\ i_w\ g} \qquad (13)$$

The optimum working range

At descent velocities between 15 and 80 feet per second, using parachutes of good structural efficiency, K has a minimum value of 22 and a maximum value of 34 (Figure 1 Reference 13). It will be seen immediately by (13) that for this range of K values and any reasonable impulse/weight ratio between 100 and 185 seconds the minimum weight system will be obtained when V_e is between 50 and 75 feet per second. Therefore, the value of K must be in the order of 30 to 34 and it develops shortly that 34 is a good number to use.

Inasmuch as the range of descent velocities being considered makes it feasible to employ very short deceleration intervals without generating significant g forces, i.e., large thrust requirements, the effect of operating time on rocket efficiency becomes an important factor.

As shown in Figure 2, Reference 13, the efficiency of rockets falls off with decreasing burning time and the variation is quite pronounced for burning times less than 2 or 3 seconds. The faired curve of i_w/i_p vs t_b was developed from the performance of a few exceptional solid propellant rockets described in Reference 13. Specific impulse values ranged between 170 and 224 seconds. The use of $i_p = 220$ seconds is considered a realistic value for the design of any new rocket for the proposed application. A tentative cut at the solution, with $i_w = 150$ seconds and $K = 34$, by (13) indicates that a descent velocity of 69 feet per second approaches the optimum for minimum weight landing systems employing parachutes and solid propellant retro-rockets. Therefore, we may determine the precise effect of rocket burning time on the system weight by letting

$$V_e = 3\sqrt{68\ i_w\ g} \qquad \text{(Eq. 13 with } K = 34\text{)}$$

and using Figure 2 to obtain corresponding values of i_w and t_b in the solution of (11b). Figure 2 is in Reference 13.

In completing the solution, it is considered desirable to let $K_e = 1$, because the problem of vehicle stabilization during the final deceleration phase will be simplified by disconnecting the parachute system at the same time the retro-rockets are fired, i.e., the entire weight will be supported solely by the rockets during this interval.

7.3.2 Numerical Relationships

From the above theory, Mr. Ewing has established the following relationships for retro-thrust parachute landing systems for vehicles landing on the Earth, Mars and Venus. He has shown that for vehicles landing on the Earth, the combination retro-thrust and parachute landing system will have a minimum weight of 2.92% of the gross weight landed. For landing on Mars, this percentage increases to 3.96%, and for a Venus landing the percentage drops to 2.79%. Thus the minimum weight retro-thrust-parachute landing system is lighter, and that for Mars is slightly heavier than for Earth in the ratios of 80% and 106% respectively. Mr. Ewing also concludes that these minimum weight systems will be obtained by designing the parachutes for rates of descent of 55 ft/sec for Venus and 92 ft/sec for Mars as compared to 64 ft/sec on Earth.

7.3.3 Conclusions

The only really new factor to contend with is the need for firing the retro-rockets at a precise distance above the landing surface. With a near-optimum combination of descent velocity and rocket burning time, significant errors in timing the start of the reaction cannot be tolerated; the difference between success and disaster at 70 feet per second is 0.65 seconds. However, the initiating height is low enough (only 40 to 50 feet) to permit a mechanical probe to be used with good efficiency; a telescoping

tube is considered to have best possibilities. The mechanical probe is, in fact, one of the few devices that also provides a means of sensing the direction and rate of horizontal drift, such that a corrective impulse could be applied by a second cluster of small rockets just prior to touchdown.

Despite the apparent violence and hazard of the proposed landing operation, the potential reliability of the system, with redundancy confined to the contact probe and control system, is high. The net average deceleration of the vehicle will be only about 1.7 g during the retro-thrust interval. When the total impulse is provided by a cluster of four or more retro-rockets, failure of one would not have disastrous consequences. A reduction in total impulse of 25 percent, for example, would give an impact velocity of about 28 fps; this is less than the design value for some present day capsules. If we are willing to trade weight for a less precipitous descent and use rockets of shorter-than-optimum burning time, the advantages include both reduced length (and weight) of contact probes and a lower impact velocity in the event of rocket malfunctions.

The general solution may be applied to the landing of a spacecraft on other planets having significant atmospheres. When the surface gravity and atmospheric density are known, new constants for equation (11) can be developed readily by the methods indicated. Landing

on both Mars and Venus is feasible employing the parachute-retro-rocket system and the anticipated cost per pound of payload makes it important to have a system of absolute minimum weight. However, it will also be important that the landing system be capable of sensing and correcting drift just prior to touchdown.

SECTION 8
LANDING SYSTEMS CONCEPTS
FOR
MARS AND VENUS SPACECRAFT

In examination of the Mars or Venus entry and landing problem, a number of concepts suggest themselves as offering solution to insure satisfactory results. The actual concept or method selected will depend on factors such as vehicle gross weight, allowable touchdown velocity, deceleration and heating tolerances of the payload, and the specific operating characteristics of the instrumentation that is collecting the environmental data in the atmosphere and on the surface of the planets.

It is shown in Section 10 that satellite entry into the Martian atmosphere may be characterized by less than half as severe a deceleration problem, and perhaps an order of magnitude less severe heating problem than in the Earth's atmosphere. On the other hand, satellite entry into the Venusian atmosphere may be characterized by the same order of deceleration and heating values as encountered upon entry in the Earth atmosphere. It is suggested in Reference 16 that if the restriction is imposed that the deceleration limits be the same in all planetary atmospheres considered, and if it is required that exit be at satellite speed in all cases, then the parabolic corridor depths in the Venusian atmosphere are about the same as those in the Earth's atmosphere, and those in the Martian atmosphere may be an order of magnitude greater than those in the Earth's atmos-

phere. The following tables from Reference 16 show this relative deceleration and heating.

	Satellite Entry		
	Deceleration G	Heating Rate $\dot{q}$	Net heat transfer per unit area, q Total heat transfer, Q
Earth	1	1	1
Mars	.4	.1	.2
Venus	.9	.8	.9

	Parabolic Entry			
	Deceleration G	Altitude Corridor h	Heating Rate $\dot{q}$	Net heat transfer per unit area, q Total heat transfer, Q
Earth	1	1	1	1
Mars	1	12	.5	.2
Venus	1	1	.9	1

8.1 SUGGESTED LANDING SYSTEM CONCEPTS

With the above in mind the following Mars and Venus spacecraft landing systems concepts are suggested.

I.
a. Drag parachute for entry deceleration and stabilization
b. Main parachute for final descent
c. Impact deceleration material such as aluminum honeycomb for impact shock absorption.

II.
a. Drag parachute for entry deceleration and stabilization
b. Main parachute for final descent
c. Landing bags or a penetration spike for impact shock absorption.

III.
a. Drag parachute for entry deceleration and stabilization
b. Main parachute for final descent
c. Landing legs with impact absorption material in the feet for final touchdown.

IV.
a. Drag parachute for entry deceleration and stabilization
b. Main parachute for final descent
c. Retro-thrust to reduce vertical and horizontal velocity to zero at touchdown. (See Section 7)

V.
a. Drag parachute for entry deceleration and stabilization
b. Main parachute for final descent
c. Balloons installed in the main parachute canopy and inflated with gas to provide a buoyant system which would allow the vehicle to remain at a fairly constant pre-selected altitude above the surface to observe the surface (television) or record atmospheric data. At a given signal the gas could be slowly valved out of the balloon and a descent to the planetary surface accomplished.

VI.
a. Paraglider or "Rogallo Sail" deployed for lifting entry and glide descent
b. Impact deceleration material or landing bags for shock absorption

VII.
a. Folded fins or wings deployed for lifting entry and glide descent
b. Same as VI.b.

If the possibility of landing on a liquid surface is suspect, a flotation bag system or styrofoam material should be incorporated.

Steerable features could be made a part of the final descent parachute system to control touchdown location if communication can be established with the descending vehicle to transmit commands.

From the above it is seen that a number of possibilities exist for design of a Mars or Venus landing system. The point is that these planets, unlike the Moon, have an atmosphere. Any landing system for spacecraft approaching these planets for a landing should take advantage of this and utilize aerodynamic drag and/or lift producing devices to accomplish the landing.

8.2 PARACHUTE WEIGHTS

In order to obtain a "feel" for the order of magnitude of final descent parachute weight a calculation was made based on the following assumptions:

a. Data capsule weight = 250 earth pounds
b. Entry angle θ = 20 to 90 degrees
c. Impact velocity = 25 and 80 feet per second
d. Parachute deployed at M = 1.0
e. Ablation nose cone is dropped allowing the capsule to impact on crushable material to absorb shock
f. Subsonic capsule $\frac{W}{C_D A}$ = not more than 300 lbs/sq. ft.

The mass of the parachute is estimated by the method given in Reference[13] as follows:

$$\frac{W_p}{W} = \frac{C_k}{V_e^2}$$

where

W_p = mass of parachute

W = gross mass landed (250 earth pounds)

V_e = equilibrium descent velocity at the surface of the planet (80 fps)

K = constant which is proportional to the ratio

C = correction factor for small parachutes (C is close to 1.3 in this system).

By substitution in above equation one gets

$$\frac{W_p}{W} = \frac{1.3K}{6400} \text{ and } \frac{1.3K}{625}$$

On the basis of the gravitational constants and atmospher c characteristics given in Reference 13, the values of K and the corresponding parachute masses for W = 250 lbs and V_e = 25 to 80 fps are:

Impact velocity = 80 feet per second

Planet	K	W_p/W	Parachute Weight (lbs)
Venus	21.1	0.0043	1.1
Mars	98.4	0.0200	5.0

and

Impact velocity = 25 feet per second

Planet	K	W_p/W	Parachute weight- lbs
Venus	13.7	0.0219	5.5
Mars	63.7	0.1020	25.5

SECTION 9

IMPACT DECELERATOR HARDWARE

A wide variety of energy absorbers were studied for possible application for a planetary spacecraft soft landing system. These absorbers included crushable materials (Honeycomb and Foam), pneumatic impact bag, cylinders (pneumatic, hydraulic, etc.) and miscellaneous devices such as spike, plastic bending struts, extruding wire, etc. A brief physical description, suggested methods of deployment, performance and outstanding characteristics of these absorbers are presented in the following paragraphs.

9.1 CRUSHABLE HONEYCOMBS

9.1.1 Aluminum Honeycomb

Aluminum honeycomb, having hexagonal cells, has been used effectively as an impact decelerator. This material is available in varying cell sizes (1/8" - 3/8") and foil thickness (.0007" - .003") in either 3003 or 5052 alloys. The crushing strength of the 5052 alloy is approximately 30 percent higher than the 3003 alloy. Aluminum honeycomb is normally used in the expanded state but can be purchased in the unexpanded condition for a special application.

Aluminum honeycomb crushed in a direction parallel to the cell axis results in a force versus stroke curve as shown below:

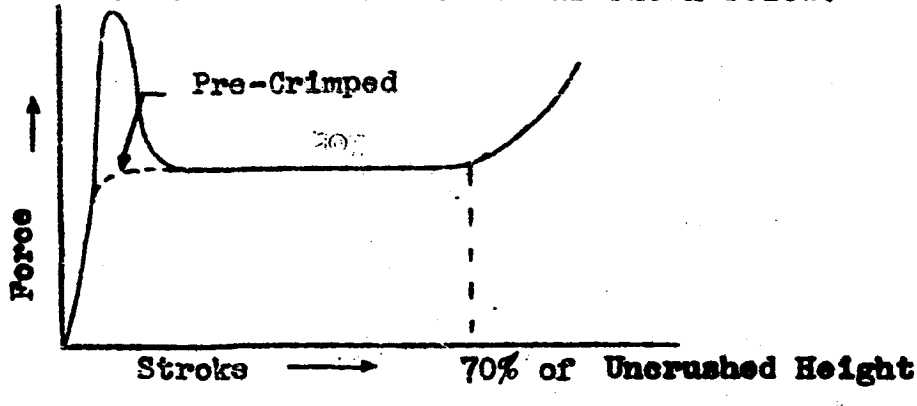

The peak at the beginning of the stroke may be eliminated by pre-crimping the honeycomb or by shaping the honeycomb so that the area in contact with the impact surface increases with stroke, (radial deployment for example).

Aluminum honeycomb normally starts to bottom out at approximately 70% of the original honeycomb height as noted by a substantial force increase on the force vs. stroke curve. Aluminum honeycomb may be deployed in a variety of ways for use in a lunar landing vehicle. It may be deployed radially, or parallel on the feet of landing struts as shown below.

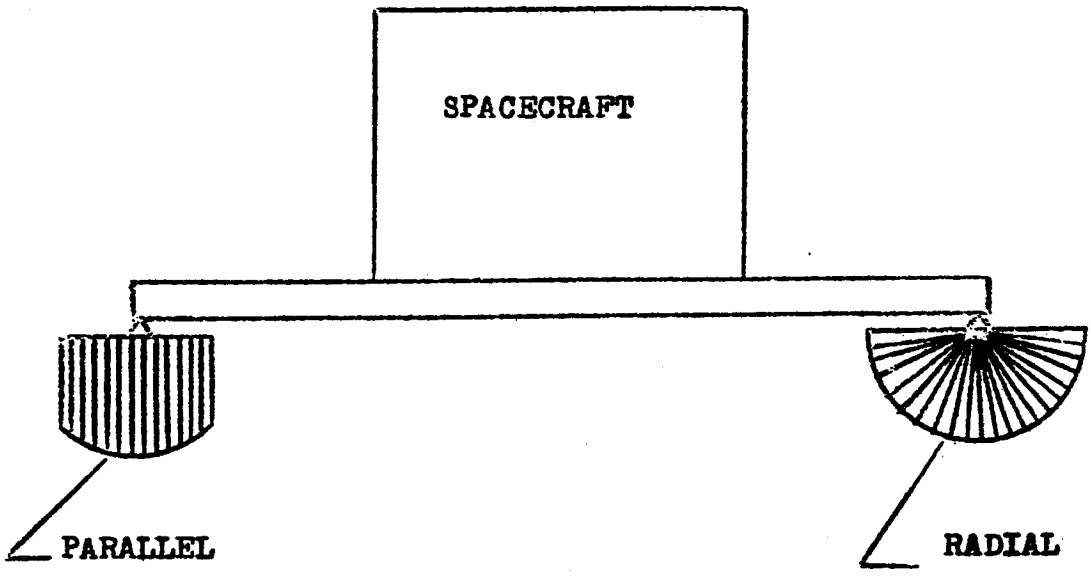

Honeycomb may also be deployed in a cylinder in which the material is crushed parallel to the cell axis. Cell sizes of 1/8" or 1/4" are recommended because of the smaller volume of material required to absorb the energy due to the higher crushing stress than 3/8" aluminum honeycomb. The crushing stress can be increased by filling the honeycomb cells with polyurethane or balsa wood. The maximum allowable deceleration will determine the minimum acceptable decelerator stroke. This minimum stroke may necessitate a large L/D ratio due to rather high crushing stress (300-800 psi). For this reason a cylinder is selected for deployment of high crushing stress materials.

This method of absorbing energy is considered to be quite efficient but overall weight of the system may be somewhat higher than deploying the material as a free expanded cushion beneath the load due to the extra cylinder weight. A sketch of this method is shown below:

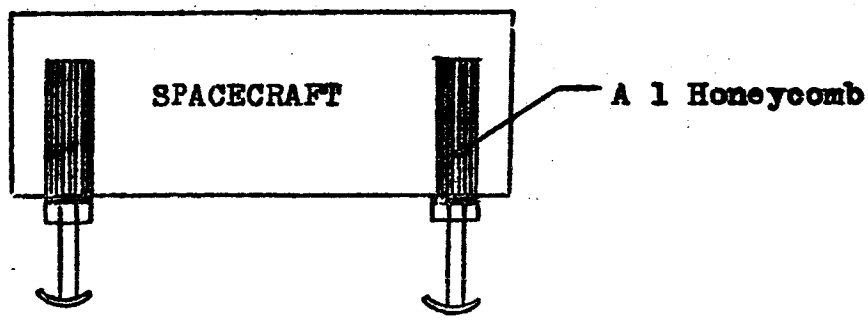

Aluminum honeycomb may be packed and expanded just prior to impact. However, a high force mechanism might be required to perform this expansion. Aluminum honeycomb has the additional advantages that is non-magnetic and requires no out-gassing. It has, however, a distinct disadvantage in that its energy absorbing capability is direction sensitive. This directional property can be illustrated by varying the angle of applied load. This is shown below:

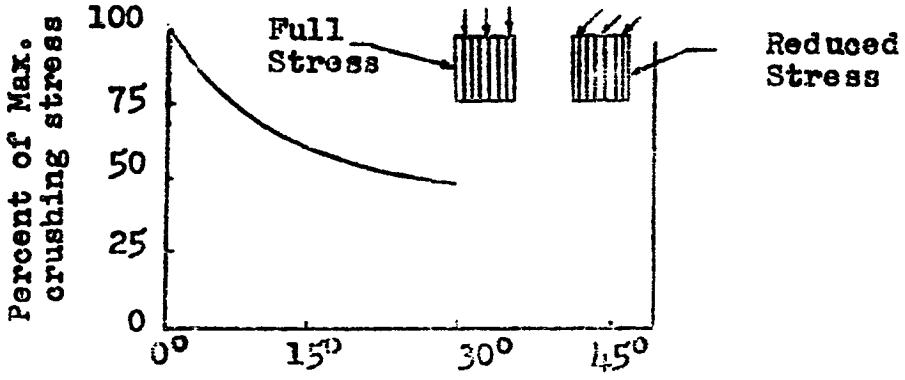

Variation of Stress with Angle of Applied Load

NOTE: Curve obtained from Hexcel Corporation Technical Publication TSB-116.

9.1.2 Paper Honeycomb

Paper honeycomb having hexagonal cells has been satisfactorily used as an energy absorber on many air cargo drops. This material is available in varying cell sizes (1/2" - 2") and thicknesses of .006" - .01". Paper honeycomb crushed parallel to the cell axis results in a force versus stroke curve similar to the curve discussed under aluminum honeycomb.

Paper honeycomb may be deployed in any of the methods suggested in the section on aluminum honeycomb. This material may be packed and expanded prior to impact. Considerably less force is required to expand paper honeycomb as compared to aluminum honeycomb. Paperboard honeycomb has the same disadvantage as aluminum honeycomb in that its energy absorbing capability is directional sensitive. However, it has the advantages mentioned under aluminum honeycomb in that it is non-magnetic and produces no out-gassing.

9.2 CRUSHABLE FOAMS

9.2.1 Styrofoam

Crushing styrofoam is an effective way to absorb energy. Styrofoam is a light-weight cellular structure which is available in various densities and chemical properties. This material could be used in a manner similar to the honeycombs discussed previously. Styrofoam is considered to be approximately 70% efficient as compared to an ideal decelerator. Styrofoam has the distinct

advantage that it can take compressive loading equally well in any direction. It is non-magnetic and produces no out-gassing.

9.2.2 Quick Setting Plastic Foams (Lockfoam)

Foamed plastic is a light-weight, highly expanded, cellular structure produced by combining liquid resin with an accelerator or foaming agent. A wide range of foam density and rigidity may be produced by the various combinations of resins and accelerators, thus allowing the production of foams of different crushing strengths and energy absorbing capabilities.

The chief advantage of this material is that it can be foamed in place, and thus, it could be stored as a liquid to conserve space until just prior to touch down. For lunar spacecraft application, the material would have to be foamed in place in a bag shaped to the proper configuration due to lack of pressure on or near the moon. Successful deployment of lockfoam depends on proper mixing, temperature control and curing time (minimum 5-10 minutes). The latter two conditions may prove difficult to achieve in a lunar vehicle landing system.

9.3 PNEUMATIC BAGS

Pneumatic impact bags have been successfully employed as energy absorbers applied to recovery of target drones, missiles, and in air drop of heavy cargo. Development is in progress on inflatable bags for cushioning the landing of emergency escape capsules and space vehicles returned from orbit. These bags are normally

fabricated of rubber coated nylon fabric or equivalent material in a range of shapes and sizes depending on the application. Bags are placed beneath the load in an arrangement to provide effective absorption of vertical descent energy, and to counter adverse landing conditions which may induce toppling. In the above applications, the bags are folded and tightly packed in a compartment within the vehicle. They are normally deployed and inflated during final parachute descent just prior to impact. The inflation pressure of the bag may range from zero to 15 psi above ambient depending on a number of design conditions including the method used to inflate the maximum allowable load factor and the maximum permissible bearing stress between bag and vehicle. Bags are equipped with exhaust orifices which are sealed by burst diaphragms designed to rupture at a preselected pressure level above the initial inflation pressure.

During impact the bag compresses under the load, raising the pressure in the bag to the rupture point of the diaphragms. Although after rupture the gas exhausts at a high rate through the orifices, the pressure will continue to rise then level off before dropping rapidly as the vehicle's downward velocity is overcome. The force with which the bag resists the downward force of the load is the product of the bag internal pressure and the bag footprint or

bearing area on the ground. A typical force versus stroke curve is shown below.

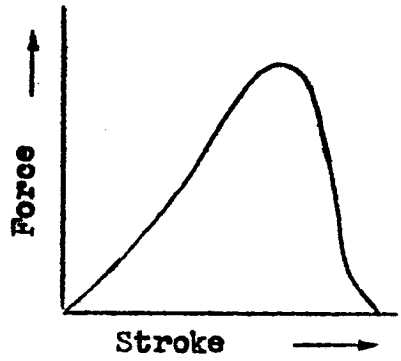

A pneumatic bag of the type described above acts as a non-linear spring during the first portion of the stroke and as a viscous damper during the remaining stroke. Bag efficiency has been improved by the use of variable orifices which level the pressure curve slightly by retarding the escape of air over the latter part of the stroke.

The above principles could apply to the use of pneumatic bags in a planet landing system. A principal difference in the bag would be the use of a smaller orifice and burst diaphragm designed to provide the same pressure versus stroke profile. The same initial inflation (differential above ambient) pressure will require a reduced weight of gas and therefore a reduced size and weight of gas storage vessel. The bag size, weight and packed volume would remain unchanged for stress and bag action considerations alone.

Pneumatic bags may be applied in much the same way as other decelerator structures in accordance with the requirements dictated by the dynamics of landing. A principal difference which must be considered is the lack of shear resistance in the flexible bag structure at low pressure. With proper design this characteristic may be turned into an advantage rather than a disadvantage.

Stowability and ease of deployment are characteristics of the pneumatic bag which make it competitive with other cushion type energy absorbers. The usual flight configuration will involve a weight penalty in providing space for an expanded landing cushion whereas the pneumatic bag occupies a minimum of space and housing structure. The flexible fabric may also be stowed in odd shaped cavities which may otherwise be wasted space within the vehicle.

9.4 CYLINDERS

9.4.1 Pneymatic Cylinders

Pneumatic cylinders, similar to aircraft actuating cylinders, might also be utilized to absorb energy during the landing of a lunar spacecraft. A cylinder of this type would be used in conjunction with a strut landing system. A pneumatic cylinder vented to the atmosphere would be mounted in each strut. This arrangement would permit the deployment of the landing system by pressurizing the cylinders to some nominal pressure.

A typical force versus stroke curve for a pneumatic cylinder, equipped with a variable orifice, is shown below:

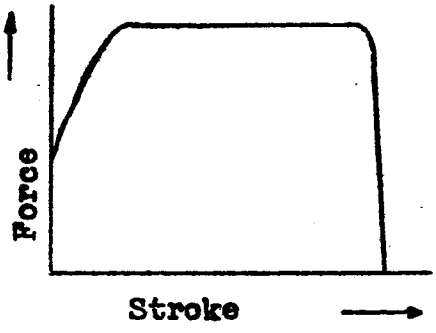

Upon impact the pressure in the cylinder is permitted to increase to some predetermined value resulting in the rupturing of a diaphragm.

This permits the gas in the cylinder to vent into the lunar atmosphere so that the maximum allowable deceleration would not be exceeded and all energy would be absorbed prior to bottoming out. This system would permit the vehicle to remain level with the lunar surface following impact.

9.4.2 Hydraulic Cylinder

Hydraulic cylinders were also evaluated as possible energy absorbers on strut type landing system. These cylinders would be deployed in the same manner as the pneumatic cylinders discussed above. The only major difference between the two systems is that the hydraulic fluid would be bled into a reservoir

to prevent contamination of the lunar environment. This system would be somewhat heavier than the pneumatic type due to the additional weight of the hydraulic fluid and reservoir.

9.4.3 Oleo-Struts

Aircraft type oleo-struts were also considered as a possible method for absorbing shock in this study for soft landing a lunar vehicle. Oleos would be employed in a manner similar to that of pneumatic and hydraulic cylinders discussed previously.

Considerable snubbing would be required to reduce rebound to an allowable value. The oleo-strut would be somewhat heavier than some of the crushing materials discussed previously. This system would, however, assure that the vehicle would be level with the lunar surface after impact.

9.4.4 Liquid Springs

Liquid springs, which have been used extensively on European aircraft to absorb shock, are another device which might be utilized to soft land a lunar spacecraft. This mechanism is relatively simple and consequently very reliable. It is a self-contained unit and requires no supporting hardware. Two major objections to using this type of an energy absorber on a lunar vehicle is that rebound is high and fluid temperature is considered critical.

Silicone oil, which is compressible up to approximately 18% at 50,000 psi, is used to fill the cylinder on both sides of the piston at an initial pressure of 500 - 750 psi. Springing is accomplished by forcing the piston rod into the cylinder, reducing the fluid volume thereby compressing the liquid. Energy is dissipated during the compression stroke by transferring fluid to the opposite side of the piston through the central spring loaded valve and small orifice in the piston. On the recoil stroke, the spring loaded valve closes restricting flow to the small open orifice, thus damping the outward movement of the piston rod.

9.4.5 Crushable Metal Tubes

Crushing of thin walled stainless steel tubes in a cylinder is another technique which has proven to be an effective means of absorbing energy. This is accomplished by the crimping of the tube using a mandrel guided by the inside diameter of the uncrushed portion of the tube. Pre-crimping is required to achieve an acceptable initial crushing stress. A device of this type would also be deployed in a strut landing system described in previous sections.

9.5 MISCELLANEOUS DEVICES

9.5.1 Balsa Wood

Crushing balsa wood in a direction parallel to the fibers provides an efficient way of dissipating energy. Balsa wood is approximately three times as efficient as 3/16" - .001" aluminum honeycomb for absorbing energy on a pound per pound basis.

Selection of balsa wood having a density of 6 - 8 lbs/cu. ft. is recommended to assure an acceptable uniform crushing stress. Balsa wood crushes very much as do paper and aluminum honeycomb as shown by the load vs. stroke curve below.

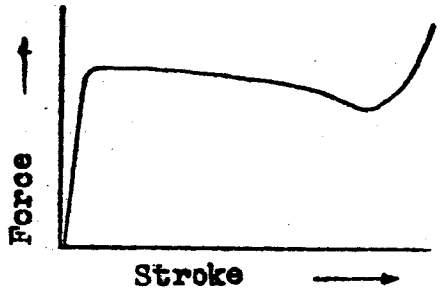

Balsa wood has a high crushing stress (1500 psi). For this reason, it would probably have to be deployed in a cylinder similar to one shown in the section on aluminum honeycomb. The crushing stress of aluminum honeycomb can be increased by placing balsa wood into the honeycomb cells.

9.5.2 Plastic Bending Struts

Outrigger arms (struts) designed for the efficient utilization of energy absorbing capabilities in plastic bending are low cost, non-deteriorating, predictable shock absorbing media. They constitute a desirable feature capable of satisfying both energy absorption and anti-toppling requirements.

On the negative side, struts which take a permanent set are apt to leave a vehicle inclined at some angle to the surfaces on which it has landed. This would probably be the case if the

vehicle lands on one leg (velocity vector inclined at some angle to the lunar surface). If considerable horizontal velocity is present, the struts may tend to dig into the surface and give rise to high side loads. To prevent this, some sort of feet would be needed. These feet could be made of additional energy absorbing material if so desired.

9.5.3 Ground Penetration Spike

A ground penetrating nose spike has been used successfully with recoverable air vehicles to absorb landing shock. Its simplicity and anti-toppling characteristics are particularly attractive, although structural considerations of landing with a horizontal velocity sometimes result in a substantial weight penalty. The kinetic energy of the descending load is absorbed by the surface through friction, displacement, and compression during spike penetration.

A major disadvantage of the spike decelerator is its inadequacy when used over terrains which may include rocks or hard surfaces. For this reasons the spike was eliminated from consideration as an energy absorber for a lunar landing system.

9.5.4 Multiple Arm Decelerators Employing Various Energy Absorbing Mechanisms

Another method of absorbing landing shock is to extend a series of arms to an outboard position. This will allow the feet to touch the ground and effect the cantilevered arms a sufficient distance, under a resistance load, to bring the system to rest before the platform touches the ground. The arms would be designed to work independently or in pairs with sufficient resistance in bending from both vertical and lateral forces to transmit the ground engaging forces to a suitable energy absorbing mechanism. The above system is similar in most respects to conventional, simple, levered landing gear linkages used by aircraft where the energy absorbing mechanism is hydraulic, pneumatic, or helical spring shock absorber.

A multiple-arm decelerator system could be adapted to a lunar landing vehicle. Deceleration may be accomplished by using a liquid spring, drawing wire through a die, or extruding metal through a die. The energy-absorbing device would be connected to and actuated by the arms. Adaptation to the vehicle includes provisions for strong support structure for each arm hinge and a bearing pad. In a liquid spring application, the shock absorber would mount close to the arm hinge.

In a drawn-wire system, a metal rod would be inserted through a reducing die and attached to an outrigger arm to produce a tensior

load on the rod. At ground contact the arms are forced upward, drawing the wires or rods through the dies and absorbing energy by reducing the size of the rods. Experience with wire-drawing techniques indicated that although the wire-drawing system would be light, simple, and inexpensive, control of the rod diameter, rod surface die size, and die finish are critical. Minor oxidation on the surface of the rod or on the drawing surface of the die, and variations in rod diameter and die size greatly affect the rate of drawing and energy absorbed, thereby making it difficult to control deceleration and overturning tendencies.

The extruded metal system is the reverse of the wire-drawing system. This system has approximately the same advantages and disadvantages as the wire drawing system. In addition, in the event of sticking, a sudden destabilization moment may be induced.

9.6 SUMMARY OF ENERGY ABSORBERS

A summary of the physical properties of the energy absorbers is presented in Table 9-1 below. No attempt was made to present all parameters studied, but only those related to the application on a planetary soft landing system. Most of the decelerator devices were considered from the standpoint of deploying same on a strut type landing system. Evaluation of these decelerators is presented in the following paragraph.

It is generally agreed that the majority of the absorbers studied could be designed to function satisfactorily in a space environment provided the proper environmental control normally required for space hardware was used.

9.7 PARAMETRIC STUDY

Evaluation of the energy absorbers discussed in previous paragraphs was accomplished by relating the parameters such as: crushing stress, energy absorbed per weight and volume of absorber, rebound, temperature limitation and cost. Parametric data for this study was obtained from miscellaneous reports on energy absorber studies conducted by government agencies, universities, private corporations and Radioplane's experience on landing bags, WADD project project on Decelerator Studies - Contract No. AF-33(616)-6875, materials, etc. Additional data was obtained from dynamic tests conducted by Radioplane on aluminum honeycomb, balsa wood and aluminum honeycomb filled with lockfoam and balsa wood. Description and results of this program are presented in Reference 17.

9.7.1 Ideal Decelerator

A description and definition of an ideal decelerator system must be understood to evaluate actual decelerator hardware. A decelerator must provide a force in the opposite direction to the velocity until the mementum of a rigid body is reduced to zero. Depending on the fragility of the object, the deceleration system must also control the magnitude of the applied force during deceleration. This system must have sufficient time to complete the deceleration before the load bears on the ground.

SUMMARY OF PHYSICAL PROPERTIES OF ENERGY ABSORBERS

TABLE 9-1

PROPERTY	Al Honey-comb	Paper Honey-comb	Styro-foam	Lock Foam	Pneu. Bag	Pneu. Cyl.	Hyd.Cyl Oleo & Liq Spr	Balsa Wood	Spike	Extruding Metal
Material Thickness	.0007" .003"	.0086"	—	—	.0017" .018"	—	—	—	—	—
Cell Size	1/8"-3/8"	1/2" - 2"	—	—	—	—	—	—	—	—
Material	3003 & 5052 Al	Impreg-nated Paper	Foamed Poly-styrene	Foamed Poly-urethane	Rubber coated nylon	Alum.	Alum	Wood Fiber	Alum.	Steel or Al.
Expanded Density (#/ft^3)	2.3 - 4.5	2.6	1.8 - 4.5	2-10	—	—	—	6-8	—	—
Packed Density (#/ft^3)	147	40	—	63	15.6	—	—	—	—	—
Operating Pressure (PSI)	None	None	None	5-10	2-15	500-3000	200-3000 Hyd 50,000 Liq Spr	None	None	None
Stowable (at less than operating size)	Yes	Yes	No	Yes	Yes	No	No	No	No	Yes
System of Employment	Impacting Cushion or cylinder			Pads or	Cushion	Strut	Strut	Cylinder	Fixed	Exter-nal
Effect of Impact on Planetary Surface	None	None	None	None	Subject to Puncture	None	None	None	No Penitra-tion	None
Space Environment (Press., Temp., Meteorites)	None	None	None	None	Puncture	Leakage	Leakage	None	None	None
Vehicle Attitude After Impact	Inclined	Inclined	Incl.	Incl.	Level	Level	Level	Incl.		Incl.

The "ideal" decelerator is defined as one which will absorb the kinetic energy of a mass at a constant maximum allowable force. The amount of energy that can be dissipated by the decelerator is given by the area under the force-stroke curve. The ideal decelerator force-stroke curve is shown below.

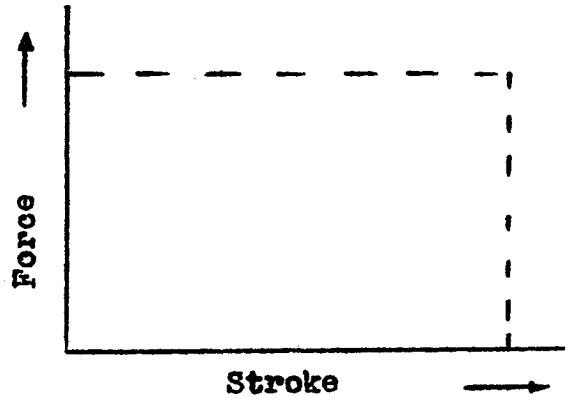

In the ideal curve the force rises immediately to its maximum allowable value and remains constant. This results in a constant deceleration until all of the enegy has been absorbed. The force then falls immediately to zero without decrease in strain (no rebound). The ideal deceleration should be capable of absorbing shock in any direction of impact on all types of terrain.

The most efficient decelerator is defined as one which has the minimum stroke without exceeding the maximum load allowed. The efficiency of any decelerator system is defined as the ratio of the area under the force versus stroke curve to the area under the force versus stroke curve of an ideal decelerator.

Reference sample case below:

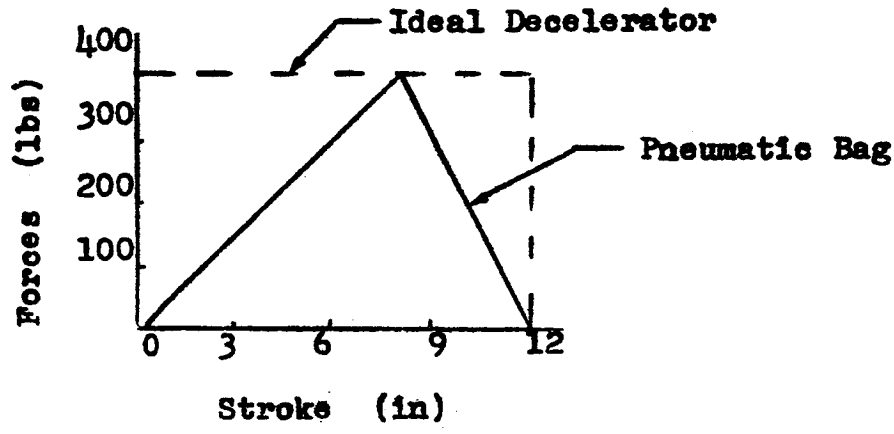

Area under pneumatic bag = 2400 in lbs.

Area under Ideal Decel. = 4800 in lbs.

Efficiency of pneumatic bag = $\frac{2400}{4800}$ = .50

The efficiencies of five representative absorbers are compared to an ideal decelerator in Figure 9-1 . The efficiencies noted are based on the load being applied parallel to the cell axis of the honeycombs and the grain of the balsa wood. It should be pointed out that these efficiencies are computed for the load versus stroke curve shown. Any deviation from these curves will change the efficiencies accordingly.

EFFICIENCY OF VARIOUS ENERGY ABSORBING MATERIALS
COMPARED TO AN IDEAL DECELERATOR

FIGURE 9-1

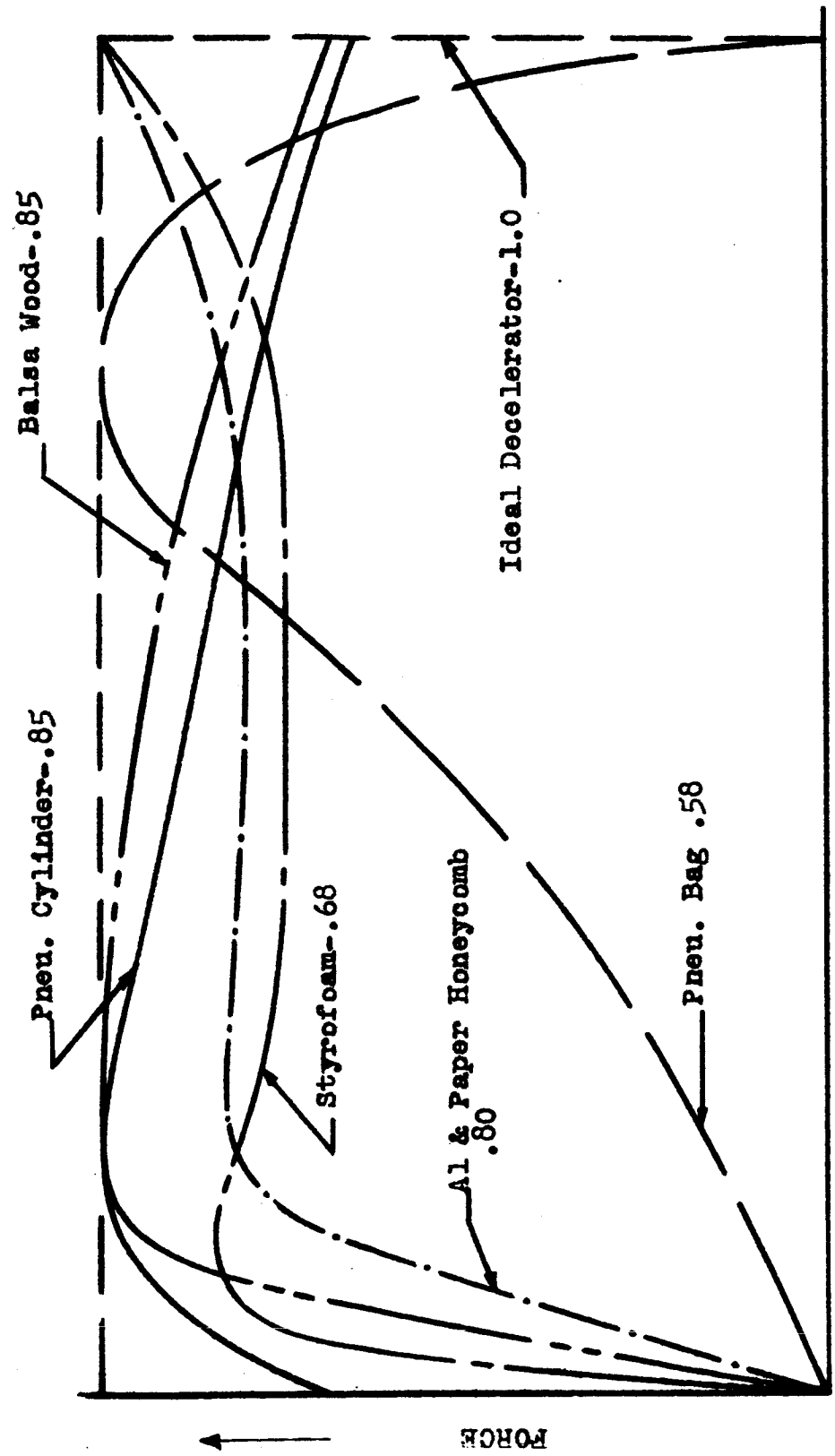

NOTE: Efficiencies based on load being applied parallel to cell axis of Honeycomb and Balsa Wood

9.7.2 Performance

9.7.2.1 Dynamic Crushing Stress

The average crushing stress of the typical energy absorbers studied are presented in Figure 9.2 . This graph is divided into two sections: (1) material having relatively low crushing stress which could be deployed as feet on a landing strut and, (2) materials having high crushing stress which can only be crushed in mechanism such as a cylinder.

It should be pointed out that initial crushing stress of uncrimped honeycomb will approach twice that of the average crushing stress, as discussed in the previous section on aluminum honeycomb.

The average crushing stress of honeycombs remains relatively constant over a range of impact velocities of 10 - 50 ft/sec. All stress values given on Figure 6 are for load applied parallel to the honeycomb cell axis and balsa wood grain. Reduced crushing stress will be experienced if load is applied at an angle of less than 90° to the cell axis.

9.7.2.2 Energy Absorbed Per Unit Weight

The energy absorbed per pound is presented in Figure 9.3. The words, energy absorber, are intended to include the absorbing material and the cylinder in which they are deployed, but not the complete landing system. For example, in a landing system employing pneumatic cylinders, the weight of the cylinders is considered, but

DYNAMIC CRUSHING STRESS OF VARIOUS MATERIALS

FIGURE 9-2

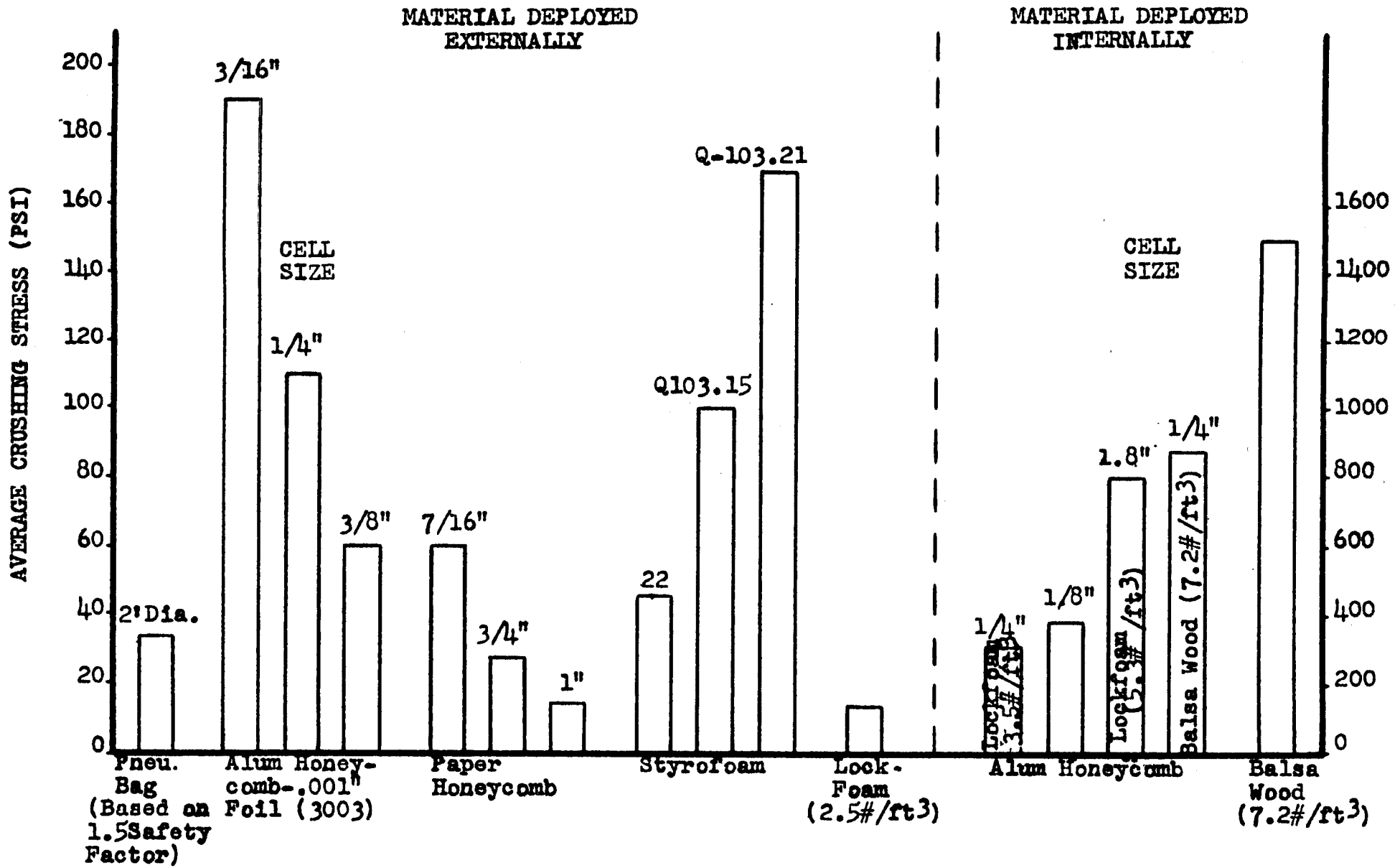

ENERGY ABSORBED PER POUND OF VARIOUS MATERIALS
(DYNAMIC CRUSHING)

FIGURE 9-3

NOTES:

1. Lockfoam ($3.5\#/Ft^3$) Filled
2. Lockfoam ($5.3\#/Ft^3$) Filled
3. Balsa Wood ($7.2\#/Ft^3$) Filled

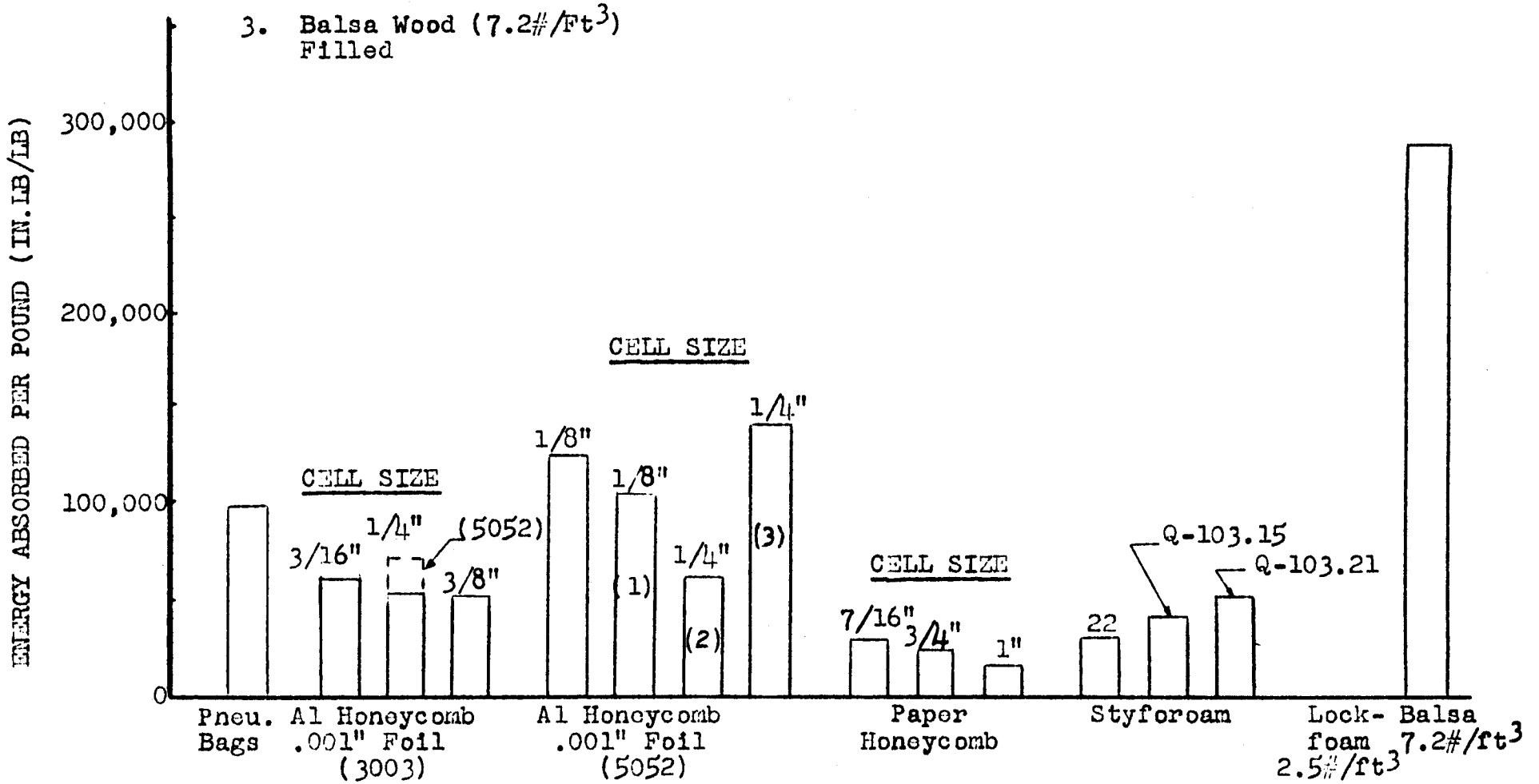

not the weight of the struts, which contain the cylinders. In the case of the pneumatic bag, the inflation equipment and the deployment hardware are included in this analysis.

The material crushed in cylinder may only weigh 10 - 20 percent of the cylinder weight. Even though the material may be quite efficient in energy absorbed per pound, this additional cylinder weight may more than off-set the use of a high energy material.

9.7.2.3 Energy Absorbed Per Unit Weight of Material Crushed in A Cylinder

The energy absorbed per pound of cylinder containing various crushable materials is presented in Figure 9-4. As the title implies, both the weight of the energy absorbing materials and the weight of the cylinders in which they are employed were considered. Any additional hardware required to deploy the decelerators is not considered in this graph.

9.7.2.4 Energy Absorbed Per Unit Expanded Volume

The energy absorbed per unit volume of expanded material is presented in Figure 9-5 . This graph is divided into two sections: (1) material having a relatively low energy absorbing capability per unit volume which could be deployed as cushions on a landing strut, and (2) materials having high energy absorption per unit volume which must be confined in a cylinder. In the first section, the volume of the material is presented, but in the second section,

not the weight of the struts, which contain the cylinders. In the case of the pneumatic bag, the inflation equipment and the deployment hardware are included in this analysis.

The material crushed in cylinder may only weigh 10 - 20 percent of the cylinder weight. Even though the material may be quite efficient in energy absorbed per pound, this additional cylinder weight may more than off-set the use of a high energy material.

9.7.2.3 Energy Absorbed Per Unit Weight of Material Crushed in A Cylinder

The energy absorbed per pound of cylinder containing various crushable materials is presented in Figure 9-4. As the title implies, both the weight of the energy absorbing materials and the weight of the cylinders in which they are employed were considered. Any additional hardware required to deploy the decelerators is not considered in this graph.

9.7.2.4 Energy Absorbed Per Unit Expanded Volume

The energy absorbed per unit volume of expanded material is presented in Figure 9-5 . This graph is divided into two sections: (1) material having a relatively low energy absorbing capability per unit volume which could be deployed as cushions on a landing strut, and (2) materials having high energy absorption per unit volume which must be confined in a cylinder. In the first section, the volume of the material is presented, but in the second section,

ENERGY (IN-LB) PER LB OF CYLINDER
CONTAINING VARIOUS CRUSHABLE MATERIALS

FIGURE 9-4

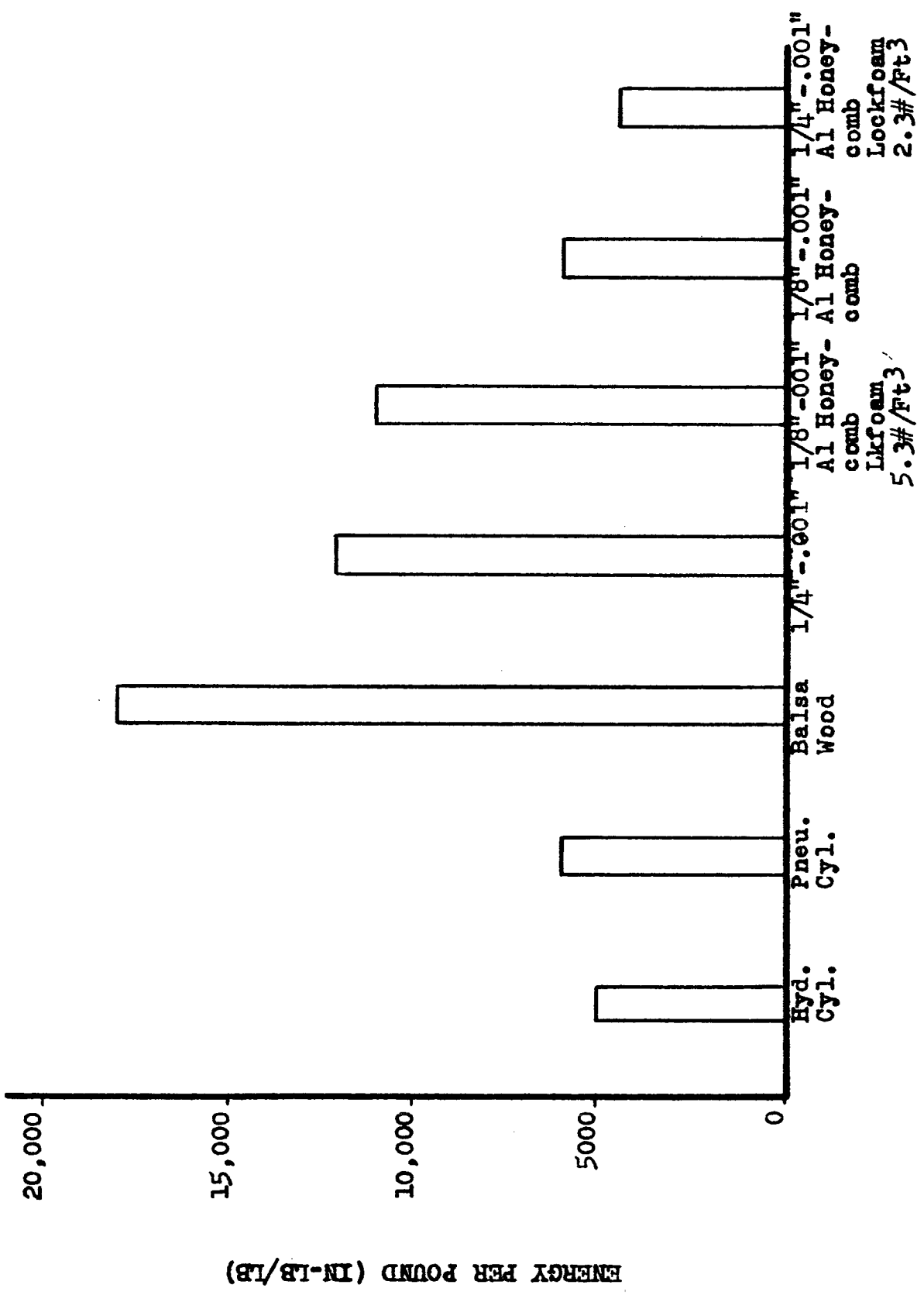

ENERGY ABSORBED PER CU. IN. OF VARIOUS EXPANDED MATERIALS

(DYNAMIC CRUSHING)

FIGURE 9-5

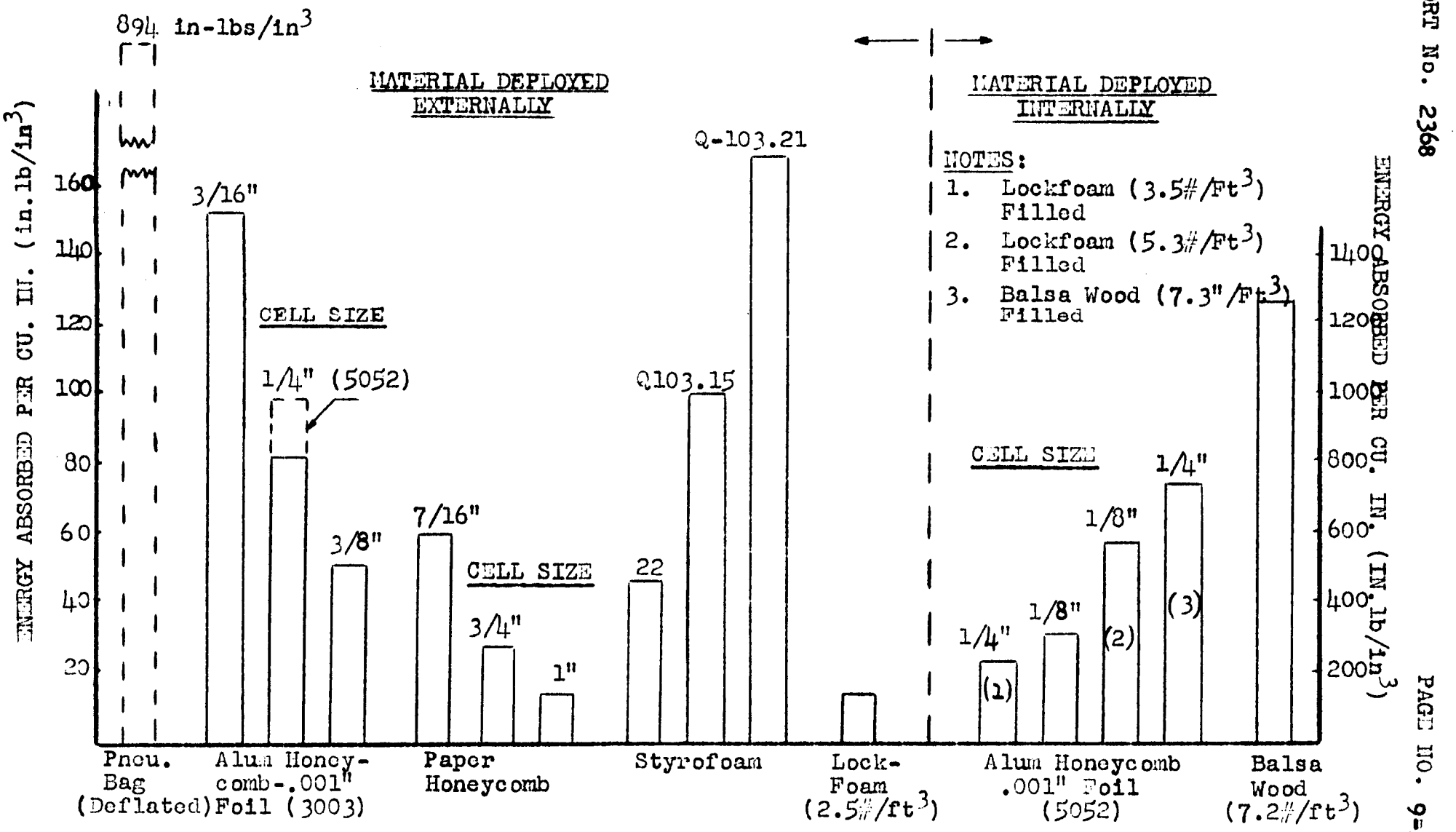

ENERGY ABSORBED PER CU. IN. OF VARIOUS PACKED MATERIALS

(DYNAMIC CRUSHING)

FIGURE 9-6

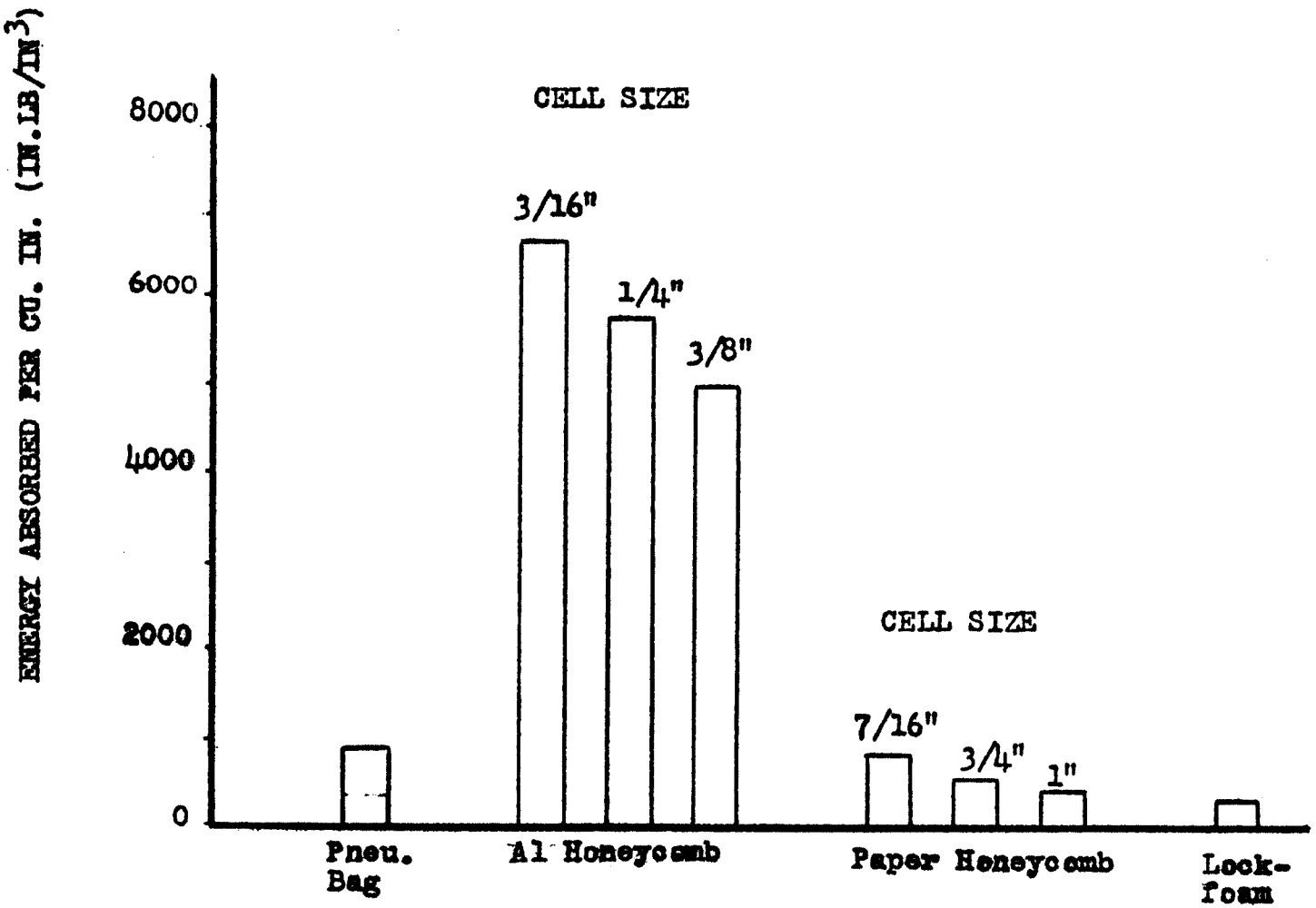

DYNAMIC REBOUND IN PERCENT OF STROKE OF VARIOUS MATERIALS

FIGURE 9-7

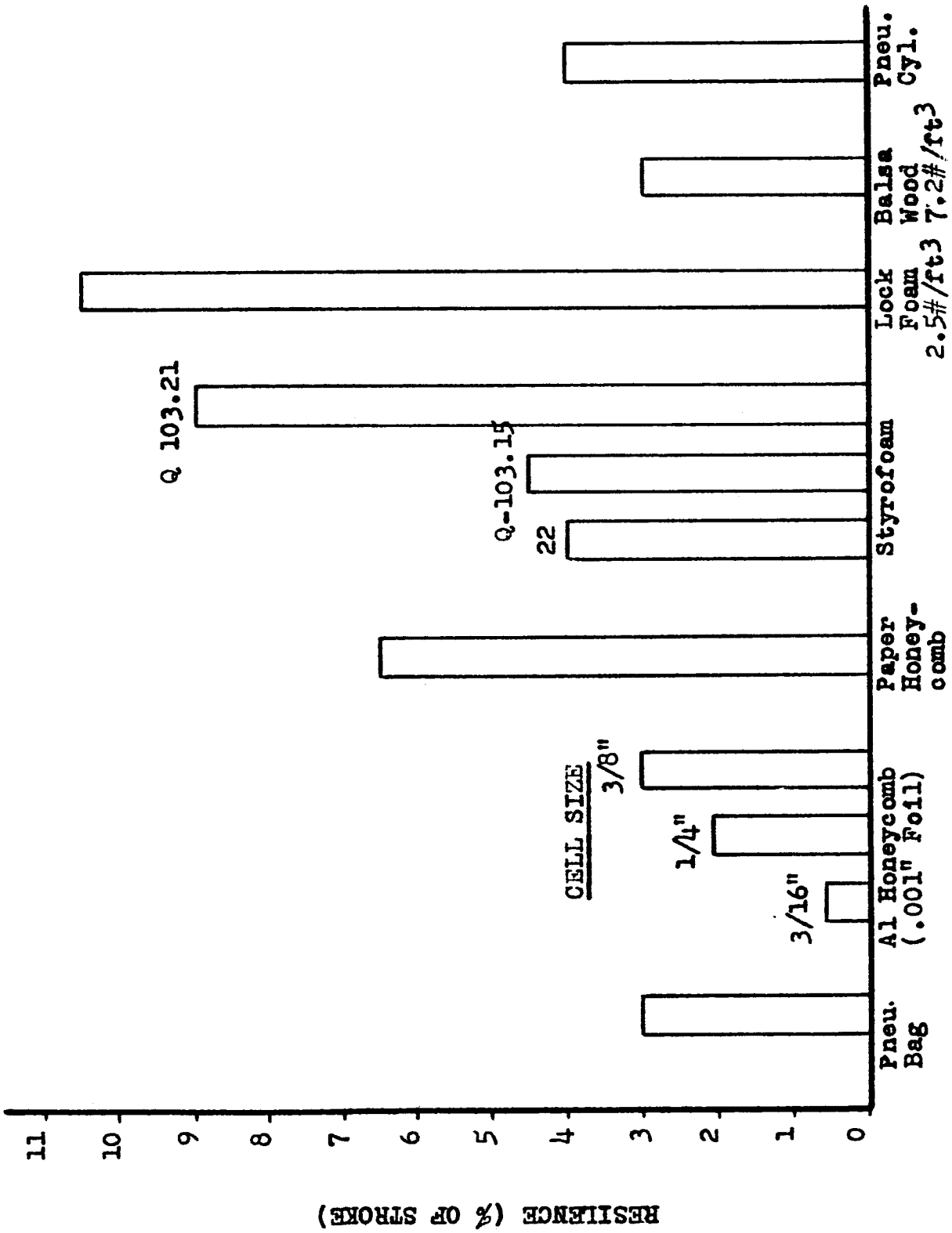

TEMPERATURE LIMITATIONS OF VARIOUS MATERIALS

FIGURE 9-8

presented in Figure 9-9. These costs are based on estimated limited production of these decelerators and do not include any research and development costs.

9.9 VEHICLE WEIGHT AND VOLUME

Figure 9-10, 9-11 & 9-13 present the weight, the packed volume, and the expanded volume respectively of energy absorbing materials vs. a range of vehicle weights. The following assumptions were made:

(1) Impact Velocity

A. Vertical - 20 ft/sec.

B. Horizontal - 0 ft/sec.

(2) 1/8" - .001" Al. honeycomb deployed in a cylinder

(3) Weight and volume curves of materials crushed in a cylinder include only the weight and volume of the material and cylinder.

(4) 35% additional weight was added to the weight of materials. Aluminum and paper honeycombs were used as foot pads to account for the weight of the facing material and attachment hardware.

(5) 100% additional weight was added to the weight of pneumatic bags to account for the inflation hardware and stowage container.

COST OF VARIOUS MATERIALS
(DOLLARS/FT-LB OF ENERGY)

FIGURE 9-9

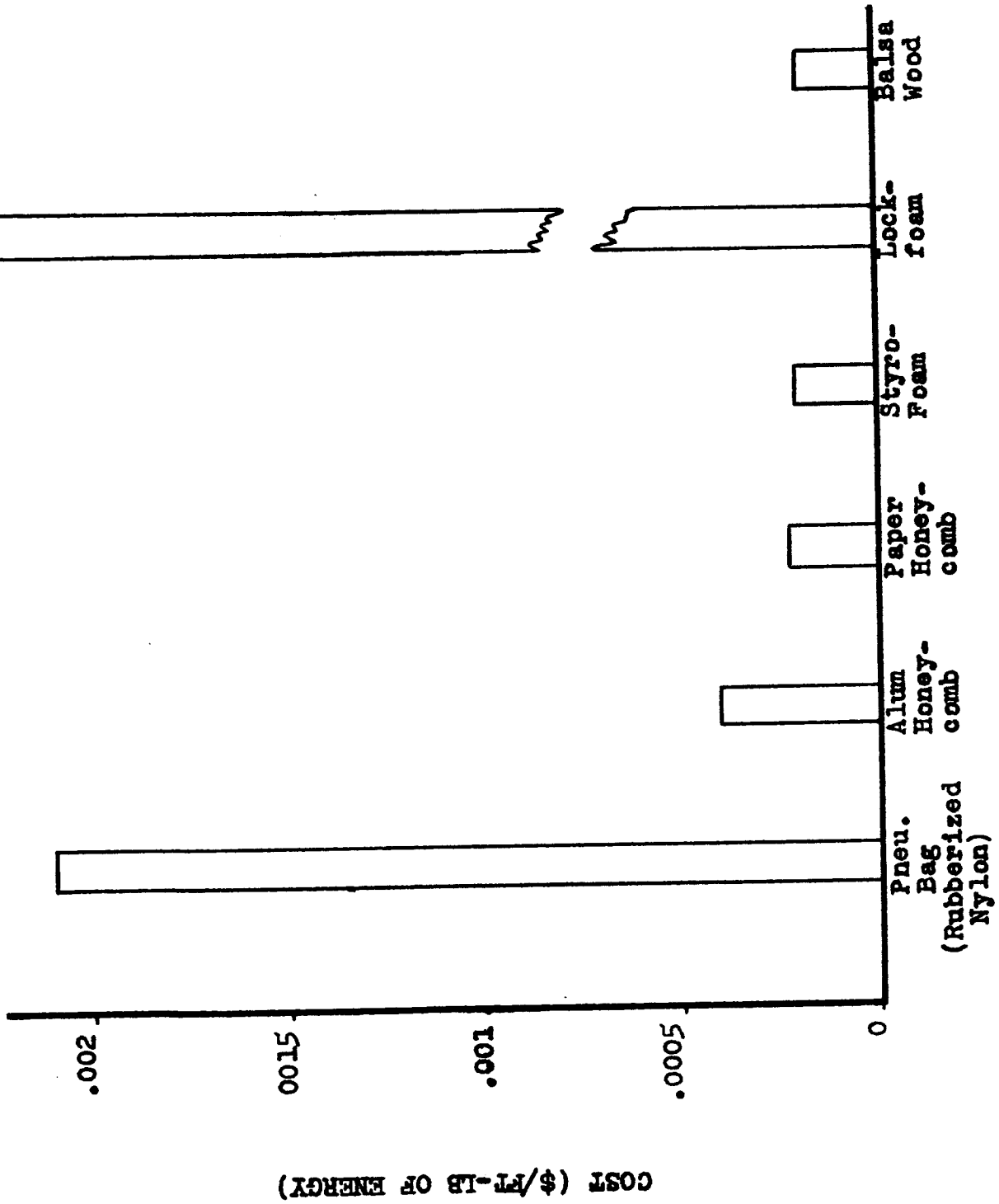

WEIGHT OF ENERGY ABSORBER MATERIALS VS RANGE OF VEHICLE WEIGHT
FIGURE 9-10

NOTE: 1. Impact Velocity
A. Vertical 20 ft/sec
B. Horizontal - 0
2. Material Weight does not include deployment devices
3. 1/8" Al. Honeycomb & Balsa Wood deployed in Cylinder

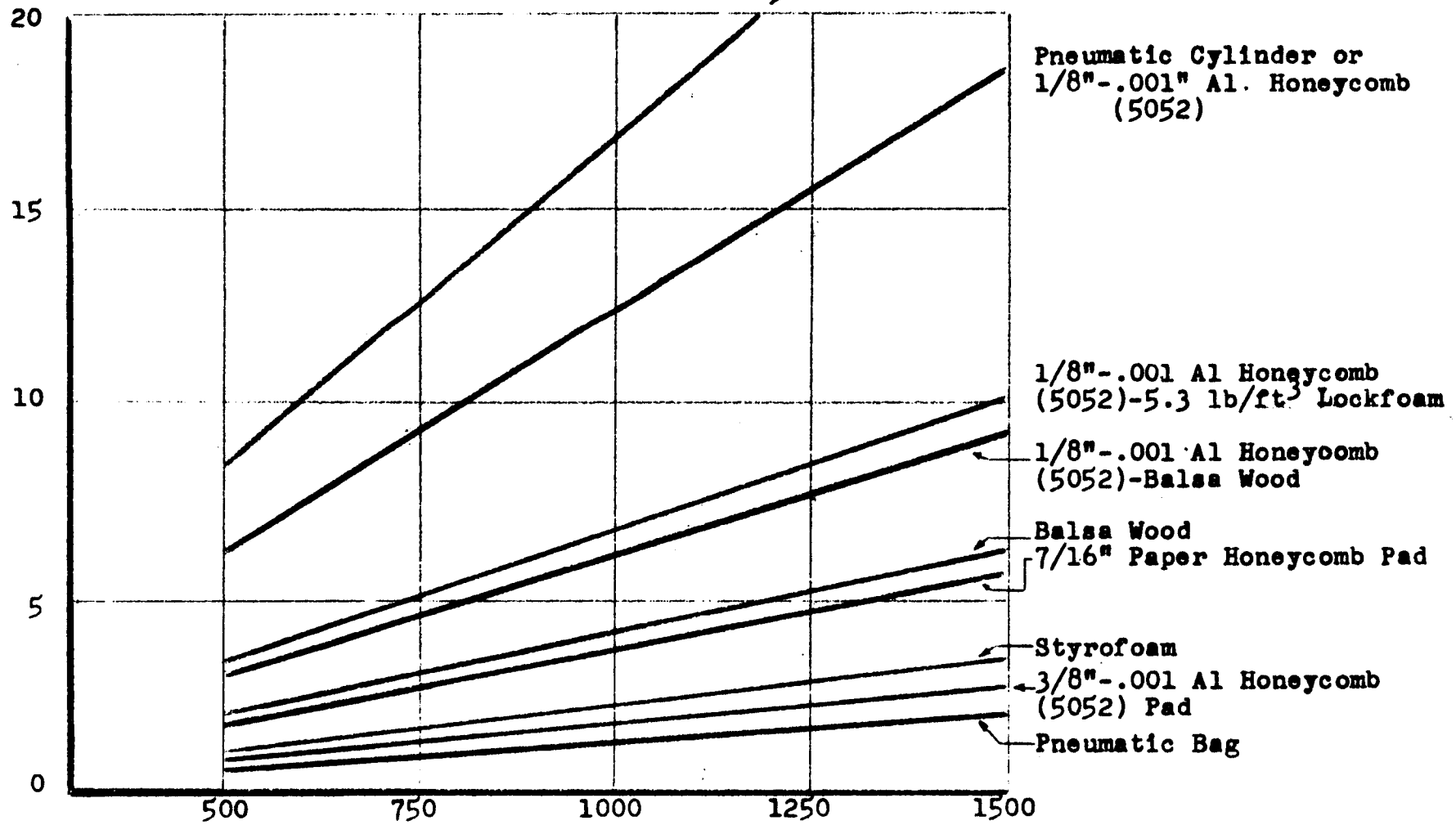

PACKED VOLUME OF ENERGY ABSORBER MATERIALS VS RANGE OF VEHICLE WEIGHTS

FIGURE 9-11

NOTE: 1. Impact Velocity
A. Vertical - 20 ft/sec
B. Horizontal - 0

2. Material does not include deployment devices such as struts

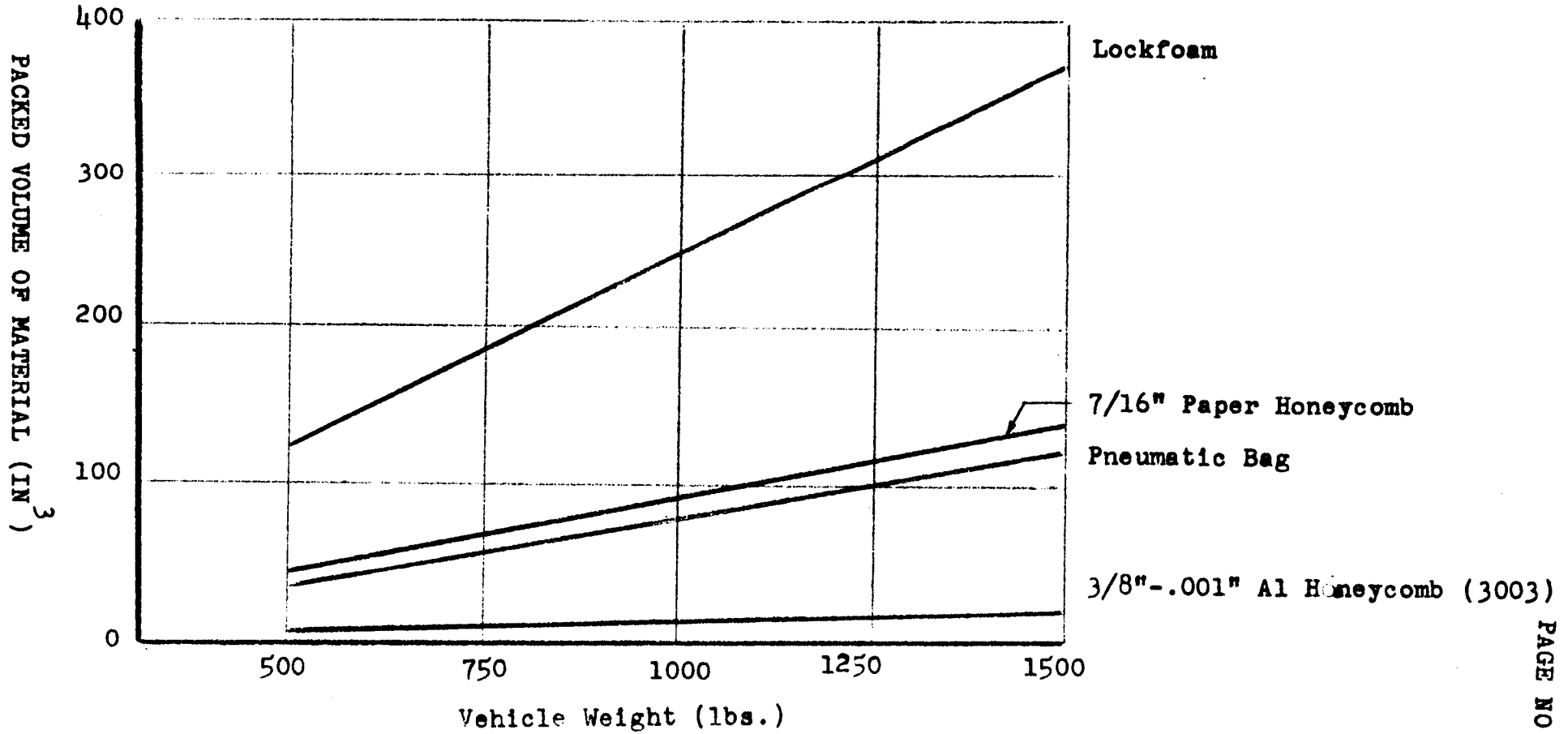

EXPANDED VOLUME OF ENERGY ABSORBER MATERIALS
VS RANGE OF VEHICLE WEIGHTS
FIGURE 9-12

NOTE: 1. Impact Velocity
A. Vertical-20 ft/sec
B. Horizontal - 0
2. Material Weight does not include deployment devices
3. 1/8" Al Honeycomb & Balsa Wood deployed in a Cylinder

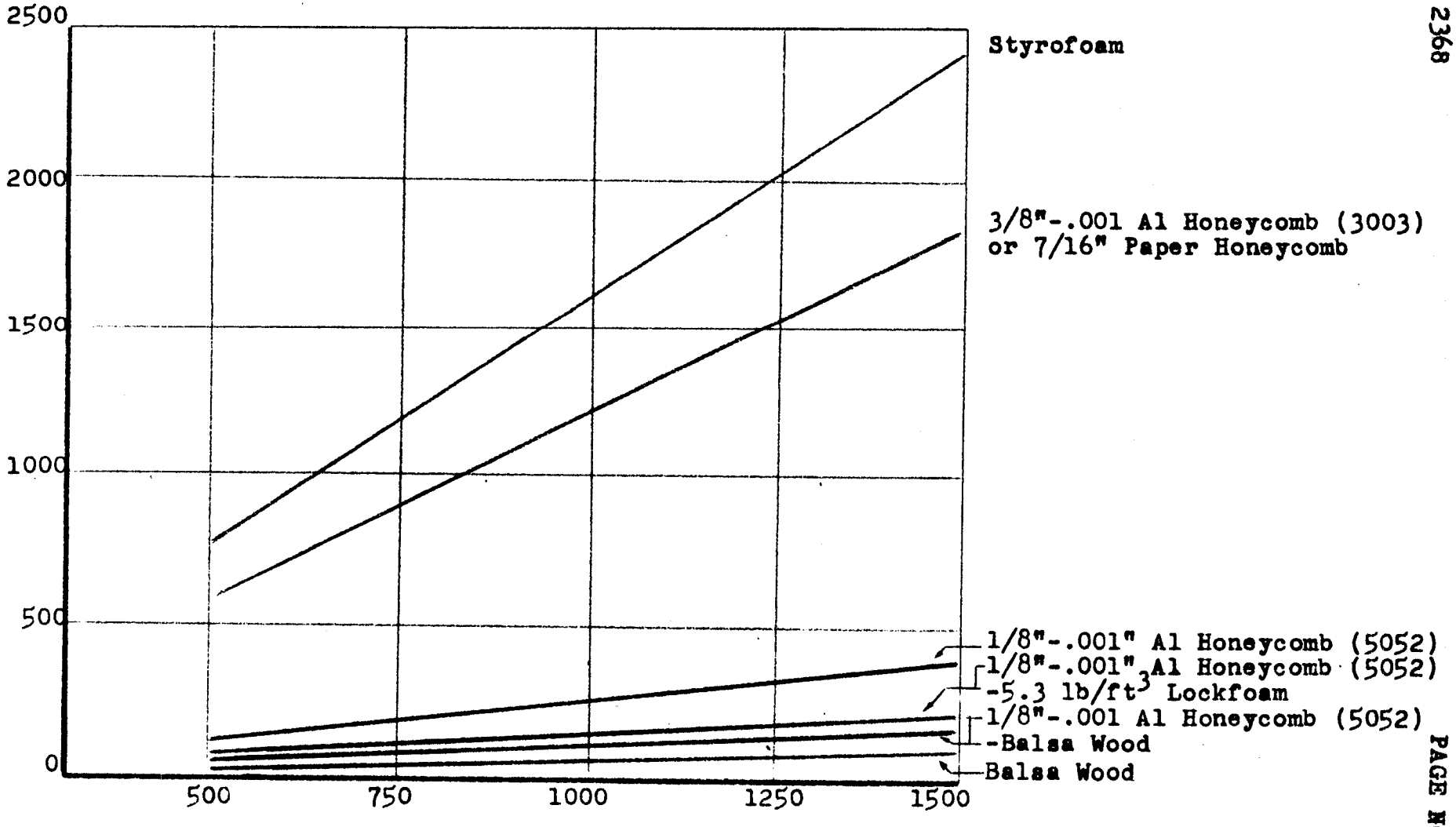

(6) 15% additional weight was added to the weight of the lockfoam for the storage container of the raw materials and the necessary hardware required to contain the foam.

(7) 25% additional volume was added to the volume of materials deployed in a cylinder to account for the volume of the cylinder.

9.10 EVALUATION

Energy absorbers discussed under Energy Absorbers were evaluated on the basis of deploying the absorbers on a spacecraft soft landing system. In order to determine the most feasible system the decelerators were evaluated on the basis of the following parameters presented in Figures 9-13 and 9-14. In some cases where little or no information was available, estimates were made in an attempt to evaluate or compare absorbers.

9.10.1 Overall Merit

(1) Average merit based on the following evaluation parameters; reliability, efficiency and weight, volume and cost per unit energy.

(2) Measure to determine relative comparison between operational decelerator systems applicable for a lunar vehicle.

Al Honeycomb
*Al Honeycomb
*Al Honeycomb-Lockfoam
*Al Honeycomb-Balsa
Paper Honeycomb
Pneu. Bags
*Balsa Wood
Styrofoam
Lockfoam
*Crush. Metal Tube
Plastic Bend. Strut
Pneu. Cylinder
Hyd. Cyl. Oleo Strut
Penetration Spike
Metal Extrusion

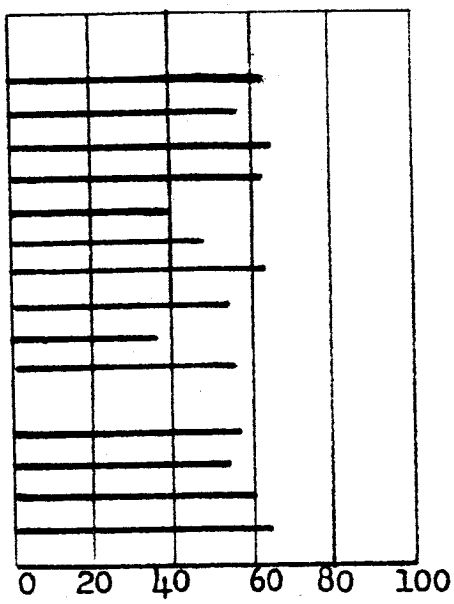

OVERALL MERIT

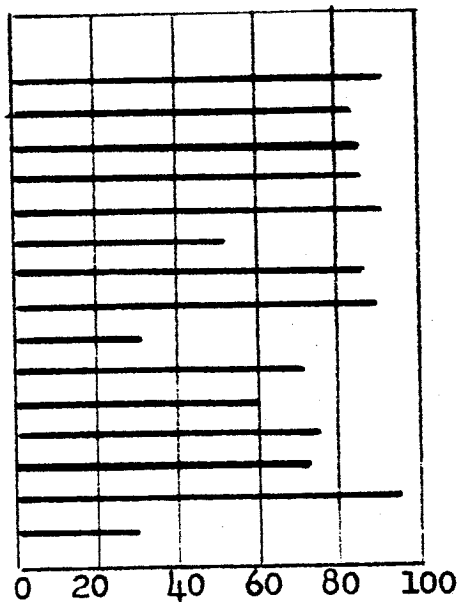

RELIABILITY

Al Honeycomb
*Al Honeycomb
*Al Honeycomb-Lockfoam
*Al Honeycomb-Balsa
Paper Honeycomb
Pneu. Bags
*Balsa Wood
Styrofoam
Lockfoam
*Crush. Metal Tube
Plastic Bend. Strut
Pneu. Cylinder
Hyd. Cyl. Oleo Strut
Penetration Spike
Metal Extrusion

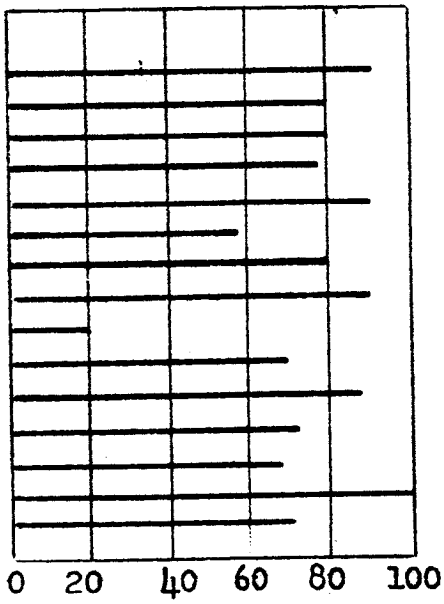

OPERATIONAL SIMPLICITY

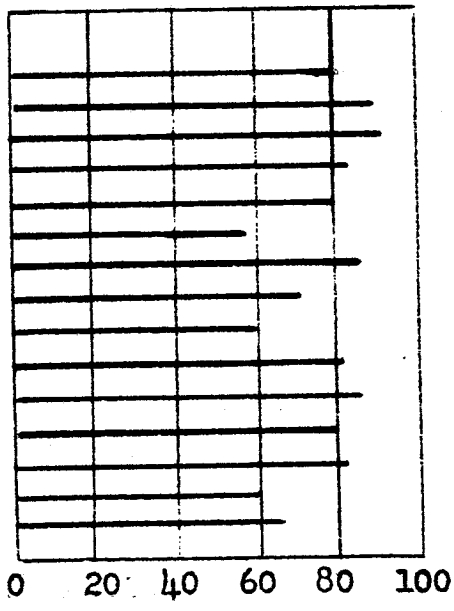

OPERATIONAL EFFICIENCY

* Crushed in a cylinder

EVALUATION OF ENERGY ABSORBERS

FIGURE 9-13

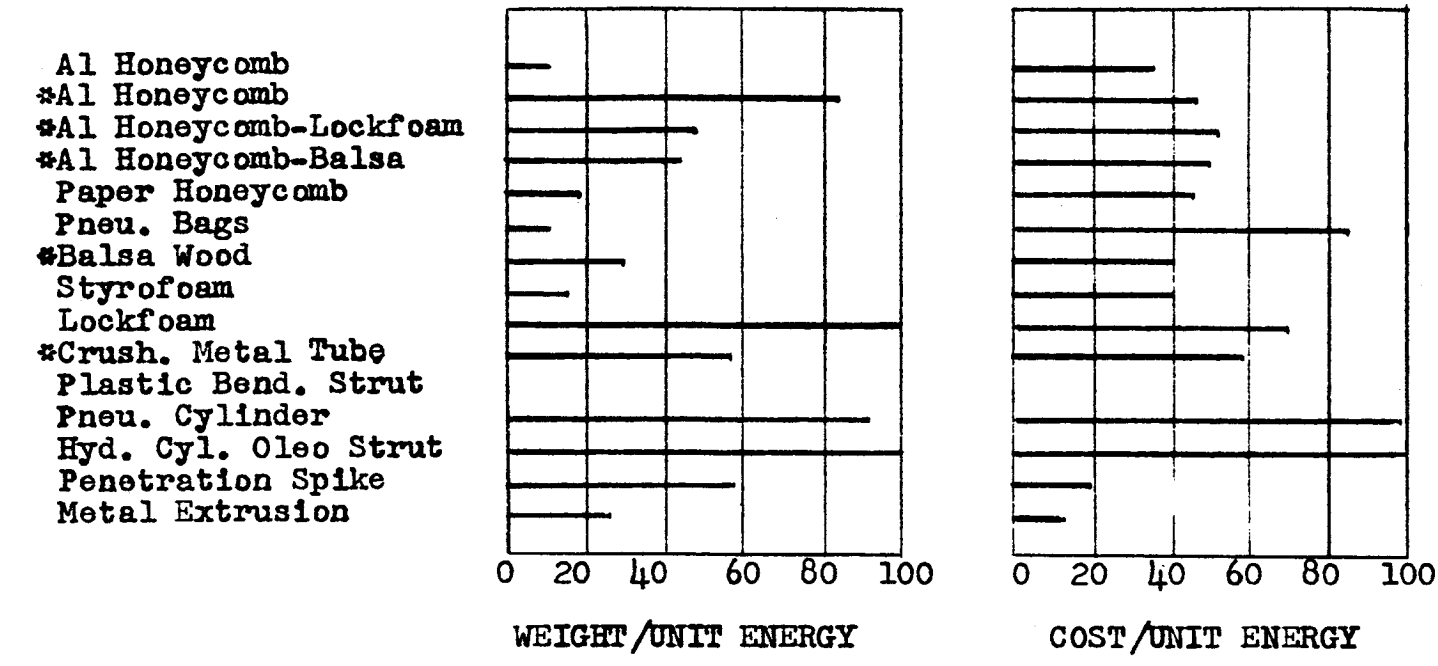

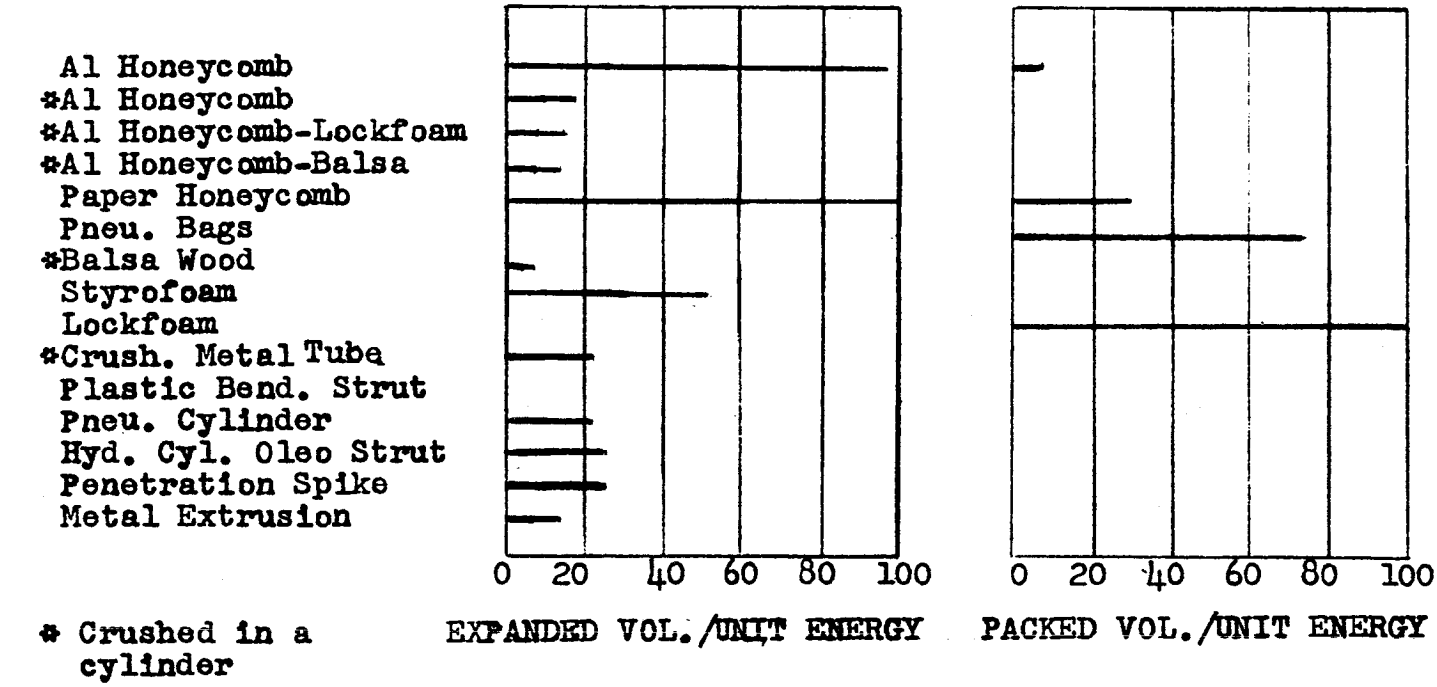

* Crushed in a cylinder

EVALUATION OF ENERGY ABSORBERS

FIGURE 9-14

9.10.2 Reliability

(1) Estimated reliability based on simplicity of system required to deploy decelerator and reliability of actual absorbers.

(2) Present state-of-the-art.

(3) Qualified per specification outlined in Section 2.3.

9.10.3 Operational Simplicity

(1) Number of parts

(2) Time required to deploy

(3) Complexity of attachment of landing system to vehicle structure

(4) Method of deployment

(5) Absorbers compared to spike which was considered to be the least complex of all absorbers.

9.10.4 Operational Efficiency

(1) Average efficiency for all possible impact conditions.

(2) Comparison with ideal decelerator (100%).

9.10.5 Weight/Unit Energy

(1) Weight of absorber

(2) Weight of cylinder if required to deploy absorber (Example: Balsa wood).

(7) Absorbers compared to paper honeycomb which requires the most storage space of all absorbers.

9.10.7 Packed Volume/Unit Energy

(1) Volume prior to expansion.

(2) 3/8" - 001" aluminum honeycomb.

(3) 3/4" and 1" paper honeycomb.

(4) Pneumatic bag.

(5) Lockfoam.

(6) Absorbers compared to Lockfoam which required largest stored volume of materials considered.

9.10.8 Cost/Unit Energy

(1) Limited production of hardware.

(2) No R&D costs.

(3) Cost of absorber.

(4) Cost of cylinder to deploy absorber.

(5) Cost of facing material and attachment hardware.

(6) Absorbers compared to hydraulic cylinder which was considered to be the most expensive of all absorbers.

The following conclusions were derived from the evaluation of the energy absorbers considered in this study program.

(1) Aluminum honeycomb in the larger cell sizes (1/4" and 3/8") should be given serious consideration when used as pads or feet on a strut for absorbing energy under all planetary and vehicle impact environmental conditions.

(2) Crushing of balsa wood or aluminum (1/8") honeycomb filled with either balsa wood or lockfoam in a cylinder also shows a definite promise as a good method for absorbing energy on impact of a spacecraft.

(3) Further investigations and studies in conjunction with a test program designed to evaluate both absorber materials and landing systems are certainly warranted.

9.11 EFFECT OF ENVIRONMENT ON IMPACT SYSTEM

The estimated Mars atmospheric and surface environment should have no detrimental effects on the impact systems discussed in the above sections. This conclusion is based on present day information on atmospheric temperature, composition and surface roughness on Mars.

Venus, however, apparently has a high surface temperature.

The surface of Venus is unknown due to the heavy cloud cover. It is quite possible, primarily due to extreme temperature effects, that some of the materials and devices discussed above will not be suitable for this program or that some environment control of the hardware may be required. Environmental control would, no doubt, also be needed to condition the landing system in space for proper functioning on landing.

SECTION 10

AEROTHERMODYNAMIC CONSIDERATIONS OF RE-ENTRY TO MARS AND VENUS

This Section discusses the considerations of entry into the atmosphere of Mars and Venus from the standpoint of velocity, deceleration, and dynamic heating. Both the ballistic and lifting re-entry cases are presented. The re-entry and recovery systems designed for spacecraft approaching Mars and Venus will have to be adapted to the aerothermodynamic conditions described in the paragraphs to follow.

The approach to Venus will be at the Venus escape velocity 34,100 feet/sec. Similarly, the approach to Mars will be at the Mars escape of 16,700 feet/sec. The Mariner vehicle, in a fly-by mission, will probably intend to pass Venus or Mars as closely as possible and the orbit could be such that the Mariner returns to the vicinity of the earth. The Voyager vehicle may be heavier than the Mariner, the additional payload weight available using the Saturn launcher could be used primarily for a retro-propulsion and terminal guidance system to put the Voyager into orbit around Venus and Mars. Retro-rockets are needed for braking from escape velocity to orbital velocity at Venus or Mars. Because of the relatively high velocity increment (7,000 - 15,000 ft/sec.) the retro-rockets must have high performance. When precise orbits are to be attained, the total rocket impulse will have to be controllable.

It is suggested that the Mariner could be designed to eject an instrumented capsule for atmospheric entry and possibly landing to obtain environmental data for the design of re-entry and landing systems of vehicles to follow. Data from the capsule could be relayed to the Mariner and stored for later transmission to the Earth. If technology permits, the data could be transmitted directly from the capsule to the Earth. Later in the program planetary soft landings could be made by Mariner or Voyager vehicles. Braking for such soft landings will probably be effected by atmospheric drag rather than by rocket power.

Developmental Mariner missions to Venus and Mars are scheduled to begin in 1966. See Section 2.

10.1 ENTRY INTO ATMOSPHERE OF VENUS OR MARS

The approach to Venus or Mars is assumed to involve the classical technique of first getting the vehicle into the planet's orbit and then "falling" into the planet or orbit as required. The approach velocity is then essentially the escape velocity of the planet - corresponding to a parabolic orbit.

10.1.1 Dynamics of Atmospheric Entry

Before entry into Mars' or Venus' atmosphere a body's motion is determined only by the principles of celestial mechanics, i.e., its motion is governed only by its own inertia and by gravitational forces. However, such motion is modified when the vehicle enters

the outer fringes of Venus' or Mars' atmosphere. In the rarefied upper atmosphere where the mean free path is large compared to vehicle dimensions, the flow is of the so-called free-molecule type and gasdynamic drag begins to act in a direction opposite to the vehicle's motion. In the free-molecule flow regime lift (i.e. normal to the direction of motion) forces are not attained at velocities of the orbital or escape magnitude. In the denser lower atmosphere, where the flow is of a continuum type, both lift and drag forces affect the vehicle's motion.

The equations of motion, when moving through a planetary atmosphere, are

$$\frac{W}{32.2}\frac{du}{dt} = \frac{W}{32.2} g \sin\theta - C_D A_c \left(\frac{1}{2}\frac{\rho}{32.2} u^2\right) \quad (1)$$

$$\frac{W}{32.2} u \frac{d\theta}{dt} = \frac{W}{32.2} g \cos\theta - \frac{W}{32.2}\frac{u^2}{r}\cos\theta - C_L A_c \left(\frac{1}{2}\frac{\rho}{32.2} u^2\right) \quad (2)$$

where the coordinate system is illustrated in Figure 10-1.

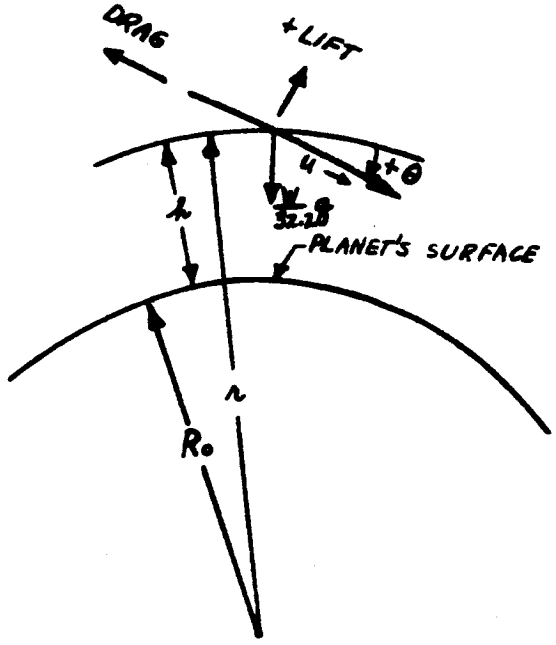

COORDINATE SYSTEM AND SYMBOLS
USED IN EQUATIONS OF MOTION

FIGURE 10-1

Here

W = mass in pounds,

u = velocity in ft/sec,

g = acceleration of gravity in ft/sec^2 at height h,

θ = path angle with local horizontal measured positively downwards,

C_D = drag coefficient,

C_L = lift coefficient,

A_c = frontal (cross-sectional) area of body,

ρ = atmospheric density in lbs/ft^3

The term $\left(\frac{W}{32.2}\right)\frac{u^2\cos\theta}{r}$ is the centrifugal force perpendicular to the trajectory.

Equations (1) and (2) can be put in the form

$$-\frac{du}{dt} = g\sin\theta + \frac{C_D A_c}{W}\frac{\rho_{SL}}{2}\sigma u^2 \qquad (3)$$

$$u\frac{d\theta}{dt} = g\cos\theta - \frac{u^2}{r}\cos\theta - \frac{C_L A_c}{W}\frac{\rho_{SL}}{2}\sigma u^2 \qquad (4)$$

where σ is given by Equation: $\sigma = \frac{\rho}{\rho_{SL}} = e^{-\frac{M'gh}{RT}} = e^{-\alpha h}$

Analytic solution of these equations is possible only for certain approximations. The following paragraphs describe solutions for various types of atmospheric entry.

10.2 DIRECT ENTRY OF A NON-LIFTING BODY (BALLISTIC CASE)

Direct entry into Venus' or Mars' atmosphere from a parabolic orbit involves an initial velocity equal to the planet's escape velocity and an essentially linear path through the atmosphere. The initial velocity is reduced due to gasdynamic drag. The following assumptions are made:

(1) The path angle θ is constant.

(2) The drag coefficient C_D is constant.

(3) The gravitational acceleration is small compared to the drag deceleration.

(4) No lifting forces.

Equation (3) becomes:

$$\frac{du}{dt} = -\frac{C_D A_c}{W} \frac{\rho_{SL}}{2} \sigma u^2.$$

Now, the exponential density variation given by Equation

$$\sigma = e^{-\alpha h}$$

may be differentiated to give

$$\frac{d\sigma}{dt} = -\alpha e^{-\alpha h} \frac{dh}{dt}$$

From the following sketch

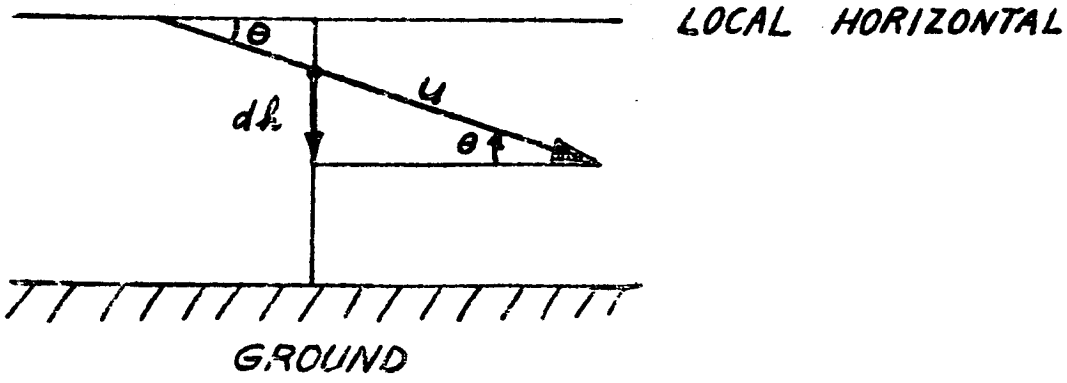

$$dh = -u \sin\theta \, dt,$$

so that $\frac{dh}{dt} = -u \sin\theta,$

and

$$\frac{d\sigma}{dt} = -\alpha\sigma\left(-u\sin\theta\right) = \alpha\sigma u \sin\theta. \qquad (6)$$

If one divides Equation (5) by Equation (6) one gets

$$\frac{du}{d\sigma} = -\frac{C_D A_c}{W\sin\theta}\frac{\rho_{SL}}{2\alpha}u. \qquad (7)$$

Thus,

$$\frac{du}{u} = -\frac{C_D A_c}{W\sin\theta}\frac{\rho_{SL}}{2\alpha}d\sigma, \qquad (8)$$

and

$$\left[\log_e u\right]_{u_{esc}}^{u} = -\frac{C_D A_c}{W\sin\theta}\frac{\rho_{SL}}{2\alpha}\left[\sigma\right]_0^{\sigma} \qquad (9)$$

or

$$\log_e\frac{u}{u_{esc}} = -\frac{C_D A_c}{W\sin\theta}\frac{\rho_{SL}}{2\alpha}\sigma, \qquad (10)$$

and

$$\frac{u}{u_{esc}} = e^{-\frac{C_D A_c}{W\sin\theta}\frac{\rho_{SL}}{2\alpha}\sigma} \qquad (11)$$

The quantity $\frac{u}{u_{esc}}$ is plotted versus

$$\frac{C_D A_c}{W\sin\theta}\frac{\rho_{SL}}{2\alpha}\sigma$$

in Figure 10-2.

Altitude is plotted versus velocity during direct entry from a parabolic orbit with $\theta = 90^\circ$ into Venus' and Mars' atmospheres for $\frac{C_D A_c}{W} = 0.1$ ft^2/lb in Figure 10-3.

VELOCITY VARIATION FOR DIRECT ENTRY INTO PLANET'S ATMOSPHERE

$$\frac{u}{u_{esc}} = e^{-\frac{C_D A_c}{W \sin\theta} \frac{\rho_{SL}}{2\alpha} \sigma}$$

$$\frac{C_D A_c}{W \sin\theta} \frac{\rho_{SL}}{2\alpha} \sigma = \frac{C_D A_c}{W \sin\theta} (10250)\, e^{-(4.88 \times 10^{-5}) h} \quad \text{FOR VENUS}$$

$$\frac{C_D A_c}{W \sin\theta} \frac{\rho_{SL}}{2\alpha} \sigma = \frac{C_D A_c}{W \sin\theta} (486)\, e^{-(6.67 \times 10^{-5}) h} \quad \text{FOR MARS}$$

FIGURE 10-2

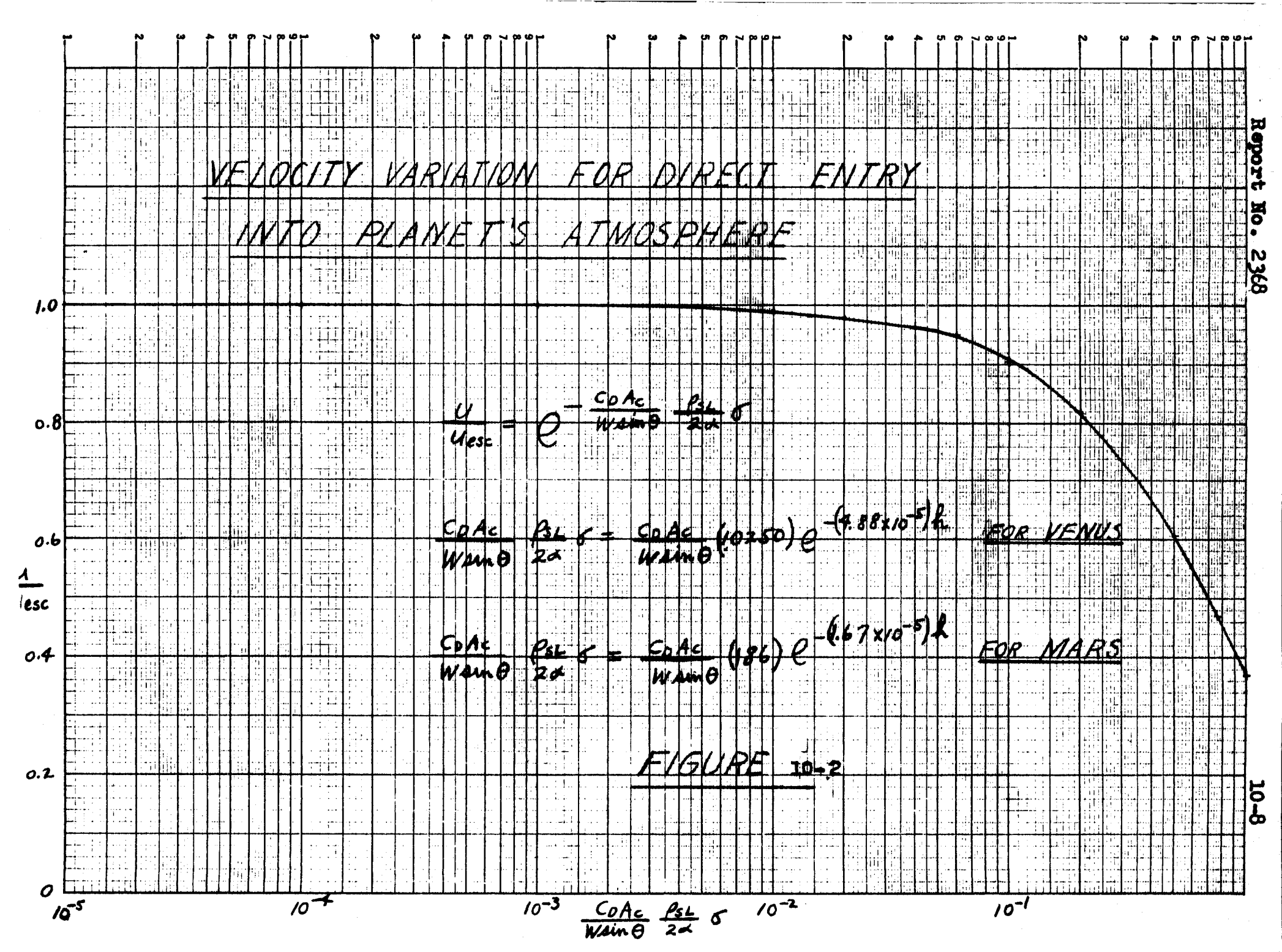

RADIOPLANE
A DIVISION OF NORTHROP CORPORATION
SYSTEMS DIVISION

ALTITUDE VERSUS VELOCITY DURING DIRECT ENTRY FROM SPACE AT $\theta = 90°$ INTO THE ATMOSPHERES OF VENUS AND MARS

FIGURE 10-3

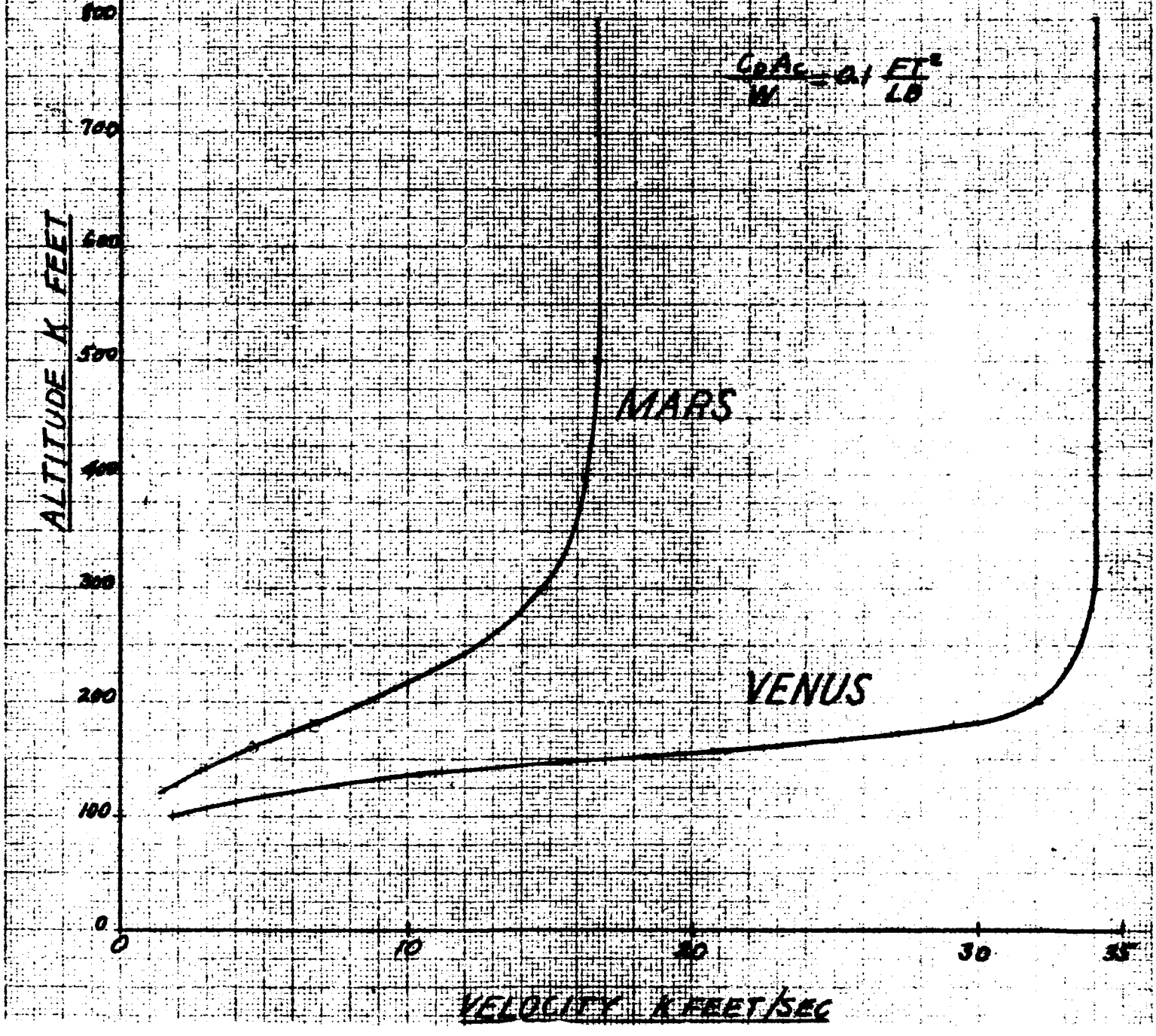

Now, for steady motion in a circular orbit with orbital velocity one has

$$\frac{m u_o^2}{r} = \frac{GMm}{r^2} = mg,$$

and $\frac{GM}{R_o^2} = g_o$ at the surface of the planet, so that

$$GM = g_o R_o^2 .$$

Thus,

$$\frac{u_o^2}{r} = \frac{g_o R_o^2}{r^2} ,$$

or

$$u_o^2 = \frac{g_o R_o^2}{r} . \qquad (12)$$

The escape velocity u_{esc} is found from

$$\frac{1}{2} m u_{esc}^2 = \int_r^\infty f\, dr = \int_r^\infty \frac{GMm}{r^2} dr = g_o R_o^2 m \int_r^\infty \frac{dr}{r^2} = \frac{m g_o R_o^2}{r},$$

or

$$u_{esc}^2 = 2 \frac{g_o R_o^2}{r} . \qquad (13)$$

Now, divide Equation (13) by Equation (12) to get

$$\frac{u_{esc}^2}{u_o^2} = 2 ,$$

or

$$\frac{u_{esc}}{u_o} = \sqrt{2} . \qquad (14)$$

Thus, one has

$$\frac{u}{u_o} = \frac{u}{u_{esc}} \left(\frac{u_{esc}}{u_o} \right) = \frac{u}{u_{esc}} \left(\sqrt{2} \right) = \sqrt{2}\, e^{-\frac{C_D A_c}{W \sin\theta} \frac{\rho_{sl}}{2\alpha} \sigma} \qquad (15)$$

or

$$\frac{u}{u_o} = \sqrt{2}\, e^{-\left(\frac{C_D A_c}{W \sin\theta} \frac{\rho_{sl}}{2\alpha} e^{-\alpha h} \right)} . \qquad (16)$$

Altitude is plotted versus $\frac{u}{u_o}$ for direct entry at $u = u_{escape}$ for $\frac{C_D A_c}{W \sin\theta}$ ranging from 0.001 to 100.0 $\frac{ft^2}{lb}$ for Venus in Figure 10-4 and for Mars in Figure 10-5.

VENUS

DIRECT ENTRY (BALLISTIC CASE)

FIGURE 10-4

(ENTER AT $U_{ESC} = \sqrt{2}\, U_o$)

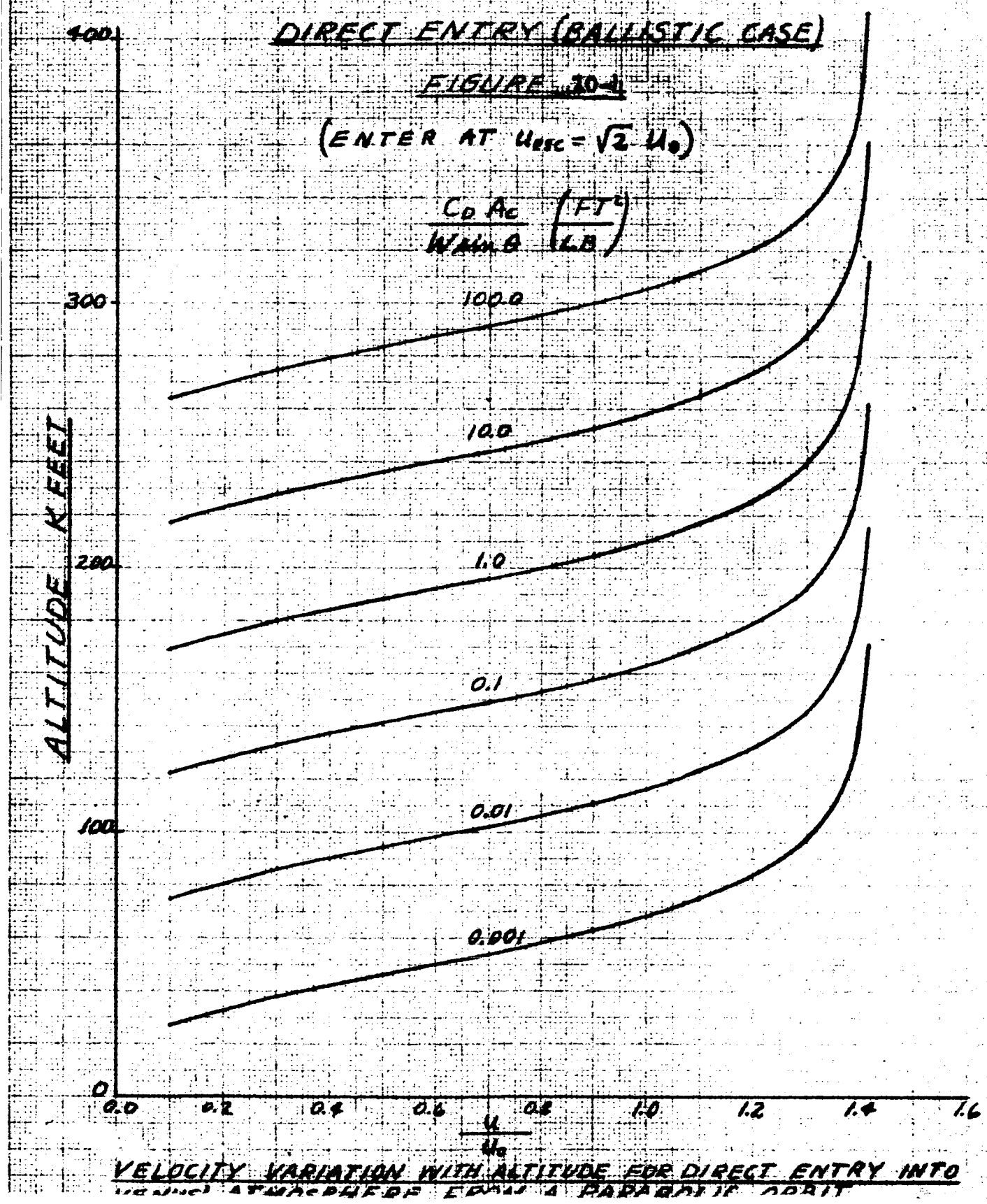

VELOCITY VARIATION WITH ALTITUDE FOR DIRECT ENTRY INTO VENUS ATMOSPHERE FROM A PARABOLIC ORBIT

RADIOPLANE
A DIVISION OF NORTHROP CORPORATION
SYSTEMS DIVISION

MARS

DIRECT ENTRY (BALLISTIC CASE)

FIGURE 10-5

(ENTER AT $U_{esc} = \sqrt{2}\, U_o$)

$$\frac{C_o A_c}{W \sin\theta} \left(\frac{Ft^2}{LB}\right)$$

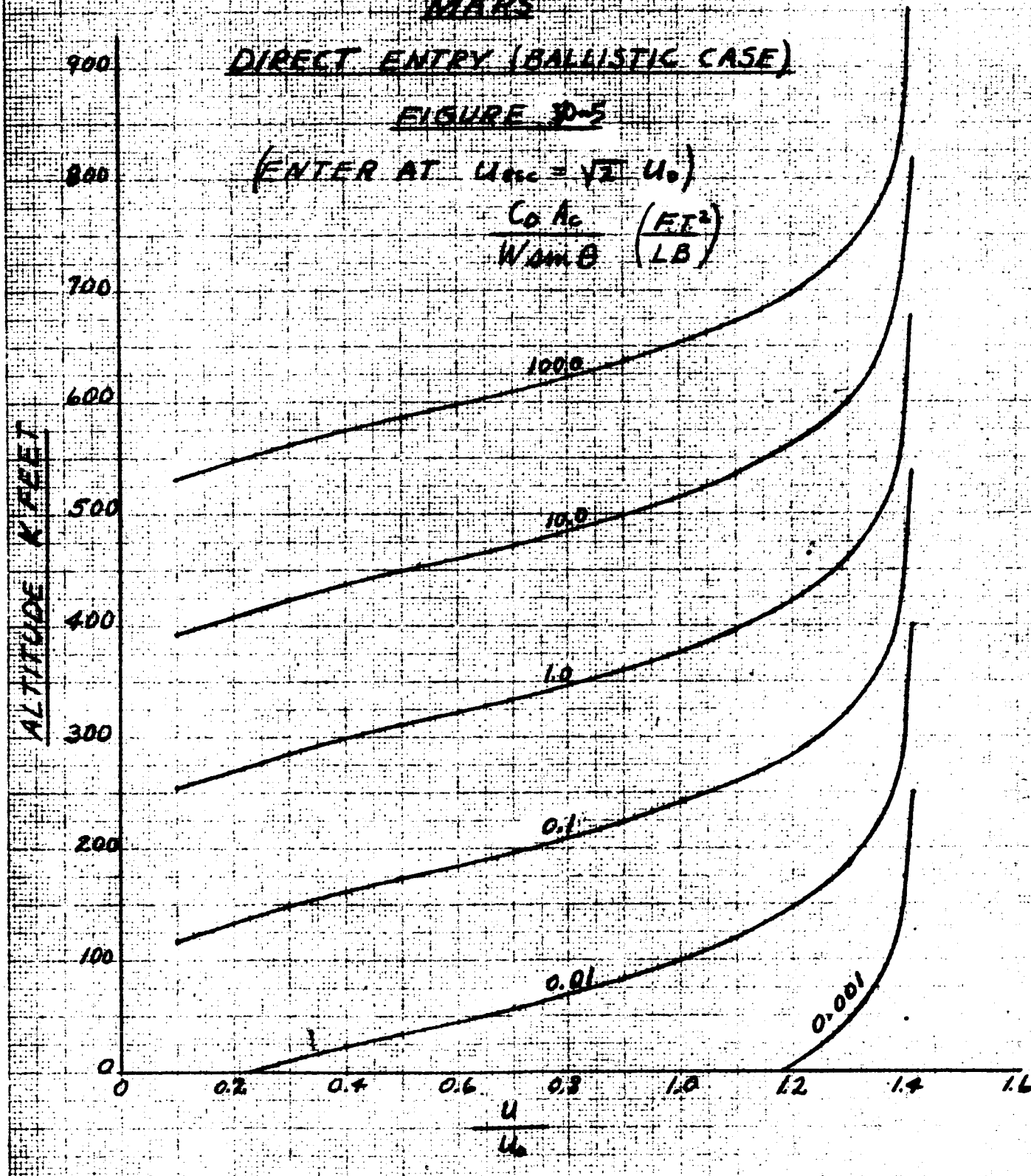

VELOCITY VARIATION WITH ALTITUDE FOR DIRECT ENTRY INTO MARS' ATMOSPHERE FROM A PARABOLIC ORBIT

Now, from Equations (11) and (6) one gets

$$-\frac{1}{32.2}\frac{du}{dt} = \frac{\alpha\, u_{esc}^2 \sin\theta}{32.2}\left(\frac{C_D A_c}{W\sin\theta}\frac{\rho_{SL}}{2\alpha}\sigma\right) e^{-2\frac{C_D A_c}{W\sin\theta}\frac{\rho_{SL}}{2\alpha}\sigma} \qquad (17)$$

or

$$-\frac{1}{32.2}\frac{du}{dt} = \frac{\alpha\, u_{esc}^2 \sin\theta}{32.2}\left(\frac{C_D A_c}{W\sin\theta}\frac{\rho_{SL}}{2\alpha}e^{-\alpha h}\right) e^{-\left(2\frac{C_D A_c}{W\sin\theta}\frac{\rho_{SL}}{2\alpha}e^{-\alpha h}\right)} \qquad (18)$$

which gives the deceleration in earth g's as a function of altitude, $\frac{C_D A_c}{W}$ and angle θ.

As an example, altitude is plotted versus deceleration during direct entry from space at escape velocity into Venus' and Mars' atmosphere at $\theta = 90^\circ$ for $\frac{C_D A_c}{W} = 0.1\,\frac{ET^2}{LB}$, in Figure 10-6.

From Equations (17) and (11) one gets

$$\frac{du}{dt} = \alpha\, u_{esc}^2 \sin\theta \left(\frac{u}{u_{esc}}\right)^2 \log_e \frac{u}{u_{esc}} . \qquad 19$$

If one sets

$$A = \frac{du}{dt},$$

$$K = \alpha\, u_{esc}^2 \sin\theta,$$

and $$x = \frac{u}{u_{esc}}$$

then Equation (19) becomes

$$A = K\, x^2 \log_e x,$$

and

$$\frac{dA}{dx} = Kx\,(1 + 2\log_e x).$$

When A is a maximum, then

$$\frac{dA}{dx} = Kx\,(1 + 2\log_e x) = 0$$

RADIOPLANE
A DIVISION OF NORTHROP CORPORATION
SYSTEMS DIVISION

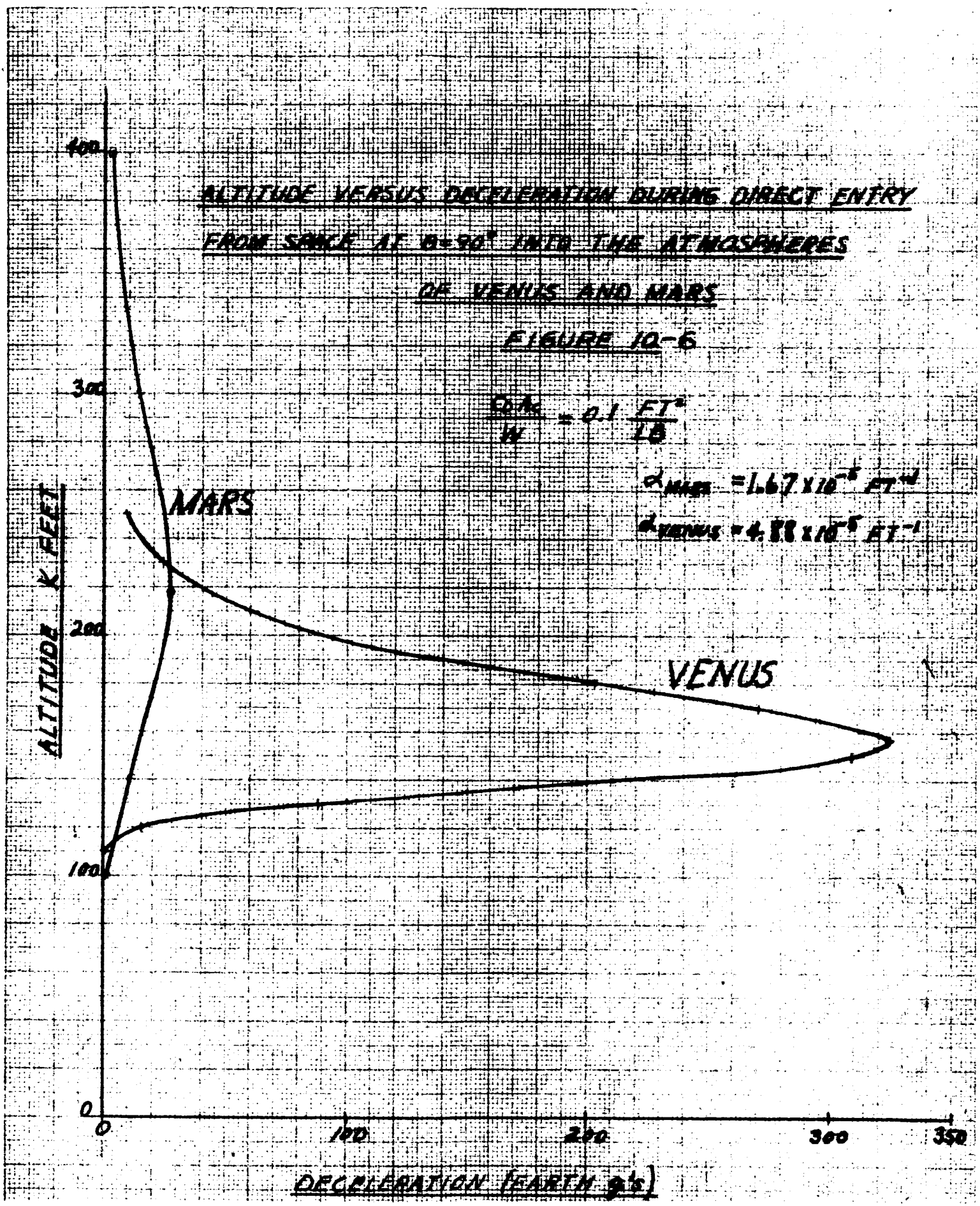

or

$$\log_e \chi = -\frac{1}{2}$$

and

$$\chi = e^{-\frac{1}{2}} = \frac{1}{e^{\frac{1}{2}}} = \frac{1}{\sqrt{2.72}} = \frac{1}{1.649} = 0.607$$

Thus, the maximum deceleration $\left(A = \frac{du}{dt}\right)$ occurs at

$$\frac{u}{u_{esc}} = 0.607 \quad . \tag{20}$$

Now, from Equation (11)

$$\log_e \left(\frac{u}{u_{esc}}\right) = -\frac{C_D A_c}{W \sin\theta} \frac{\rho_{SL}}{2\alpha} \epsilon = -\frac{1}{2} \quad ,$$

or

$$\frac{C_D A_c}{W \sin\theta} \frac{\rho_{SL}}{2\alpha} e^{-\alpha h} = \frac{1}{2} \quad , \tag{21}$$

when maximum deceleration occurs.

With $\frac{u}{u_{esc}} = \frac{1}{e^{\frac{1}{2}}}$ at maximum deceleration,

the value of $\left(\frac{du}{dt}\right)_{max}$ is, from Equation (19),

$$\left(\frac{du}{dt}\right)_{max} = \alpha u_{esc}^2 \sin\theta \left(\frac{1}{e^{\frac{1}{2}}}\right)^2 \left(-\frac{1}{2}\right) = -\frac{\alpha u_{esc}^2 \sin\theta}{2e} \tag{22}$$

Now, from Equation (13), with

$$r = R_o$$
$$g = g_o$$

one gets

$$u_{esc}^2 = 2 g_o R_o \quad ,$$

and Equation (22) becomes

$$-\left(\frac{du}{dt}\right)_{max} = \frac{\alpha (2 g_o R_o) \sin\theta}{2e} = \frac{\alpha g_o R_o \sin\theta}{e} \quad . \tag{23}$$

Thus, the maximum deceleration is proportional to α .

If entry is made at orbital speed, from Equation (8) one gets

$$\left[\log_e u\right]_{u_o}^{u} = -\frac{C_o A_c}{W \sin\theta}\,\frac{\rho_H}{2\alpha}\left[\sigma\right]_{\sigma_o}^{\sigma} \quad , \tag{24}$$

or

$$\frac{u}{u_o} = e^{-\frac{C_o A_c}{W \sin\theta}\,\frac{\rho_H}{2\alpha}(\sigma-\sigma_o)} \quad , \tag{25}$$

and

$$\frac{du}{dt} = \alpha u_o^2 \sin\theta \left(\frac{u}{u_o}\right)^2 \log_e\left(\frac{u}{u_o}\right) \quad , \tag{26}$$

and

$$\left(\frac{du}{dt}\right)_{max} = -\frac{\alpha u_o^2 \sin\theta}{2e} \quad , \tag{27}$$

and

$$\frac{\left[\left(\frac{du}{dt}\right)_{max}\right]_{\text{entering at escape velocity}}}{\left[\left(\frac{du}{dt}\right)_{max}\right]_{\text{entering at orbital velocity}}} = \frac{u_{esc}^2}{u_o^2} = 2 \tag{28}$$

Thus, the maximum deceleration with entry at escape velocity is twice the maximum deceleration with entry at orbital velocity.

In Table 10-1 maximum deceleration during direct entry into the atmospheres of Venus, and Mars is given for direct entry at escape velocity ($\theta = 20^\circ$ and 90°) and orbital velocity ($\theta = 5^\circ$, 20° and 90°).

TABLE 10-1

MAXIMUM DECELERATION DURING DIRECT ATMOSPHERIC ENTRY

(Values Given in Earth g's)

Planet	Direct Entry at Escape Velocity		Direct Entry at Orbital Velocity		
	$\theta = 20^\circ$	90°	$\theta = 5^\circ$	20°	90°
Venus	112	326	14.3	56	163
Mars	9.2	26.6	1.16	4.6	13.3

10.3 ENTRY WITH GASDYNAMIC LIFT

The use of a lifting body for planetary entry enables a more gradual descent. For a given value of $\frac{C_D A}{W}$ a lifting descent is more gradual than the descent of a non-lifting body. Since gasdynamic lift is negligible for velocities of the orbital range at high altitudes (i.e., free-molecule flow), we will consider only the use of a lifting device with descent from a circular orbit, or during the later stages of a shallow direct entry. That is, only descent from an orbit is considered here.

The assumption is made of a small, slowly-changing path angle. Thus, one has

$$\sin\theta \ll 1 ,$$

$$\cos\theta \cong 1 ,$$

$$\frac{d\theta}{dt} \cong 0 ,$$

$$g\sin\theta \ll \frac{du}{dt} .$$

Equations (3) and (4) become

$$-\frac{du}{dt} = \frac{C_D A_c}{W}\frac{\rho_{SL}}{2}\sigma u^2 \tag{29}$$

$$\frac{C_L A_c}{W}\frac{\rho_{SL}}{2}\sigma u^2 = g - \frac{u^2}{r} . \tag{30}$$

Equation (30) can be put in the form

$$\alpha r \frac{L}{D}\frac{C_D A_c}{W}\frac{\rho_{SL}}{2\alpha}\sigma u^2 = gr - u^2 , \tag{31}$$

or

$$u^2\left(1 + \alpha r \frac{L}{D}\frac{C_D A_c}{W}\frac{\rho_{SL}}{2\alpha}\sigma\right) = gr = u_0^2 , \tag{32}$$

and

$$\frac{u}{u_0} = \frac{1}{\sqrt{1+\alpha r \frac{L}{D}\frac{C_D A_c}{W}\frac{\rho_{SL}}{2\alpha}e^{-\alpha h}}} \tag{33}$$

This can be solved for altitude h and yields

$$h = \frac{1}{\alpha} \log_e \left[\frac{\frac{L}{D} r \frac{\rho_{SL}}{2} \frac{C_D A_c}{W}}{\frac{1}{\left(\frac{u}{u_0}\right)^2} - 1} \right].$$

Altitude h is plotted versus velocity $\frac{u}{u_0}$ for $\frac{L}{D} = 1$ for Venus in Figure 10-7 and for Mars in Figure 10-7a.

Now, using

$$C_L = \frac{L}{D} C_D ,$$

and

$$u_0^2 = g r ,$$

Equation (31) becomes

$$\frac{L}{D} \frac{C_D A_c}{W} \frac{\rho_{SL}}{2} \sigma u^2 = g - \frac{u^2}{\left(\frac{u_0^2}{g}\right)} = g - g \frac{u^2}{u_0^2} = g\left(1 - \frac{u^2}{u_0^2}\right),$$

so that

$$-\frac{du}{dt} = \frac{C_D A_c}{W} \frac{\rho_{SL}}{2} \sigma u^2 = \frac{g\left(1 - \frac{u^2}{u_0^2}\right)}{\frac{L}{D}} . \qquad (34)$$

Now from Equation (34)

$$1 - \frac{u^2}{u_0^2} = 1 - \left(\frac{1}{1 + \alpha r \frac{L}{D} \frac{C_D A_c}{W} \frac{\rho_{SL}}{2\alpha} \sigma} \right) = \frac{\alpha r \frac{L}{D} \frac{C_D A_c}{W} \frac{\rho_{SL}}{2\alpha} \sigma}{1 + \alpha r \frac{L}{D} \frac{C_D A_c}{W} \frac{\rho_{SL}}{2\alpha} \sigma} ,$$

and

$$-\frac{du}{dt} = \frac{g}{\left(\frac{L}{D}\right)} \left[\frac{1}{\frac{1}{\alpha r \frac{L}{D} \frac{C_D A_c}{W} \frac{\rho_{SL}}{2\alpha} \sigma} + 1} \right]$$

or

$$-\frac{du}{dt} = \frac{g}{\frac{L}{D} + \left(\frac{1}{\alpha r \frac{C_D A_c}{W} \frac{\rho_{SL}}{2\alpha} e^{-\alpha h}} \right)} . \qquad (35)$$

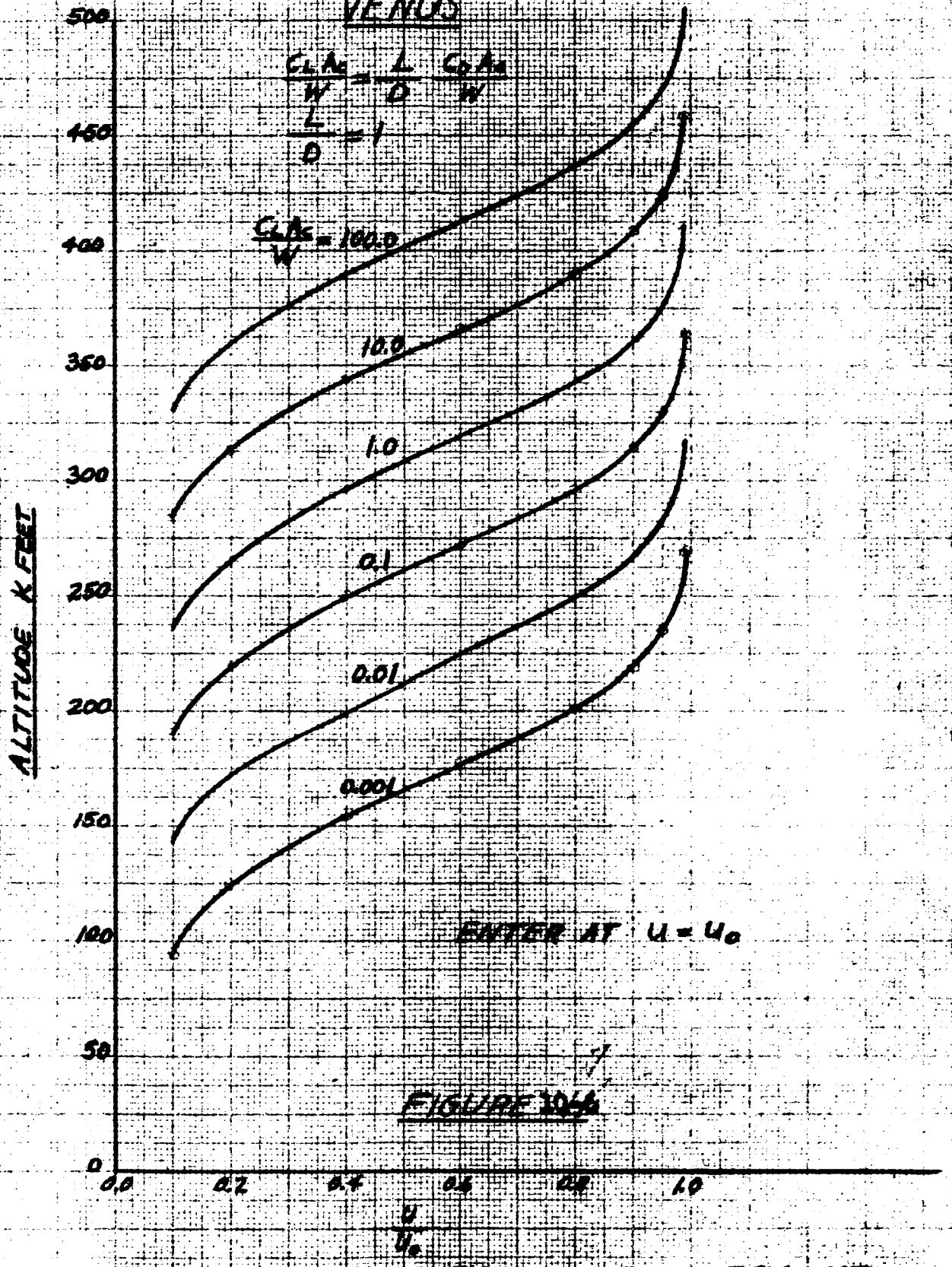

FIGURE 3066

ALTITUDE VERSUS VELOCITY RATIO FOR ENTRY INTO VENUS' ATMOSPHERE OF A BODY WITH GASDYNAMIC LIFT

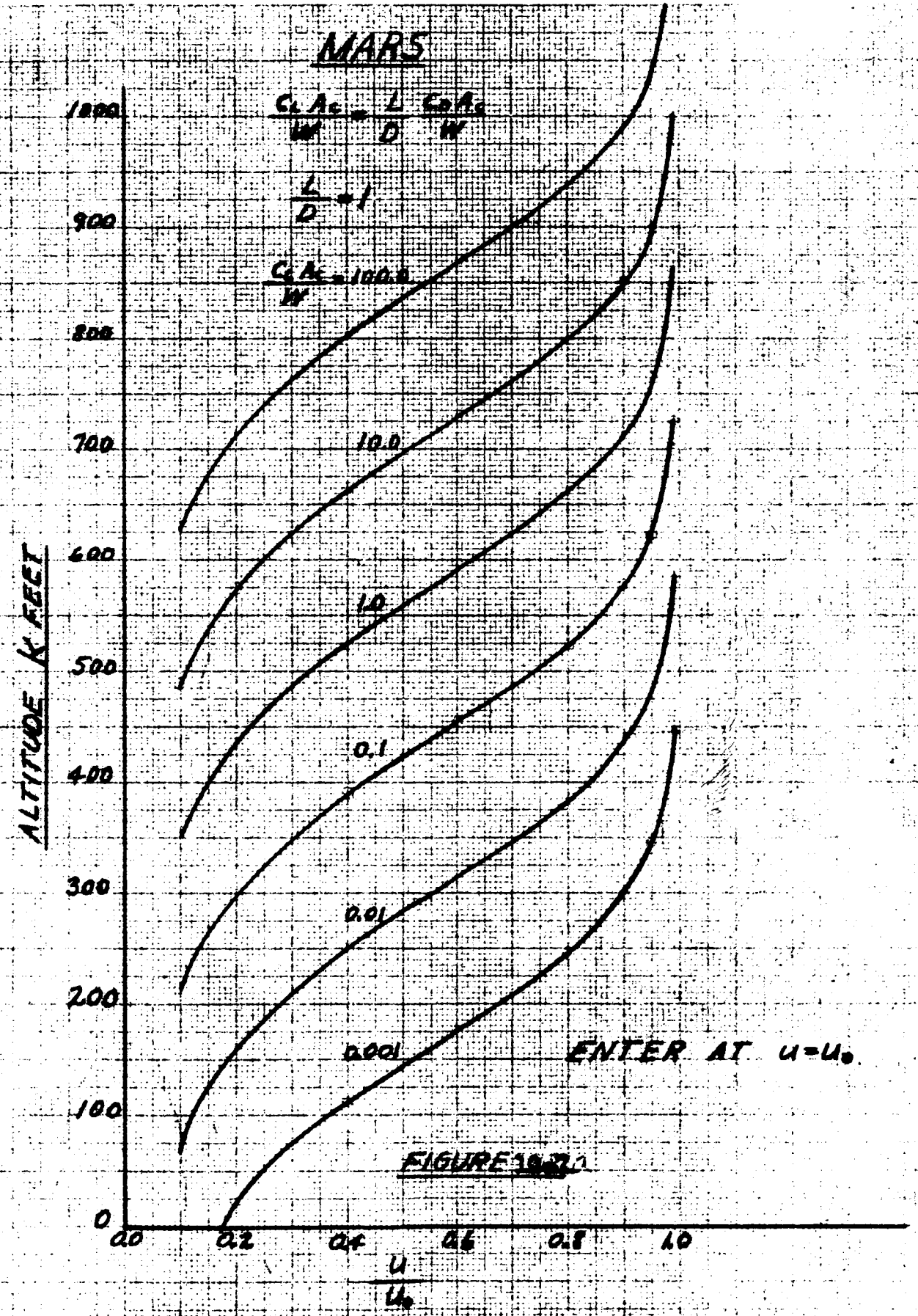

FIGURE 10-7

ALTITUDE VERSUS VELOCITY RATIO FOR ENTRY INTO MARS ATMOSPHERE OF A BODY WITH GASDYNAMIC LIFT

No maximum deceleration occurs during the glide. The deceleration increases continuously during the glide, asymptotically approaching the value

$$-\left(\frac{du}{dt}\right)_{max} = \frac{g}{\left(\frac{L}{D}\right)} \tag{36}$$

as the velocity is reduced.

For a given value of $\frac{C_D A_c}{W}$ the decelerations during a lifting descent are much lower than those in the direct entry case.

Equation (35) can be solved for altitude and yields

$$h = \frac{1}{\alpha} \log_e \left\{ \rho \frac{\rho_{SL}}{2} \frac{C_D A_c}{W} \left[\frac{\left(\frac{g}{32.2}\right)}{\left(-\frac{du}{dt}\right)} - \frac{L}{D} \right] \right\} \tag{37}$$

where g is the gravitational acceleration at the surface of the planet. Altitude h is plotted versus deceleration

$$-\frac{\left(\frac{du}{dt}\right)}{32.2}$$

for $\frac{L}{D} = 1$ for Venus in Figure 10-8 and for Mars in Figure 10-9.

RADIOPLANE
A DIVISION OF NORTHROP CORPORATION
SYSTEMS DIVISION

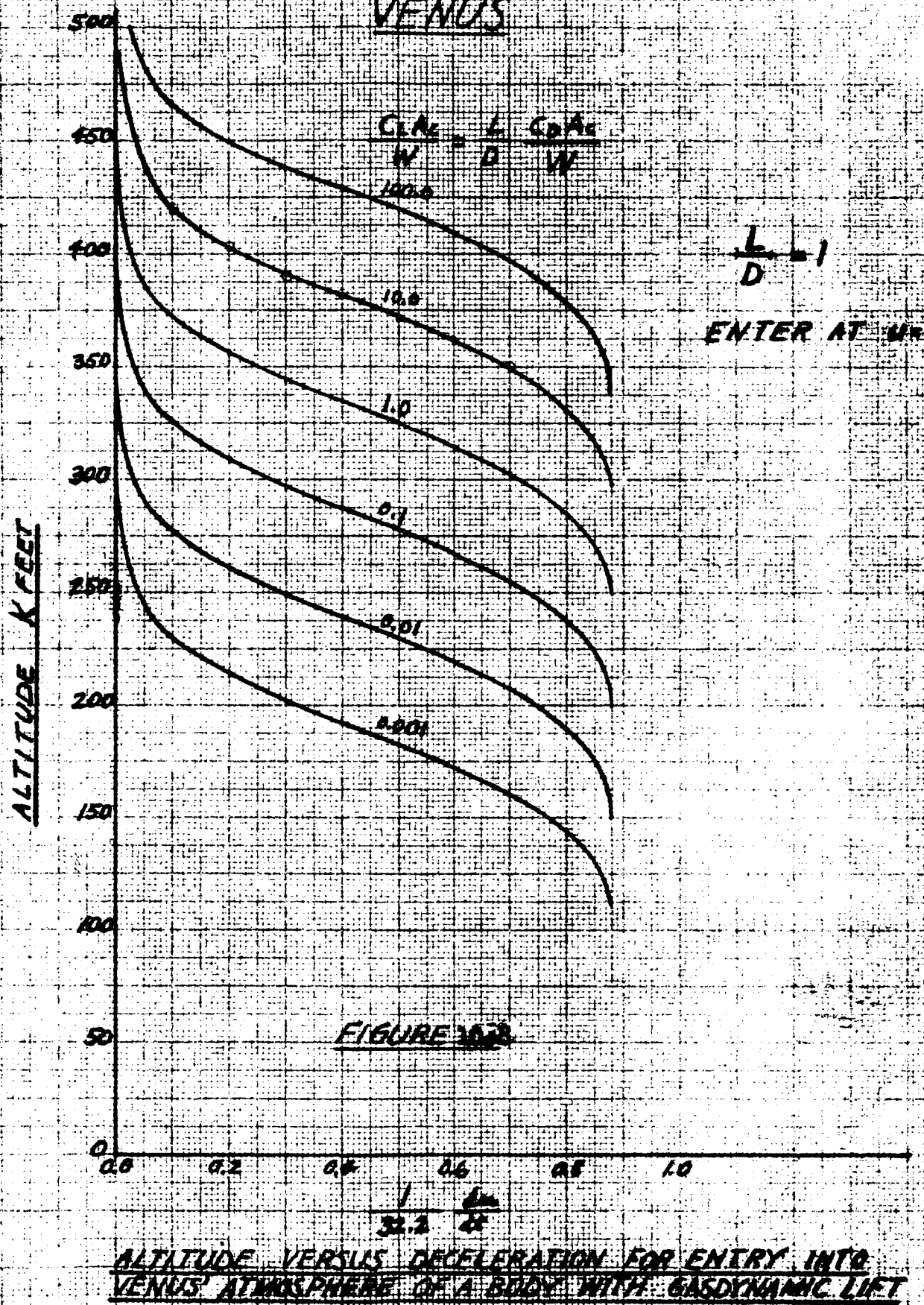

FIGURE 10-8

ALTITUDE VERSUS DECELERATION FOR ENTRY INTO VENUS' ATMOSPHERE OF A BODY WITH GASDYNAMIC LIFT

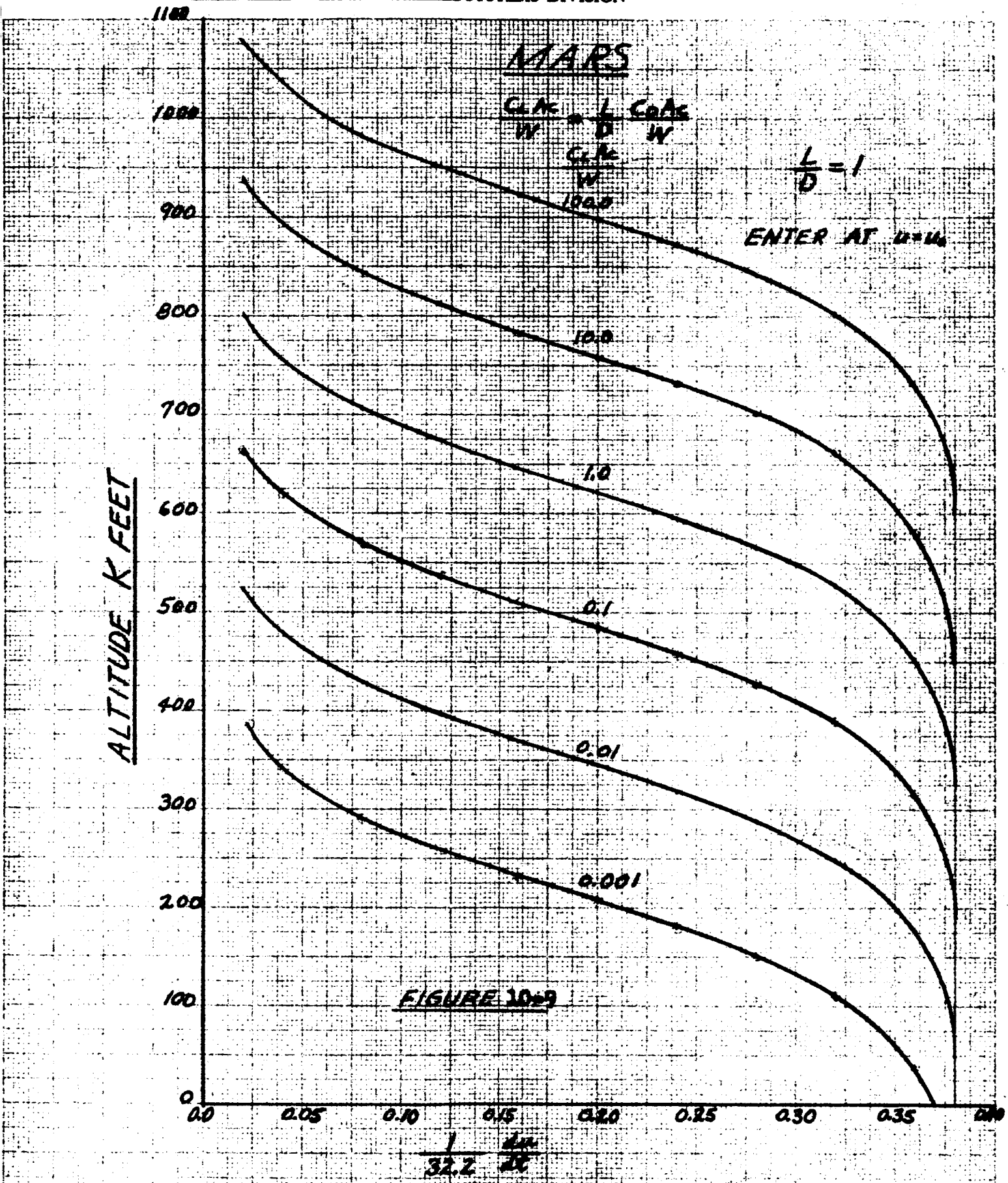

FIGURE 10-9

ALTITUDE VERSUS DECELERATION FOR ENTRY INTO MARS' ATMOSPHERE OF A BODY WITH GASDYNAMIC LIFT

The maximum deceleration during lifting re-entry with gasdynamic drag given by Equation (36) is tabulated in Table 10-2.

Table 10-2

Maximum Deceleration During Entry of Lifting Vehicle at Orbital Velocity (Values Given in Earth g's)

Planet	$\frac{L}{D} = 1$	2	5
Venus	0.88	0.44	0.18
Mars	0.38	0.19	0.076

10.4 Heating

The heat transfer rate q to a body (per unit frontal area) may be expressed as

$$\frac{q}{A_c} = h_c (H_{aw} - H_w)$$

where h_c is the heat transfer coefficient based on the enthalpy difference $H_{aw} - H_w$, where H_w is the enthalpy corresponding to wall temperature and H_{aw} is the adiabatic-wall enthalpy (Reference 5).

Now, define a dimensionless heat transfer coefficient

$$C_{H_0} = \frac{h_c}{\rho u},$$

and an enthalpy recovery factor

$$\eta_R = \frac{H_{aw} - H_1}{H_0 - H_1}, \qquad (38)$$

where H_0 is stagnation enthalpy.

The gasdynamic heating rate q for hypersonic speeds may be approximated as

$$\frac{q}{A_c} = \frac{1}{2} C_{H_c} \eta_R \rho u^3 . \qquad (39)$$

In the upper atmosphere the flow can be considered as free-molecule flow, and (Reference 5),

$$C_{H_c} \eta_R \cong 1 , \qquad (40)$$

while in the laminar continuum regime

$$C_{H_c} \eta_R \cong \sqrt{\frac{M}{R_e}} \qquad (41)$$

where

M = Mach number,

R_e = Reynold's number = $\frac{d u \rho}{\mu}$

d = Characteristic dimension of body,

μ = Viscosity.

For the intermediate (slip-flow regime) lying between the free-molecule and the continuum regimes, the following expression has been deduced from a crude flow model (Reference 5):

$$C_{H_c} \eta_R = \frac{1}{1 + \sqrt{\frac{R_e}{M}}} . \qquad (42)$$

This checks the available data reasonably well. Equations (40), (41) and (42) are shown in Figure 10-10 as a function of $\frac{R_e}{M}$

The ratio of Reynolds number R_e to Mach number M is

$$\frac{R_e}{M} = \left(\frac{R_e}{Md}\right)_{SL} \frac{\rho}{\rho_{SL}} d = \left(\frac{R_e}{Md}\right)_{SL} \sigma d$$

Values of $\left(\frac{R_e}{Mx}\right)_{SL}$ are from Reference 5 and are tabulated in

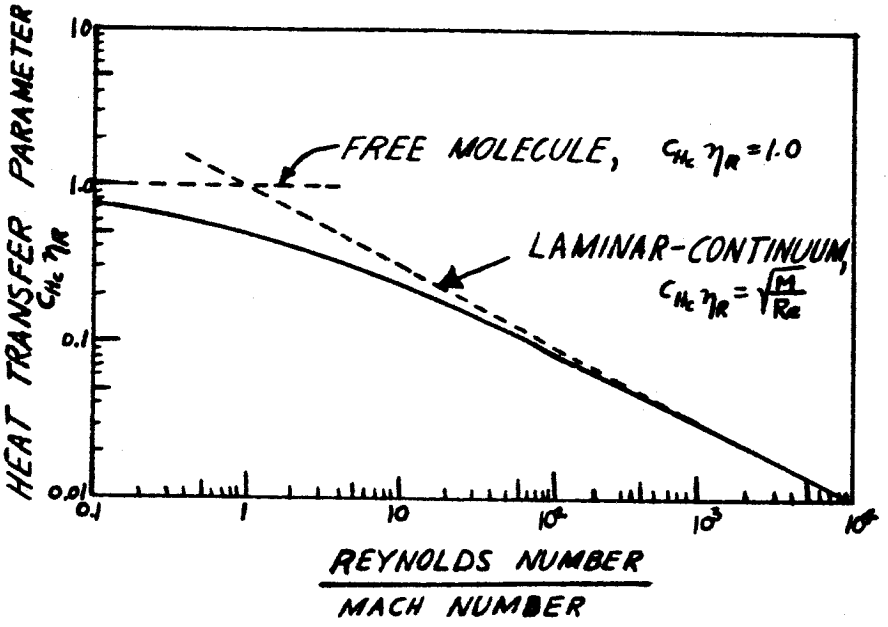

HYPERSONIC HEAT TRANSFER APPROXIMATION

FIGURE 10-10

Table 10-3 below. Here x is distance measured in the flight direction.

Table 10-3

Planet	$\left(\frac{Re}{Mx}\right)_{SL}$
Venus	$(1.0 \times 10^{8})\,ft^{-1}$
Mars	$(6.1 \times 10^{5})\,ft^{-1}$

The atmospheric density in the altitude region of free-molecule flow is so low that the heating rates are also relatively low. For the purposes of this study it appears sufficiently accurate to use Equation (41) for laminar continuum heating. While this will give heating rates which are somewhat too high in the upper atmosphere (see Figure 10-10) the heating rates here are low compared to those at lower altitudes.

A turbulent boundary-layer condition results in heating rates which are higher, by an order of magnitude or so, than the laminar heating rates. It is expected that the turbulent condition will be encountered only in the lower atmosphere, below 100,000 ft. altitude for Mars and Venus (Reference).

The expression for the gasdynamic heating rate then becomes

$$\frac{q}{A_c} = \frac{1}{2} C_{H_c} \eta_R \rho U^3 = \frac{1}{2}\sqrt{\frac{M}{Re}}\,\rho U^3 = \frac{1}{2}\left(\sqrt{\frac{1}{\left(\frac{Re}{Md}\right)_{SL}\sigma d}}\right)\rho U^3$$

or

$$\frac{q}{A_c} = \frac{1}{\sqrt{\left(\frac{Re}{Md}\right)_{SL} d}}\;\frac{1}{\sqrt{\sigma}}\;\frac{\rho_{SL}}{2}\left(\frac{\rho}{\rho_{SL}}\right)U^3 ,$$

or

$$\frac{q}{A_c} = \frac{1}{\sqrt{\left(\frac{R_e}{Md}\right)_{SL} d}} \frac{\rho_{SL}}{2} \sqrt{\sigma}\, u^3 . \qquad (43)$$

For a particular vehicle entering a particular planet's atmosphere, only the density ratio $\sigma = \frac{\rho}{\rho_{SL}}$ and the velocity u vary during descent.

Now,

$$\sigma = e^{-\alpha h},$$

and

$$\frac{u}{u_0} = \sqrt{2}\, e^{-\left(\frac{C_D A_c}{W \sin\theta} \frac{\rho_{SL}}{2\alpha} \sigma\right)}, \qquad \text{(See Eqn 15)}$$

for direct entry at escape velocity,

and

$$\frac{u}{u_0} = \frac{1}{\sqrt{1 + \alpha h \frac{L}{D} \frac{C_D A_c}{W} \frac{\rho_{SL}}{2\alpha} \sigma}} \qquad \text{(See Eqn 23)}$$

for lifting entry at orbital velocity.

A generalized dimensionless heating rate parameter Φ may be formulated from Equation (44) as follows:

$$\frac{\frac{q}{A_c} \sqrt{\left(\frac{R_e}{Md}\right)_{SL} d}}{\frac{\rho_{SL}}{2} u_0^3} = \sqrt{\sigma} \left(\frac{u^3}{u_0^3}\right)$$

Multiply both sides through by $\sqrt{\frac{C_D A_c}{W} \frac{\rho_{SL}}{2\alpha}}$ to get

$$\Phi = \frac{\frac{q}{A_c} \sqrt{\left(\frac{R_e}{Md}\right)_{SL} d} \sqrt{\frac{C_D A_c}{W} \frac{\rho_{SL}}{2\alpha}}}{\frac{\rho_{SL}}{2} u_0^3} = \sqrt{\frac{C_D A_c}{W} \frac{\rho_{SL}}{2\alpha} \sigma} \left(\frac{u}{u_0}\right)^3 . \qquad (44)$$

For a given vehicle and a given planet Φ is directly proportional to $\frac{q}{A_c}$ the heating rate per unit area.

Using Equations (15) and (33) for direct entry and lifting entry at orbital velocity results in the following maximum heating rates (Reference 5).

1. Direct entry: $\Phi_{max} = 0.70 \sqrt{\sin\theta}$ occuring at $\frac{u}{u_{esc}} = 0.846$

$$\frac{C_D A_c}{W} \frac{\rho_{SL}}{2\alpha} \sigma = \frac{\sin\theta}{6} \qquad (45)$$

2. Lifting entry: $\Phi_{max} = \frac{0.384}{\sqrt{\alpha R \frac{L}{D}}}$ occuring at $\frac{u}{u_0} = 0.816$

$$\frac{L}{D} \frac{C_D A_c}{W} \frac{\rho_{SL}}{2\alpha} \sigma = \frac{1}{2\alpha R} \qquad (46)$$

The maximum heating rate occurs when the velocity has been reduced to 80-85% of the initial value in each type of entry. The altitude of maximum heating will vary with the values of $\frac{C_D A_c}{W}$ and $\frac{L}{D}$. An increase in $\frac{C_D A_c}{W}$ will push the point of maximum heating to higher altitude.

Reference 18 gives stagnation-point heat transfer rates measured in a shock tube using hypervelocity flows of gas mixtures simulating the atmospheres of Venus and Mars. The gas mixtures

used were as follows:

Venus - 10% N_2 , 90% CO_2

Mars - 95% N_2 , 5% CO_2 .

The measured heat transfer rates were used to determine heating rates that vehicles would experience during a ballistic entry at escape velocity. For Venus, stagnation point heat transfer rate versus altitude during direct entry at escape velocity for $\frac{C_D A_c}{W \sin \theta} = 0.031$, 0.1 and 3.1 $\frac{ft^2}{lb}$ is given in Figure 10-11. Similar results are given for Mars in Figure 10-12. On the basis of results obtained to date, it appears that stagnation-point heat transfer rates experienced during direct entry into the atmosphere of Venus may be as much as 50 percent higher than those which would be experienced during re-entry into the Earth's atmosphere. Mars' entry heating rates are only a few percent of those for Venus or for the Earth (Reference 18).

For lifting re-entry from orbit there is relatively gradual descent and essentially all of the gasdynamic heating can be dissipated by thermal radiation from the vehicle skin. Such a procedure requires either a high-temperature insulating coating or a sufficiently moderate heating rate so that excessive temperatures do not occur in the primary structural skin. In the case of a thin (low thermal capacity skin), the heat accumulated in the skin is small compared to the gasdynamic heating rate and to the radiation cooling rate. In this case the skin attains the "radiation-equilibrium wall temperature" T_{wr} , the surface temperature corresponding to a radiation cooling rate just sufficient to balance the gasdynamic heating rate, with

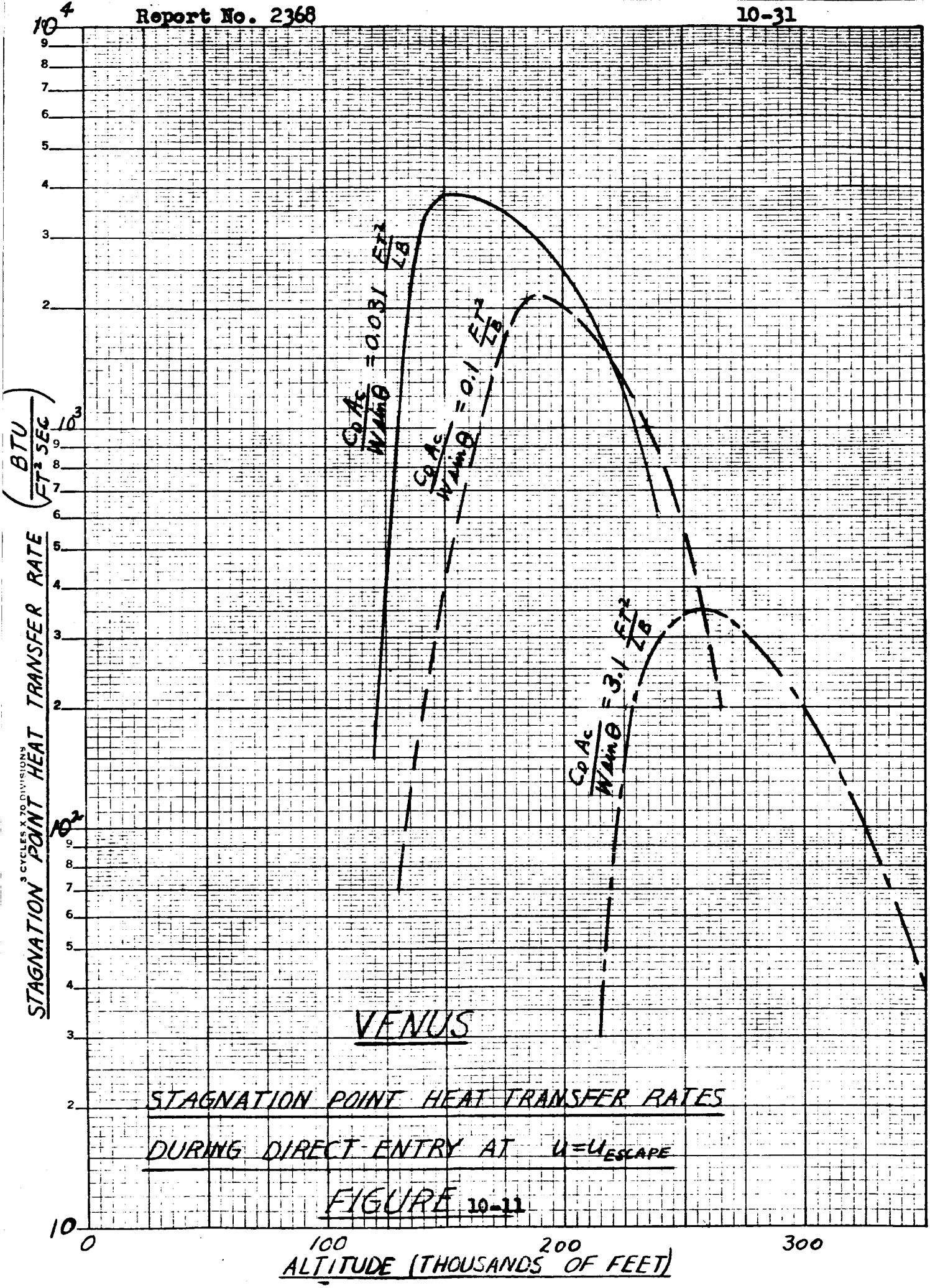

STAGNATION POINT HEAT TRANSFER RATES

DURING DIRECT ENTRY AT $U = U_{ESCAPE}$

FIGURE 10-11

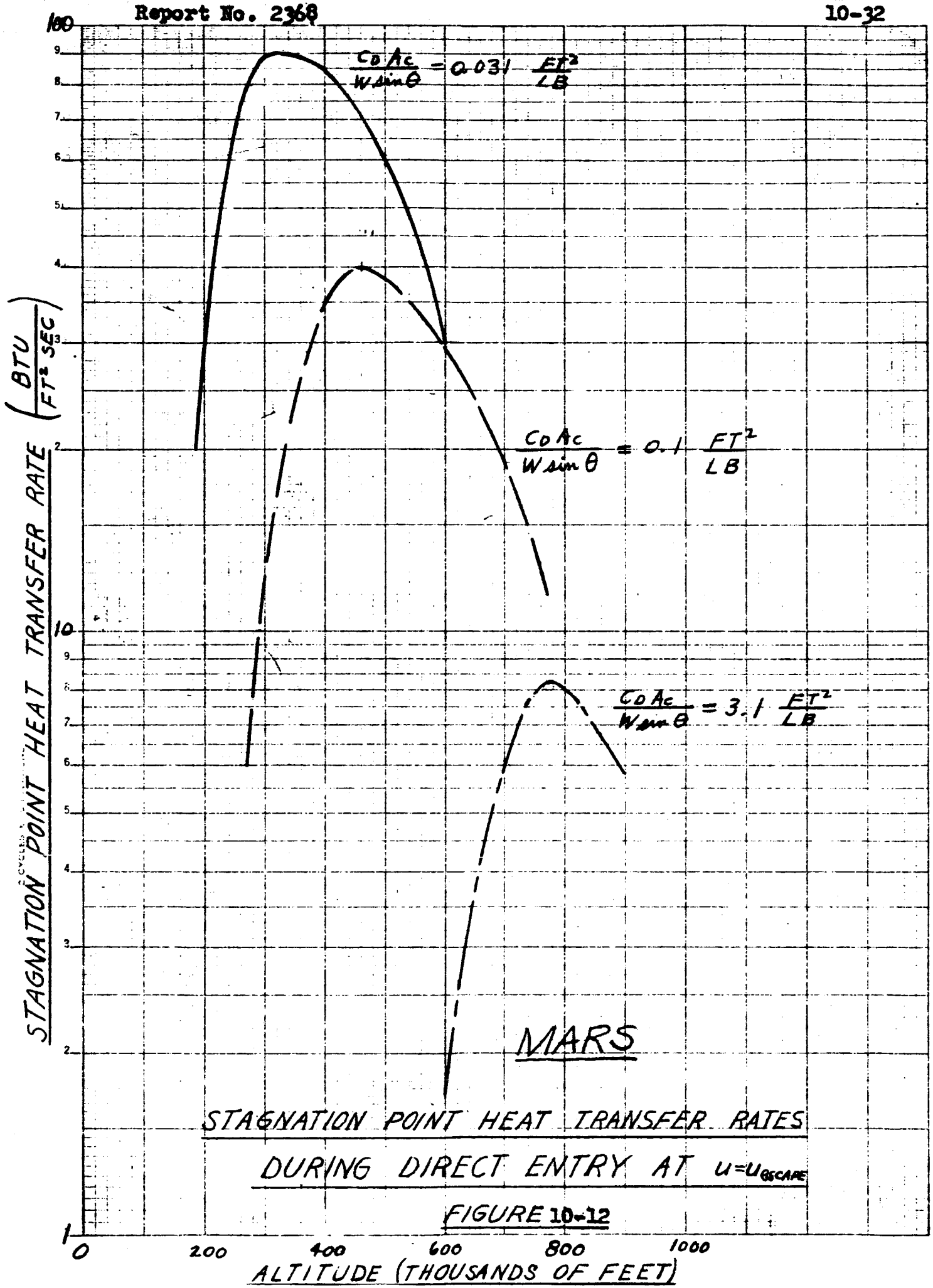

STAGNATION POINT HEAT TRANSFER RATES

DURING DIRECT ENTRY AT $u = u_{ESCAPE}$

FIGURE 10-12

$$\epsilon \sigma_B T_{we}^4 = \left(\frac{\dot{q}}{A_c}\right)\left(\frac{A_c}{A_s}\right) \qquad (47)$$

where

ϵ = Emissivity of surface,

σ_B = Stefan-Boltzmann constant,

A_s = Skin area of vehicle.

The maximum surface temperature occurs when the heating rate is a maximum, and is

$$T_{max} = \left[\frac{1}{\epsilon \sigma_B}\left(\frac{\dot{q}}{A_c}\right)_{max}\left(\frac{A_c}{A_s}\right)\right]^{\frac{1}{4}} \qquad (48)$$

From Equation (44) one has

$$\left(\frac{\dot{q}}{A_c}\right)_{max} = \frac{\frac{\rho_{SL}}{2} u_o^3 \Phi_{max}}{\sqrt{\left(\frac{Re}{Md}\right)_{SL} d}\ \sqrt{\frac{C_D A_c}{W}\frac{\rho_{SL}}{2\alpha}}} \qquad (49)$$

Thus, Equation (48) becomes

$$T_{max} = \left[\left(\frac{1}{\epsilon \sigma_B}\right)\frac{\frac{\rho_{SL}}{2} u_o^3 \Phi_{max}}{\sqrt{\left(\frac{Re}{Md}\right)_{SL} d}\ \sqrt{\frac{C_D A_c}{W}\frac{\rho_{SL}}{2\alpha}}}\left(\frac{A_c}{A_s}\right)\right]^{\frac{1}{4}} \qquad (50)$$

For the entry of a body with d = 2 ft, $\frac{A_s}{A_c} = 2$ and $\epsilon = 0.8$, Equation (50) gives the maximum average temperature to be expected over the face of a hemispherical nose of diameter of two feet. The maximum temperature at the stagnation point of this body is greater by a factor of $(2)^{\frac{1}{4}} = 1.19$, and is plotted in Figure 10-13 for lifting descent from orbit at $\frac{L}{D} = 1$ for Mars and Venus (Reference 5).

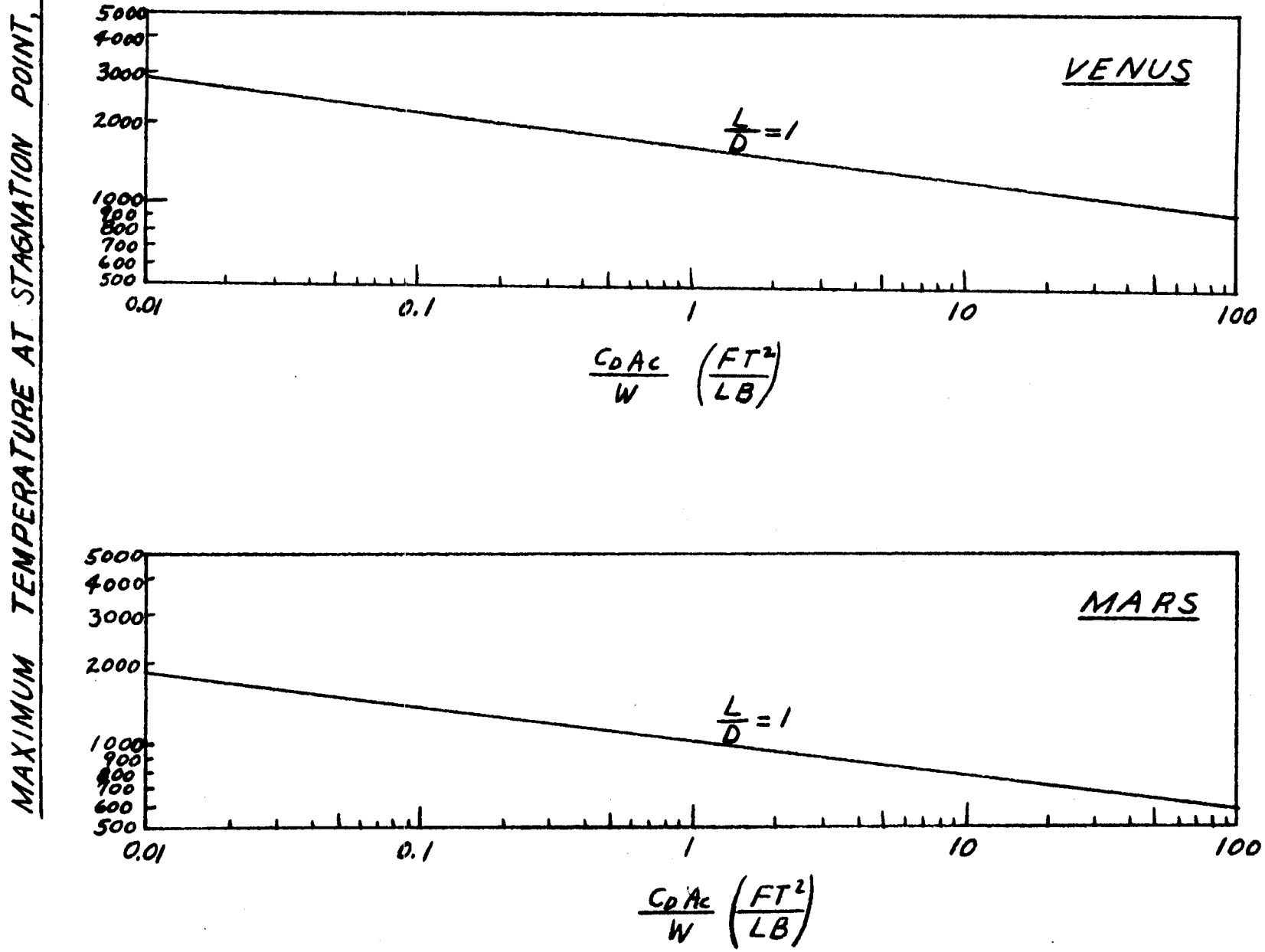

MAXIMUM TEMPERATURE AT STAGNATION POINT DURING PLANETARY ENTRY FOR d=2 FT, $\frac{A_z}{A_c} = 2$, $\epsilon = 0.8$

FIGURE 10-13

The maximum radiation equilibrium temperature (T_{max}) given by Equation (50) is tabulated in Table 10-4 (taken from Reference 19) for $\frac{C_D A_c}{W} = 0.1 \frac{\text{sq ft}}{\text{lb}}$, for Venus and Mars.

The cases tabulated are direct entry at escape velocity at $\theta = 20^\circ$ and 90° and direct entry at orbital velocity for $\theta = 5^\circ$, 20° and 90°. Also included is entry of a lifting vehicle at orbital velocity at $\frac{L}{D} = 1$, 2 and 5.

TABLE 10-4

MAXIMUM TEMPERATURE EXPERIENCED DURING VARIOUS TYPES OF ATMOSPHERIC PENETRATION FOR:

$$\frac{C_D A_c}{W} = 0.1 \frac{FT^2}{LB} \ *$$

(VALUES EXPRESSED AS EQUIVALENT RADIATION EQUILIBRIUM TEMPERATURE $^{\circ}R$)

Planet	Direct Entry at Escape Velocity		Direct Entry at Orbital Velocity			Entry of Lifting Vehicle at Orbital Velocity		
	$\theta = 20^{\circ}$	90°	$\theta = 5^{\circ}$	20°	90°	$\frac{L}{D} = 1$	2	5
Venus	5500	6300	3600	4200	4900	2300	2100	1900
Mars	2800	3200	1900	2200	2500	1500	1350	1200

*Note that the maximum heating rate, unlike the maximum deceleration, is dependent upon the mass-drag parameter.

SECTION 11

REFERENCES

1. Jet Propulsion Laboratory - Industry Conference Proceedings, JPL, NASA, October 26, 1960, at JPL, Pasadena, California.

2. Gin, Winston and Piasecki, L., Solid Rockets for Spacecraft, Page 32 of March 1961 Issue of Astronautics Magazine.

3. Kopal, Zdenek, Aerodynamic Effects in Planetary Atmospheres, December 1960 Issue of Aerospace Engineering Magazine.

4. Space Facts, A Handbook of Basic and Advanced Space Data for Scientists and Engineers, by Missile and Space Vehicle Department, General Electric Co., 1960.

5. Deceleration and Heating of a Body Entering a Planetary Atmosphere from Space, Carl Gazeley Jr., Rand Report P-955, 1957.

6. An Approximate Analytical Method for Studying Entry into Planetary Atmospheres by Dean R. Chapman, NACA, TN 4276, May 1958.

7. Vehicles for Exploration on Mars, T. F. Cartaino, Rand Report RM-2539, April 1960.

8. Öpik, E. J., Physics of Meteor Flight In The Atmosphere, Interscience, 1958.

9. Ehricke, Krafft, A. and Pence, H., Re-entry of Spherical Bodies Into the Atmosphere at Very High Speeds, Paper 428-57 presented at the ARS Spring Meeting, Washington, D. C., April 4-6, 1957.

10. Allen, H. J. and Eggers, A. J., Jr., A Study of the Motion and Aerodynamic Heating of Ballistic Missiles Entering the Earth's Atmosphere at High Supersonic Speeds, NACA Report 1381, (supercedes 4047), 1958.

11. Allen, H. J., Motion of a Ballistic Missile Angularly Misaligned with the Flight Path Upon Entering the Atmosphere and its Effect Upon Aerodynamic Heating, Aerodynamic Loads and Miss Distance, NACA, TN 4048, October 1957.

12. Bird, John D., Stability of Ballistic Re-entry Bodies, NACA Conference on High Speed Aerodynamics, March 18-20, 1958.

13. Ewing, E. G., A Minimum Weight Landing System for Inter-Planetary Spacecraft, Paper Presented at the Recovery of Space Vehicles Symposium by the Institute of Aerospace Science, Los Angeles, California, October 31-September 1, 1960.

14. WADC TR55-265, USAF Parachute Handbook, Parachute Branch, WADC, December 1956.

15. R-65, Handbook for the Design of Guided Missile Recovery Systems, Radioplane, March 1951.

16. Eggers, Jr., A. J., and Wong, Thomas J., NASA, Ames Research Center Moffett Field, California, Motion and Heating of Lifting Vehicles During Atmosphere Entry, Paper Presented at American Rocket Society on Lifting Reentry Vehicles, April 4-6, 1961, Palm Springs, Calif.

17. Radioplane Report 2324, Impact Deceleration Systems Applicable to Lunar Landing Vehicles, 21 November 1960.

18. Shock Tube Experiments Simulating Entry Into Planetary Atmospheres, Rutowski, R. W., and Chan, K. K., Advances in Astronautical Sciences, Volume 5, 1960, Proceedings of the American Astronautical Society, Los Angeles Meeting, August 4-5, 1959.

19. The Penetration of Planetary Atmospheres, Gazley, Jr., C., ASME Paper No. 59-AV-27 a presentation at the Aviation Conference, Los Angeles, California, March 9-12, 1959, of the American Society of Mechanical Engineers.